UNIVERSITÀ DEGLI STUDI DI PADOVA

DIPARTIMENTO DI INGEGNERIA INDUSTRIALE

CORSO DI LAUREA MAGISTRALE IN INGEGNERIA CHIMICA
E DEI PROCESSI INDUSTRIALI

Tesi di Laurea Magistrale in

Ingegneria Chimica e dei Processi Industriali

OPTIMISATION OF A CARBON-FREE, FLAME-ASSISTED CONTINUOUS SYNTHESIS OF $LaFeO_3$

Relatore: ***Prof. Paolo Canu***
Correlatori: ***Ing. Nicola Zanetti***
Ing. Benedetta Oliani

Laureanda: CAMILLA MATTEAZZI

ANNO ACCADEMICO 2019-2020

Abstract

Flame assisted spray pyrolysis (FASP) is a continuous technique that allows the production of perovskites by spraying a precursor solution directly into a flame. In this thesis work, this technology was applied for the synthesis of $LaFeO_3$ to be employed in the abatement of flue gases.

The lab-scale plant had been constructed during previous thesis projects and it consisted of a hydrogen-fed burner with eight momentum-controlled downwards-directed flames arranged in a conical configuration that surrounded a spray gun that nebulised the precursor solution directly into the cone of flames. Because of the high temperatures reached inside the flames, the $LaFeO_3$ synthesised had a perovskite crystalline structure right after being collected and therefore it did not necessitate to undergo any further treatment.

The reliability of the lab-scale plant was enhanced and the greatest improvements were carried out in the feeding section of the plant. The old system was discarded and substituted by four atomisers that utilised ultrasonic membranes to nebulise the precursor solution. The new feeding system allowed the synthesis of smaller particles and a more substantial collection of the catalyst which did not stop on the walls of the reactor.

The $LaFeO_3$ was synthesised by varying various parameters to understand which were the best conditions for its production that would lead to the perovskite with the greatest catalytic activity. The parameters, whose influence on the catalytic performance was investigated, were the flowrate of combustible and oxidising gas fed to the burner, the concentration of precursor solution utilised to synthesise the perovskites and the powder recovery method.

The results obtained from the catalytic tests, conducted on the various types of $LaFeO_3$, indicated that the recovery of the powder by means of ultrasonic cleaning of the filters improved significantly the catalytic activity of the perovskites.

These data, on the optimal synthesis conditions and powder recovery method, will be the basis for the synthesis of doped $LaFeO_3$.

Riassunto

La “flame assisted spray pyrolysis” (FASP) è una tecnica continua che permette la produzione di perovskiti nebulizzando una soluzione direttamente nella fiamma. In questo lavoro di tesi, questa tecnologia è stata applicata per la sintesi di $LaFeO_3$, che verrà utilizzata per l’abbattimento dei gas di scarico delle automobili.

L’impianto è stato costruito durante precedenti lavori di tesi e consisteva in un bruciatore alimentato ad idrogeno con otto fiamme direzionate verso il basso e disposte in una configurazione conica. Questo cono di fiamme circondava l’aerografo che nebulizzava la soluzione direttamente all’interno del cono di fiamme. Grazie alle alte temperature raggiunte all’interno delle fiamme, la $LaFeO_3$ sintetizzata aveva una struttura perovskitica cristallina subito dopo essere stata prodotta, senza la necessità di essere sottoposta ad ulteriori trattamenti.

L’affidabilità dell’impianto iniziale è stata ottimizzata ed importanti miglioramenti sono stati effettuati al sistema di alimentazione della soluzione. Il vecchio sistema di alimentazione è stato sostituito da quattro atomizzatori che utilizzano membrane ad ultrasuoni per nebulizzare la soluzione. Il nuovo sistema di alimentazione permette la sintesi di particelle con diametro inferiore ed un recupero più consistente del catalizzatore dal pacco filtri perché le particelle non si fermano più lungo le pareti della colonna.

La $LaFeO_3$ è stata sintetizzata variando vari parametri per capire quali fossero le migliori condizioni produttive che portassero ad ottenere la perovskite con la migliore attività catalitica. I parametri, per i quali è stata investigata una possibile influenza sull’attività catalitica, sono le portate di gas combustibile e ossidante alimentate al bruciatore, la diluizione della soluzione utilizzata per sintetizzare le perovskiti e la metodologia di recupero delle polveri dai filtri.

I risultati ottenuti dai test catalitici, condotti su diverse tipologie di $LaFeO_3$, hanno indicato che la polvere recuperata dopo la pulizia dei filtri in sonicatore ha un’attività catalitica significativamente migliore rispetto a quella raschiata dai filtri.

Le informazioni ottenute sulle condizioni ottimali di sintesi e recupero delle polveri saranno la base per ottimizzare la sintesi di $LaFeO_3$ dopata.

Index

Introduction

In the chemical industry, catalysts have always played an essential role in many sectors. In particular, their usage is of fundamental importance in the abatement of flue gases. Platinum-group metals (PGMs) have been and are still widely used for automotive applications because they are extremely efficient in terms of pollutants removal.

However, PGMs are very expensive and therefore, in recent years, the research has focused on finding more cost-efficient catalysts for this application and perovskites have occupied a significant role since they have been the most investigated alternative to PGMs.

Flame assisted spray pyrolysis (FASP) is a technique that allows to synthesise perovskites spraying a precursor solution directly into a flame. The application of this technology for the production of catalysts has become an interest of the research group K-INN Lab at the University of Padua, where a flame assisted spray pyrolysis lab-scale plant was constructed.

The primary objective of this thesis work is to optimise the lab-scale plant that was constructed during previous thesis projects to enhance its performances and improve its reliability in the production and recovery of the powder.

The optimised lab-scale plant is employed to synthesise $LaFeO_3$ varying the conditions of synthesis, such as the flowrates of combustible and oxidising gas feeding the flames, the concentration of the precursor solution sprayed and the powder recovery method. All the perovskites synthesised are characterised and catalytically tested because the second objective of this thesis work is to understand if the perovskites produced are catalytically active and which are the economically sustainable synthesis conditions that allow to synthesise the $LaFeO_3$ with the greatest catalytic activity. For a thorough comprehension, the catalytic tests are executed with different gas reacting mixtures and they are repeated for different values of weight hourly space velocity (WHSV).

This thesis work is structured as it follows. In Chapter 1, the bibliographic research is carried out with the aim of providing a general view on flame assisted spray pyrolysis (FASP) and on the various apparatuses constructed and utilised in research laboratories worldwide. Then, the bibliographic research gave an understanding of the parameters that influence the characteristics of the perovskites synthesised with this technique and on why flame assisted continuous synthesis is better than batch processes for the production of the catalysts.

The lab-scale plant constructed in previous thesis projects and utilised to synthesise the $LaFeO_3$ is described in Chapter 2. In this chapter all the improvements executed on the lab-scale plant for its optimisation are also reported.

In Chapter 3, the experimental set-up utilised to test the catalytic activity is described together with all the instruments necessary for the analysis of the gas mixture and the characterisation of the perovskites.
Chapter 4 reports the results obtained from the various analyses conducted for the characterisation of the perovskites, while Chapter 5 reports the results of the catalytic tests executed on the different types of $LaFeO_3$.

Chapter 1

State of the art

Flame technology is a continuous, scalable technique for the production of large quantities of nanoparticles. For years, this method has been utilised only for the production of commodities. During the years, it was decided to utilise this process for the preparation of catalyst supports and photocatalysts. It was then proposed by some researchers to adopt flame technology to produce more complex catalytic materials such as perovskites [1].
Flame assisted spray pyrolysis, the aerosol method in which a liquid precursor solution is fed into a flame after being atomised to produce nano-sized particles, has become an interest of the research group at K-INN Lab at the University of Padova for the production of perovskites as catalytic material for the abatement of harmful gases in automotive exhaust gas [2],[3].
In the following paragraphs, an overview of the studies conducted on this type of technology will be presented in order to provide a better understanding of this process and of all the aspects that influence the production of nanoparticles by means of this technique, with the purpose of validating the fact that betting on this technology is a good idea.

1.1 Batch processes for the production of perovskites

K-INN Lab works closely with the laboratory of Professor Glisenti of the Department of Chemistry at the University of Padua. They produce oxides with perovskite structure through the citrate sol-gel method, which is a batch process. In sol-gel chemistry, the formation of metal oxides, with perovskite structure, is achieved by mixing metal precursors (such as nitrates) in an aqueous solution to force them to react together to form a network structure called wet-gel. In order to obtain this network of metallic ions, a chelating agent (such as citric acid) is needed, and the solution has to be heated up to 80 °C in a water bath in order to promote solvent evaporation. The gel is treated for a couple of hours at high temperature (400 °C) in air in order for the organic framework to decompose and for the metal precursors to oxidise. Afterwards the powder has to be grinded and calcinated at 900 °C to obtain the crystalline phase [4].
In addition to the sol-gel method, many other batch processes are used to produce perovskites. For example, there is the co-precipitation method, where two or more components are precipitated by using a suitable precipitating agent and then the resulting product has to be centrifugated, washed with water and ethanol for several times, dried and calcinated [5].

Another possible batch synthesis technique is the combustion of a solution, that consists of rapid, self-sustaining, exothermic chemical reactions between a metal oxide dissolved in hydrogen peroxide and ammonia and a suitable organic fuel (such as citric acid). In this case, most of the heat required for the synthesis is supplied by the reactions themselves; therefore, the mixture of reactants needs to be heated up only to a temperature that is significantly lower than the actual phase formation one [6].
The citrate sol-gel method, as the other batch processes, is very laborious because it consists of many passages to obtain the final product and some of these procedures are very lengthy, as for example the formation of the network structure which lasts overnight. Therefore, at K-INN Lab it was thought to substitute the sol-gel method for the production of perovskites with a continuous process such as flame assisted spray pyrolysis.

1.2 Flame assisted spray pyrolysis

Flame assisted spray pyrolysis is based on the oxidation of a solid phase dissolved in an aqueous solution which takes place into the flame where the solution is sprayed. The fine droplets of solution, created by means of an atomiser, evaporate and the metal precursors oxidise. The small particles, that are formed, are cohesive and, due to the electrostatic interaction between them, they tend to generate clusters which will then sinter because of the high temperature in the flame. Due to the oxygen abundance in the flame environment and to the high temperatures, the particles, which are collected after exiting the flame, are usually fully oxidised and crystallised. The environment, that is created around the flame, allows the production of powders in the size range of nanometers with a high specific surface area.
Flame assisted spray pyrolysis (FASP) derives from another technique which is the flame spray pyrolysis (FSP). These two techniques are similar, but there are also some substantial differences between the two. In fact, in FSP an organic solvent is utilised for the preparation of the precursor solution instead of water and the flame, where the oxidation of the metal precursors takes place, derives from the combustion of the above-mentioned organic solvent.
One advantage of producing perovskites via flame assisted spray pyrolysis is that the metallic precursors, that are needed to form the final product, are mixed homogeneously at the atomic level from the start since they are in solution before being dispersed into the flame.
Another advantage of operating via FASP is the low cost of preparation of the precursor solution due to fact that the solvent utilised is water and also to the possibility of using low cost metal precursors that, combined during synthesis, allow the production of complex and mixed oxides such as perovskites [7].
To control the morphology of the nanostructured powders produced and, as a consequence, their catalytic properties and thermal stability, it is possible to act on different aspects of the process, such as the residence time, the temperature of the flame, the concentration of metallic

precursors in the aqueous solution or the size of the droplets into which the solution is nebulised. The manipulations on the process and their effects will be describe later on in this chapter.

1.2.1 Advantages of a continuous process

There are many reasons for which continuous processes, such as flame assisted spray pyrolysis, are better than batch processes, such as the sol-gel method, to produce catalytic materials.
First of all, flame assisted spray pyrolysis, as a continuous process, allows to produce particles at a higher rate with respect to batch processes and for this reason alone it is much more appealing for industries.
Flame assisted spray pyrolysis is a simpler and more direct method for the production of nanoparticles. In fact, it is a one-step process and it does not require several post-production treatment steps for obtaining the final product, in contrast to batch processes. For example, particles produced by FASP do not need to undergo a calcination process at 700 °C to be fully oxidised and crystallised because the sintering temperatures, which are reached inside the flame, are sufficient to form crystallised particles if the residence time is enough. Therefore, this is proof that FASP is a one-step technique.

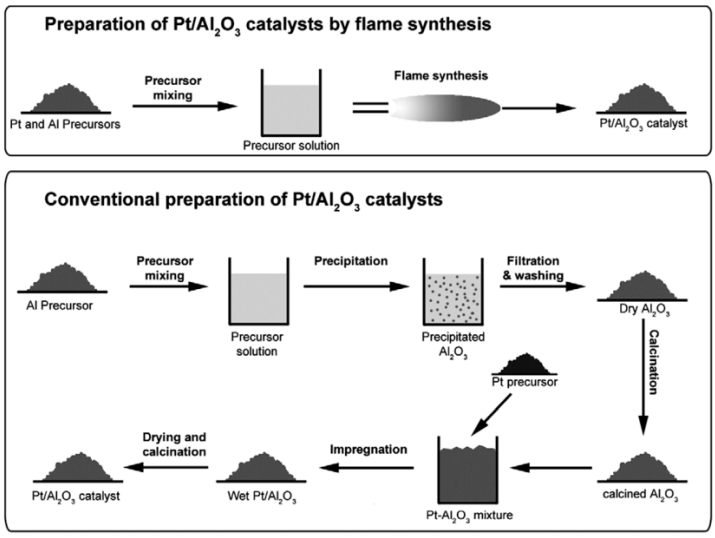

Figure 1.1: Production steps of a continuous process vs a batch process.

In Figure 1.1, it is possible to notice how much more elaborated the batch processes are with respect to flame synthesis for the production of metallic oxides utilised as catalysts.

1.2.2 FASP variables that influence the morphology of particles

The morphology and the catalytic activity of the particles produced by FASP is influenced by many factors, which include the temperature, the residence time of the particles in the high temperature zone, the concentration of the precursor solution, the percentage of solvent present in the initial solution and the system through which the liquid solution is atomised before being

fed to the flame. The temperature in the zone were the particles are formed depends itself on many factors such as, the composition and the flowrate of the gas mixture fed to the burner to produce the flame, the flowrate of secondary air that might enter the system near the reaction zone, the geometry of the system and the possible thermal dispersions towards the environment. The combustible gas and the oxidising gas which are chosen to feed the flame have an effect on the flame temperature which needs to be high enough in order for the liquid precursor solution to evaporate, oxidise and fully convert into the desired crystalline phase and in order to completely eliminate the organic matter such as the precursor anions.

The oxidising gas could be air or oxygen, with the latter allowing to reach a higher flame temperature. Higher temperatures could be achieved not only by utilizing oxygen, but also by choosing the right combustible gas. In fact, working with hydrogen instead of a paraffine, such as methane, allows to reach much higher temperatures inside the flame.

The flame temperature depends mostly on the combustible gas and oxidising gas chosen, but also on their equivalence ratio, ϕ, which is an indication of whether the gas mixture fed to the burner is fuel lean, stoichiometric or fuel rich. The equivalence ratio is defined as the molar ratio of the flowrate of fuel and the flowrate of oxidant effectively used divided by the molar ratio of the flowrate of fuel and the flowrate of oxidant in stoichiometric conditions and it can be expressed as:

$$\phi = \frac{\left(\dot{n}_F / \dot{n}_{OX}\right)_{real}}{\left(\dot{n}_F / \dot{n}_{OX}\right)_{stoich}} \tag{1.1}$$

As it is possible to notice from Figure 1.2, the majority of combustible gases reaches the maximum temperature very close to the stoichiometric condition ($\phi = 1$), while some other fuels, such as acetylene and carbon monoxide, attain the maximum flame temperature at an equivalence ratio greater than one.

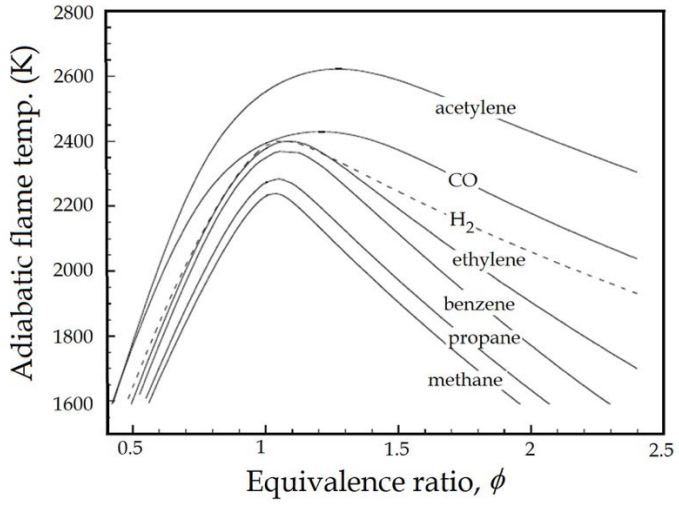

Figure 1.2: Adiabatic flame temperature of various fuels in air in function of ϕ [8].

The graph reported in Figure 1.2 is referred to a feeding gas mixture where the oxidising agent is air, but the temperature profiles obtained with a mixture containing oxygen would be very similar to those ones, just with higher peaks. However, the equivalence ratio of the feeding mixture affects other properties of the flame other than its temperature such as for example its width, which gets narrower if ϕ decreases. Moreover, while maintaining ϕ constant, the flowrates of oxidant and fuel are directly related to the length of the flame; in fact, if the flowrates decreases, also the length of the flame will decrease and vice versa [9].
Furthermore, in the case of FASP, oxygen is not only utilised for the formation of the flame, but it is also employed to oxidise the solid phase which means that an excess of oxygen will be needed with respect to the one required by the equivalence ratio selected.
Therefore, in order to obtain a high enough temperature inside the flame for the production of perovskites, it is important to choose the right fuel and oxidant, but also to select the most suitable equivalence ratio remembering all the specifics that need to be satisfied in order for the set-up to work correctly.
Another crucial factor for the correct formation of perovskites is their residence time inside the flame. In fact, the permanence of the droplets at high enough temperature must be sufficient to assure the complete evaporation of the solution, the total conversion of the metal precursors into the desired catalytically active crystalline phase and to guarantee a sufficient thermal stability of the produced powder.
The incrementation of the residence time of the particles from its minimal required value has a direct effect on the particles' sintering. If the particles remain for a short period inside the flame, the process of sintering will barely take place and therefore the specific surface area (SSA) of the perovskites will be extensive. Instead, the longer the particles will stay in a high temperature environment, the greater their sintering will be, consequently lowering their specific surface area. The larger the specific surface area of the oxide, the greater its catalytic activity will be, even though its thermal stability will decrease. Therefore, it is important to produce perovskites with an appropriate SSA in order to have both good catalytic activity and thermal stability.
Depending on the set-up that is utilized for the FASP, there could be different factors that regulate the residence time of the particles inside the flame; for example the velocity of the particles could be regulated by the velocity of the gas that is utilized as a dispersing agent for the solution.
The specific surface area of the perovskites produced via FASP is affected also by the concentration of the metal precursors in the liquid solution. In fact, a high precursor concentration is preferable because it leads to high productivity, but beyond a certain limit it causes issues in terms of sintering of the powders, causing a drop in the value of the specific surface area. Consequently, diluted solutions are desirable to ensure a sufficiently small particle size.

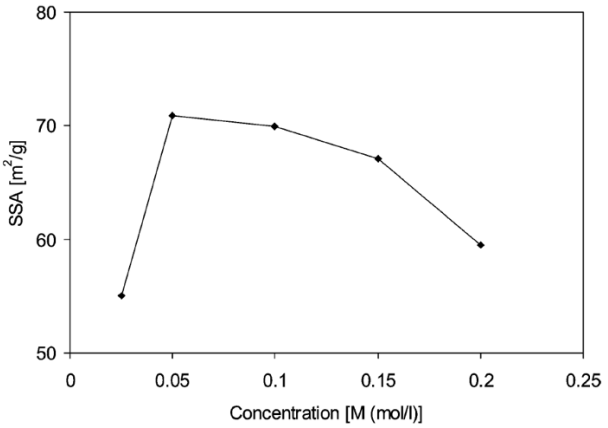

Figure 1.3: Specific surface area of perovskites as a function of the molar concentration of the precursors in the liquid solution.

The plot reported in Figure 1.3 is a good representation of the concept exposed in the previous paragraph. A solution with a higher concentration leads to single droplets of nebulised solution with a greater quantity of metal precursors inside that will produce particles with a bigger size and consequently a lower SSA. Moreover, a more concentrated solution favours the increment of the concentration of primary particles in the flame which promotes frequent particle collision and sintering, resulting in bigger particles and lower SSA. Hence diluted solutions are preferable for preparing small, high-surface area particles. The first point in the plot represented in Figure 1.3 (for a concentration of 0.025 M) is due to the formation of overly small primary particles, which sinter more easily in the hottest zone of the flame.

Moreover, in order to obtain perovskites with a high SSA, it is crucial to spray into the flame fine droplets because the smaller the diameter of the starting droplets, the smaller the one of the metal oxide particles will be.

Equation (1.2) shows the relation of the theoretical diameter of the particles with the molar concentration of metal precursors in the solution and also with the diameter of the droplets of the initial solution.

$$D_p = D_d \sqrt[3]{\frac{M * N_A * V_{uc}}{Z}} \tag{1.2}$$

where D_p is the diameter of the particle, D_d the diameter of the droplet, M the molar concentration of the solution, N_A the Avogadro number, V_{uc} the crystal unit cell volume and Z the number of molecules per unit cell [10].

Another factor that influences the morphology of particles produced via FASP is the fraction of solvent present in the aqueous precursor solution. According to Rudin *et al.*, the percentage of solvent, such as ethanol, present in the precursor solution could affect the size distribution of the particles produced by flame assisted spray pyrolysis [11].

Their researches show that it is possible to produce homogeneous bismuth oxide nanopowders by flame assisted spray pyrolysis starting from a solution of Bi-nitrate as metal precursor, pure

water as a solvent and acetylene or hydrogen as fuel gas. If the solvent is pure water, in order to obtain crystals of homogeneous size, the flowrate of the fuel gas has to be substantial enough to provide high flame temperatures which facilitate the complete conversion of the metal precursor and the nanoparticle formation by the gas-to-particle route to assure homogeneous nano powders. For each fuel gas, the minimum flowrate required is different; for example, C_2H_2 requires a flowrate of only 5.5 L/min, while the minimum one for H_2 is 21.6 L/min.
If the precursor solution contains also a percentage of ethanol, then it is possible to obtain homogeneous nano powders with a smaller flowrate with respect to the one used when the solvent is pure water. Rudin *et al.* studied how the percentage of ethanol in the solution influences the particle size distribution when the fuel gas utilized is C_2H_2 with a flowrate of 2.5 L/min [11]. Above the percentage of 60%, the particles have a unimodal distribution but, below that, they start showing a bimodal one. This percentage depends on the fuel and on its flowrate [11].
All the argumentations above are referred to the production of bismuth oxide; for other types of oxides the reasoning could be different because of the different properties of the metal precursors.

1.3 Reference Flame Synthesis set ups

In this paragraph, some reference FS set-ups, used for the synthesis of perovskites or other nano-scaled materials, are described in order to acquire a better understanding of how flame synthesis works.
The first distinction to make while talking about liquid aerosol flame synthesis is referred to the solvent which is used to disperse the metallic precursors in the liquid solution. In fact, if the solvent is combustible and it drives itself the flame process, contributing to more than 50% of the energy, then the process is called Flame Spray Pyrolysis (FSP). Instead, if the solvent utilized in the starting solution is non-combustible such as in this thesis work, where water is used, the synthesis is denominated Flame Assisted Spray Pyrolysis (FASP).
In the set-ups described below, the most adopted system to create either the auxiliary flame utilized to initiate the fuel in the solution in FSP or the main flame needed in FASP is an annular burner or a set of flamelets disposed in a ring in order to replicate the effect of the annular burner. In FASP, the annular configuration is not the only option for setting up the flames because they could be arranged differently in order to force the nebulised solution to actually go through the flames and not only transit in the high temperature zone created around the flames.
The flames are fed with a mixture of fuel (which could be a hydrocarbon or hydrogen) and an oxidising agent such as oxygen or air; the fuel and the oxidiser could be either pre-mixed or not. Oxygen or air are utilised as dispersing agents to create small droplets of the precursor

solution; the first is mostly used in order to optimise the combustion and to reach higher temperatures.

At the Department of Mechanical and Process Engineering in Zurich, over the years two apparatuses were constructed, one for the FSP [12] and the other one for the FASP [11].

Mueller proposed an FSP apparatus devoted to the production of silica nanoparticles at a higher production rate (up to 1200 g/h) compared to other lab-scale set-ups. The annular burner, fed with CH_4 and O_2, created a diffusion flame; the starting solution, fed to the atomizer, was composed by the silica precursor and ethanol as a solvent and O_2 was utilised as a dispersing agent. Particles were collected on the outer surface of four PTFE-coated Nomex baghouse filters by means of an air suction ventilator and they were removed every 30 s from each one of the baghouse filters by air pressure shocks. Moreover, another small glass fiber filter was present, which was used to collect small samples of particles, by means of a vacuum pump, in order to test them [12].

An illustration of the set-up is shown in Figure 1.4.

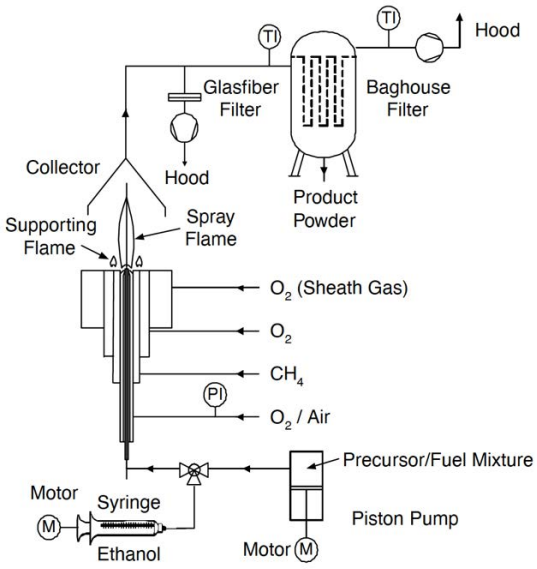

Figure 1.4: Representation of the FSP set-up constructed at the Institute of Process Engineering in Zurich.

Instead, Rudin proposed an apparatus that could be used for the synthesis of oxide nanoparticles produced by means of FASP [11]. The fuel (C_2H_2 or H_2) to feed the spray flame was issued by twelve holes placed on a cylindrical torus ring. The precursor solution, atomized by a co-axial flux of oxygen, was provided through the central nozzle by a syringe pump. A shielding tube was added between the nozzle and the flame ring in order to protect the solution spray from the entrainment of air. The collection of powders was achieved on water-cooled glass microfiber filters by means of a vacuum pump [11]. A representation of the set-up is shown in Figure 1.5.

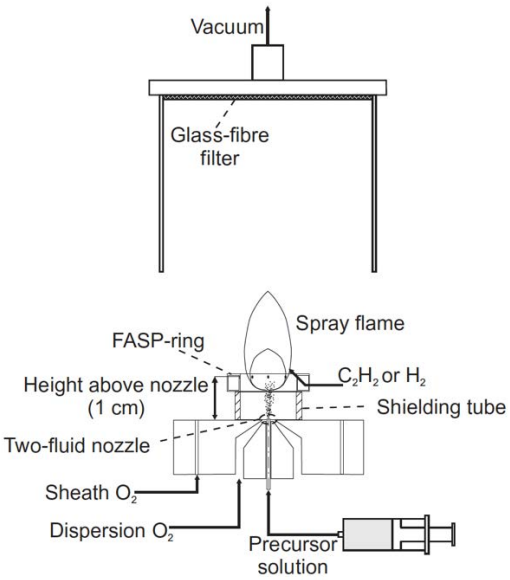

Figure 1.5: Representation of the FASP set-up constructed at the Institute of Process Engineering in Zurich.

A different set-up was built by Betancur-Granados at the Materials and Minerals Department of the University of Colombia, where an FSP apparatus was built in order to produce ceramic nano pigments with a spinel structure. In this apparatus, the alcoholic solution was pumped in the aerosol generator where air was used as a dispersing agent and then the dissolved solution entered a chamber where it was initiated by two cross torches alimented by premixed acetylene and oxygen. Afterwards the powders were collected manually [13]. It is possible to see an illustration of this set-up in Figure 1.6.

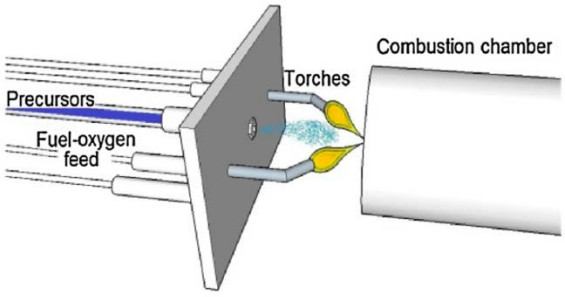

Figure 1.6: Representation of the FSP set-up constructed at the University of Colombia.

1.4 Perovskites: general concepts

The structural family of perovskites is a large family of compounds having the crystal structure related to the mineral perovskite $CaTiO_3$. The chemical formula of this structural family is ABX_3, where X is usually oxygen, but it could also be a large atom such as fluorine, chlorine or bromine. In this thesis work, the interest is directed towards compounds where the anion X is oxygen, therefore the chemical formula becomes ABO_3.

A is a cation that has a comparable radius with the anion X (oxygen) and it usually is an alkaline, earth alkaline or rare earth cation. Instead, the B cation has a smaller radius and it typically is a transition metal. The A cation needs a coordination number of 12, while B requires only a coordination number of 6, which corresponds to an octahedral site. The larger cations, together with the anions, create a crystalline structure with a high packing level.
The representation of an ideal perovskite oxide is represented in Figure 1.7, where it is possible to observe its structure from three different perspectives. From Figure 1.7 (a), it is possible to notice how the perovskite structure is a network of corner linked oxygen octahedra which are occupied for one fourth of their volume by the smaller cations. An alternative point of view of the perovskite structure is given by Figure 1.7 (b), where it is possible to observe that the A cation occupies the centre of the cube while the B cations are positioned at the corners and the oxygen ions are placed at the centre of the edges. An additional point of view is given by Figure 1.7 (c), where the B cation is found at the centre of the cube, the A cations at the corners and the oxygen ions in the centre of the cubic faces.

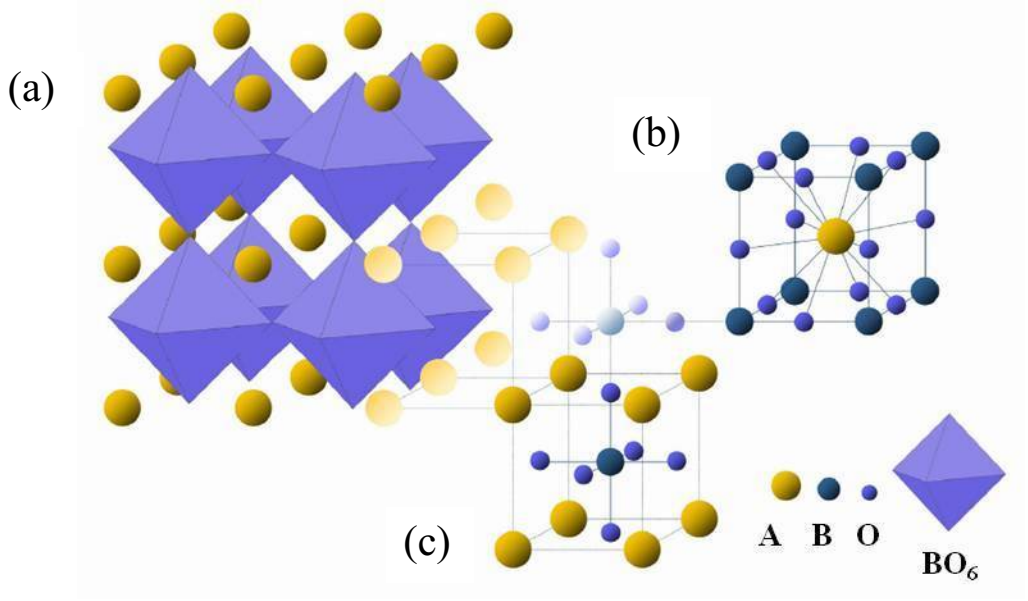

Figure 1.7: Representation of the perovskites structure.

In the ideal case, the distance between two B cations corresponds to the cubic cell axis, a; therefore, the distance between the B cation and the oxygen ion can be written as $a/2$ and the distance between the A cation and the oxygen ion as $a\sqrt{2}/2$. Therefore, the relation between the ionic radius of the elements can be written as:

$$(r_A + r_O) = \sqrt{2}(r_B + r_O) \tag{1.3}$$

where r_A, r_B and r_O are respectively the radius of cation A, B and the oxygen ion. From the relation reported above it is possible to obtain the Goldschmidt's tolerance factor, *t*, which is an indicator of stability and distortion in crystal structures:

$$t = \frac{(r_A + r_O)}{\sqrt{2}(r_B + r_O)} \tag{1.4}$$

In the ideal case, the parameter *t* has a unitary value and in the case of some structural transformations this value could vary. In order to have a compound with a stable perovskite structure, the tolerance factor must be between $0.75 < t < 1$.

However, only few compounds with perovskite structure actually have an ideal cubic structure at room temperature. In fact, most of these sustain some structural transformations which produce small local distortions that consequently lead to a non-symmetric structure. The local distortions could be caused by the displacement of cations from their equilibrium position, by the creation of a cation or anion vacancy or by the addition of a different cation in the A or B site or even in both. These structural transformations could modify the properties of the perovskites and enhance their catalytic activity [14].

1.5 Perovskites as catalysts

The current catalysts used in commercial vehicles, which are noble metals belonging to the platinum-group metals, are very efficient in the abatement of automotive exhaust gases; but scientific studies are always active in order to identify some other types of catalyst which are less costly.

Many materials have been found suitable to substitute PGMs. Among these, also perovskites have been studied as a possible alternative. In fact, perovskites have been considered by researchers because of their stability, their capability to oxidise and their ability to promote the reduction of NO_x. This is why the perovskites, obtained from flame assisted spray pyrolysis at K-INN Lab, are produced with the intentions of utilizing them as catalyst for the abatement of automotive exhaust gases.

Perovskites are very versatile metal oxides and most of the studies concerning them as catalysts, revolve around the possibility of doping them with different metals in order to achieve a specific reactivity towards a certain reaction or set of reactions.

The doping of metal oxides with perovskite structure consists on the partial substitution of cations in position A and B to create further oxides with the generic formula $A_xA'_{1-x}B_yB'_{1-y}O_3$ and this is achieved by metals with different oxidation states. The catalytic activity of these metal oxides is mainly due to the redox properties of the B cations. However, also the doping of the A site, by cations with a different valence, that leads to the formation of structural defects, can contribute to enhancing the catalytic performance, due to the action on the oxygen exchange capacity and thus on oxygen ions mobility which greatly influences the reactivity.

In the literature, it is possible to find studies performed on distinct types of perovskites where their activity is investigated with respect to exhaust gases. However, it has to be noted that the most active compounds towards a specific reaction (as for example oxidation) are not

necessarily high-performance for the activation of other types of reactions. Therefore, the catalytic activity has been evaluated for a doping system capable of replacing, even in part, the PGMs currently in use in the automotive sector.

For example, the most active perovskites for the simultaneous removal of soot and NO, that acts as the oxidising agent, have lanthanum (La) in the A-site and manganese (Mn), cobalt (Co), iron (Fe), nickel (Ni) or titanium (Ti) in the B-site. $LaNiO_3$ are also studied for oxidation and steam reforming, while $LaMnO_3$ shows high performances in the oxidation of CO and hydrocarbons.

In the literature, it is also possible to come across studies conducted on the most appropriate metals to utilise as dopants. Manganese-based compounds, which are already active towards oxidation, may achieve greater efficiency with the addition of strontium (Sr) in the A-site and cobalt-doped samples are more active than those doped with nickel in the B-site. Catalytic tests showed that the presence of copper (Cu) increases the activity of $LaCoO_3$, exhibiting an interesting compromise of oxidation and NO reduction, while substituted lanthanum ferrites are featured with a higher oxygen content on the surface, improving its mobility and consequently the catalytic activity for the soot combustion and NO_x reduction.

Many studies have been conducted on potassium (K), which is considered an interesting cation activator, very efficient in the oxidation of soot. The effect of K seems to be related to the possibility of inducing the formation of vacancies on the surface of metal oxides with perovskite structure, thus improving oxygen mobility and exchange capacity [15].

In this thesis work, only one type of perovskites, $LaFeO_3$, has been synthesised, but the FASP key variables have been varied during production. Therefore, the catalytic testing has the aim to detect how the catalytic activity and reactivity of a specific perovskite is affected by varying the FASP conditions.

Chapter 2

Experimental set-up

This chapter describes the experimental equipment utilised for the synthesis of perovskites via flame assisted spray pyrolysis. The set-up described in the first paragraphs is the one constructed and employed in the previous thesis work [3]. This is the starting point for all the improvements, implementations and changes performed which are also reported in this chapter.

2.1 Initial set-up configuration

Several versions of the experimental set-up for the synthesis of the perovskite were designed and constructed in previous thesis projects. In the next paragraphs, all the various components of the initial set-up will be described in order to give a better understanding of how the apparatus works and how the catalyst is produced.

2.1.1 The burner

A very important part of the experimental set-up for the flame synthesis of perovskites is the burner displayed in Figure 2.1. In order to produce the catalyst by flame synthesis, the nebulised metallic precursor solution had to pass through the flame and the only method to assure its passage in the high temperature zone is to surround the exiting point of the nebulised solution with the flame. To achieve this, a burner with multiple flames arranged in a conical configuration was constructed.

The burner was designed with eight nozzles to produce an equivalent number of premixed momentum-controlled downwards-directed flames. To provide a good distribution of the gas in each nozzle, a mixing chamber was needed. If the nozzles had been placed directly under it, the mixing chamber would have heated up with the consequent risk of flash back, since both fuel and oxidant were present inside of it. Therefore, it was thought that each nozzle had to be kept at a distance by means of a metallic tube.

The body of the burner was realized by Polidoro S.p.A. in carbon steel to provide a good mechanical resistance and to avoid thermal deformations. The nozzles were standard 0.8 mm diameter acetylene welding nozzles with female thread to be screwed onto the tubes.

The mixing chamber of the burner was filled with 2 mm glass spheres to reduce the volume occupied by the gas and to prevent a possible flash back of the flame. The glass spheres were confined by a metallic grid to keep them from falling in the underlying tubes.
The flames were not wide enough to ensure the passage of the nebulised solution through them if directed straight down. Therefore, the tubes were bent of 15° with respect to the vertical so that the flames could create a cone and assure the passage of the solution not only in the high temperature zone but also through them.
Two metallic poles were attached to the burner structure to move it more easily during the ignition of the flames and to sustain it on two supports when placed on top of the column during the synthesis.

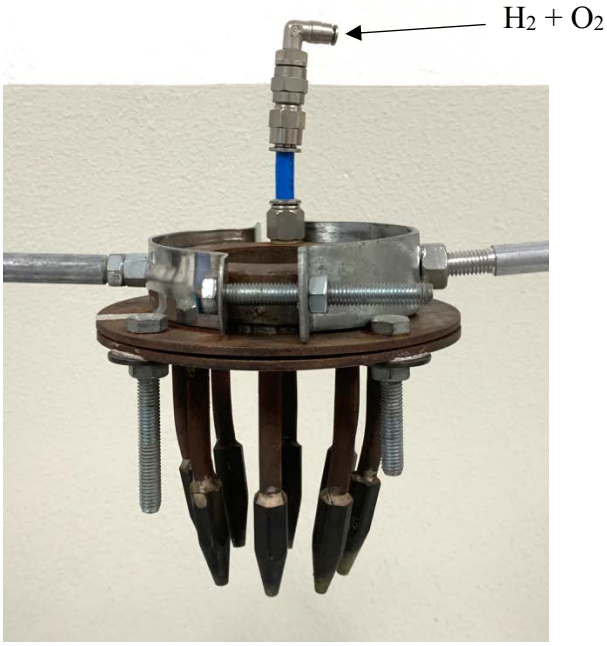

Figure 2.1: Burner

The combustible and oxidising gas needed to feed the burner were stored in two tanks. Two lines were arranged to connect the tanks to the burner. The two lines were merged just before entering the mixing chamber of the burner because, for safety reasons, the mixing of hydrogen and oxygen had to be made as close as possible to the burner, to have the smallest possible volume of gas in the flammable region. Each line was equipped with a safety tap from which the flux of gas from the tank could be stopped, a rotameter to modulate the flow and a non-return valve to avoid that one of the gases could flow back to the source of the other if there were a difference in pressure. The two lines were merged together with a Y connection just before the line entered in the mixing chamber of the burner. The two rotameters utilised to modulate the flow of combustible and oxidising gas were originally designed for a flow of air, but they were recalibrated for the two type of gases utilised. The range of the rotameter for the

oxygen was 0-9 l/min, while the one for the hydrogen had a range of 0-13 l/min. The set-up for the feeding of the gases is shown in Figure 2.2.

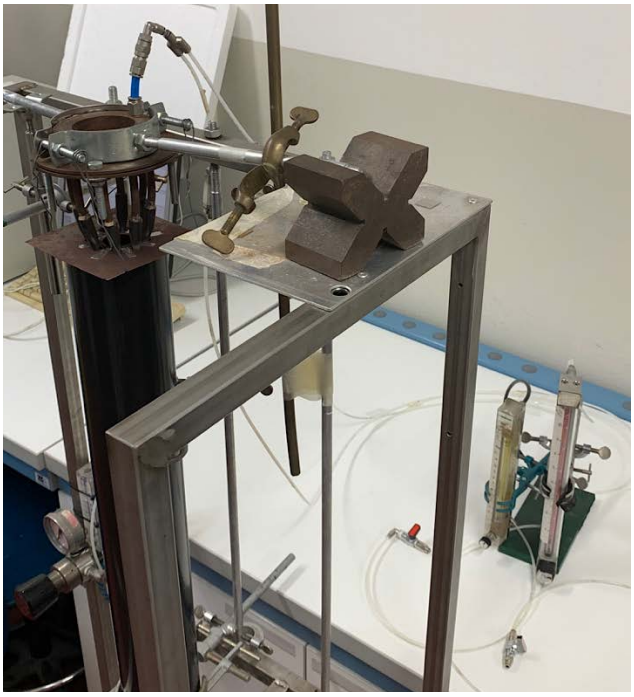

Figure 2.2: Feeding set-up of the gases

2.1.2 The atomiser

The atomiser, utilised to nebulise the solution, consisted in an airbrush (Fengda 134K) and it was mounted at the centre of the annular burner. The airbrush was connected to the air compressor to function properly and the pressure of the air flow could be regulated by a manometer installed on the rack that sustained the column. The solution was fed to the airbrush through a tube connected to it, as it is possible to observe in Figure 2.3. The solution was aspired from a beaker situated at a higher level with respect to the tip of the airbrush to let the solution flow by means of the venturi effect.

The solution was nebulised by the high velocity of the air flow from the compressor in the circular gap between the nozzle and the needle present inside the airbrush. The flowrate of solution and the width of the spray were strongly influenced by the position of the needle.

The airbrush had a trigger to modulate the air flow and consequently the liquid flow, but in this specific case it was blocked in the open position because the airbrush had to work continuously and operate as soon as the air from the compressor was fed.

The airbrush was equipped with three nozzles of increasing diameters and their related needles. The one utilised in this thesis project had a 0.3 mm diameter, to ensure a fine spray and to avoid the clogging of the tip by fouling.

The flowrate of liquid depends on the diameter of the nozzle, on the needle position and on the pressure of the dispersing air, while the spray angle seemed to be independent on all these variables and it is between 24° and 28° [3].

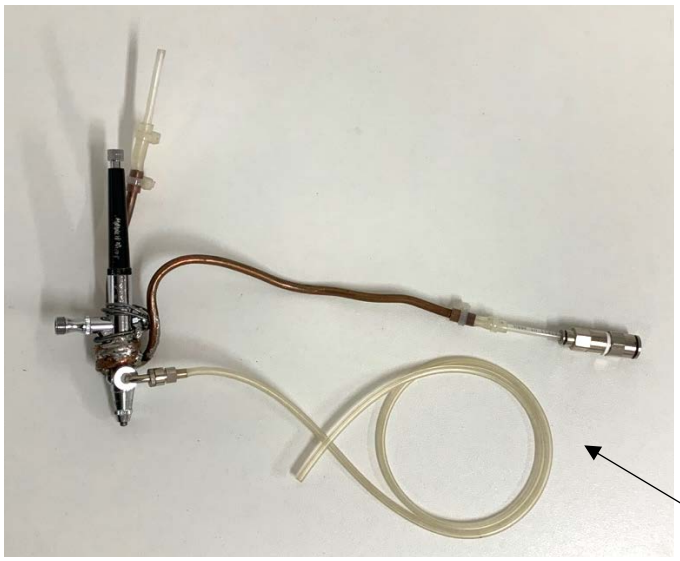

Figure 2.3: Atomiser

The spray gun was equipped with a cooling system (Figure 2.4) in order to prevent the occlusion of its tip by fouling. This problem could be caused by the precursors solution itself that could leave small solid particles on the tip of the spray gun as a consequence of the evaporation of the solution at high temperatures. To overcome this issue, a cooling circuit was developed. A copper tube was shaped to form a coil and it was wrapped around the tip of the atomiser and its body. The cooling circuit was split in two coils for practical reasons; in fact, the first part was permanently attached to the body of the air brush, while the second part, that had to cool down the tip of the atomiser, had to be removeable in order to be able to dismount the feeding apparatus from the burner structure and disassemble it to clean it. The two coils were connected at the top with a junction so that the cooling water exiting from one coil could enter the second one.

Figure 2.4: Cooling system of the atomiser

The atomiser had to be disassembled and thoroughly clean in the ultrasonic bath after each synthesis to prevent the clogging of the tip or the malfunctioning of some internal piece because of fouling.

2.1.3 The reaction column

The catalyst had to be synthesised in a closed space to avoid the dispersion of powder in the environment. Therefore, the flames were directed inside a column so that the synthesis could be confined.

The column was obtained by utilising a thin carbon steel tube which, as it is displayed in Figure 2.5, was mounted on a rack because it needed to be suspended on top of the filter pack.

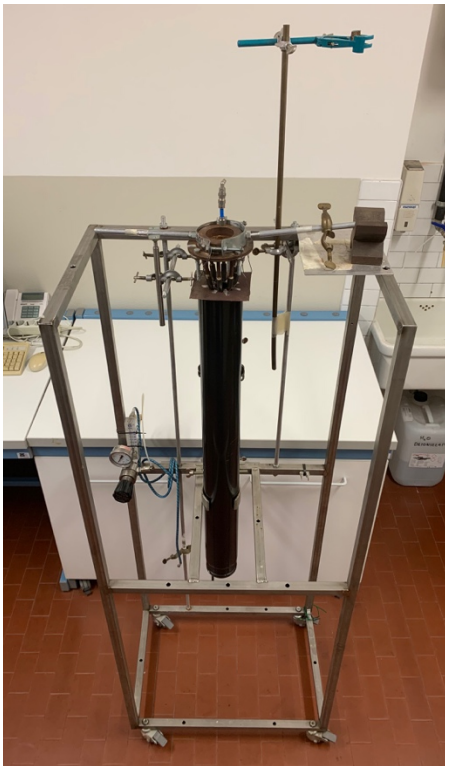

Figure 2.5: Reaction column mounted on the rack closed on top by the burner

The burner described in the previous paragraph was placed on top of the column and to partially close it. A plate was attached to the structure of the burner in order to stop the burner and nozzles from entering inside the column during the synthesis and being exposed to high temperatures. Holes were created on the plate so that the tip of the nozzles and of the atomiser could pass through.

A thin gap was left between the top of the column and the plate to let in a certain quantity of air to create a protection layer around the walls so that the synthesised particles would not stick to them. However, it was also important not to let in too much air in order not to cool down too much the environment inside the column. To help the fluid dynamics inside the column and be able to create this shield of air around the walls, a piece of tube with a smaller diameter than that of the column was attached underneath the burner's plate. With this addition to the plate, the air coming in from the top was directed straight down alongside the walls and not radially towards the centre of the column. Figure 2.6 shows all the details added to the structure of the burner.

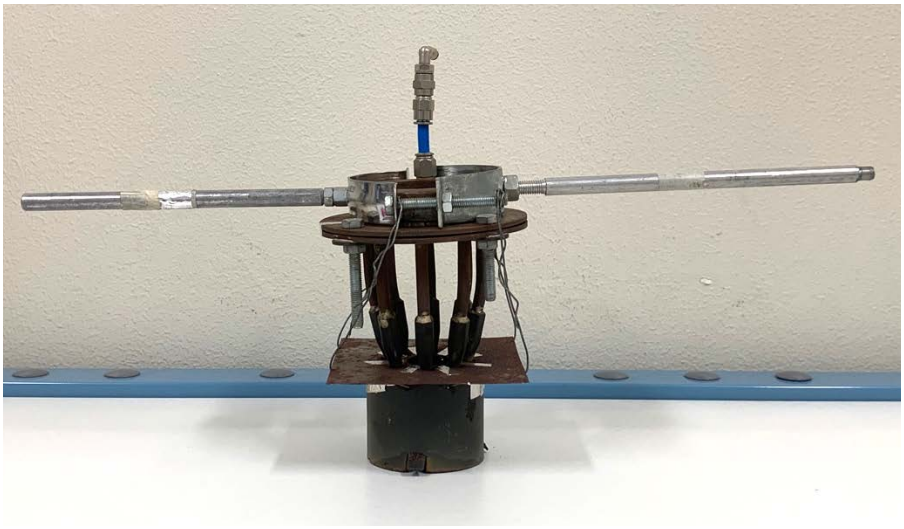

Figure 2.6: Burner with its additional structure

As it will be explained in the next paragraphs, the air that enters in the blower cannot have a temperature greater than 125 °C. Therefore, the set-up had an entrance of fresh air after the column, obtained by placing a cone shaped stainless steel junction on top of the filter pack. The depression created in the funnel junction by the blower attracted both the hot gases and powders from the column and the fresh air form the environment. The temperature of the flow of gases entering the filter pack and consequently the blower was influenced by the free section between the funnel and the column.

If the free section between the column and the filter pack decreased, the flowrate of fresh air decreased and the overall temperature of gases entering the blower increased, but at the same time, the flow of air entering from the aperture at the top, between burner and column increased.

On the bottom edge of the column, there were some holes utilised to position the metallic tube attached to the OPC which is a sensor that quantifies the number of particles dividing them in class sizes.

2.1.4 The filter pack

The filter pack (Figure 2.7) was located underneath the column. It consisted of six metallic flanges between which the five filters were positioned. The filters were metallic grids with various mesh spacings on which the powder deposited after they were invested by the flux of gases containing the catalyst. They were positioned in series, with the filters with wider meshes at the top and the ones with tighter meshes at the bottom. The mesh spacings employed were 494, 207, 114, 76 and 52 μm.

In previous thesis projects, it was observed that the first filter occluded in a short amount of time, therefore it was necessary to create a 2 cm hole in the centre, but then also the successive filters presented the same problem. Therefore, the final configuration provided an alternation between filters with one and two holes, while the last and finest filter presented no holes, to

collect the most part of the powders. This system created a sinuous path for the gases, whereas the powders had more inertia and a higher chance to collide against the filters and stopping there.
As it was explained in a previous paragraph, the first flange of the filter pack had a cone shaped stainless steel junction fixed on top of it, while the last one had a metallic tube attached to it to connect the filter pack to the blower by means of a flexible tube.
Two metal poles were attached to the body of the filter pack to suspend it above the ground so that the flexible tube, connecting it to the blower, could be secured to its bottom piece. Two clamp holders, fixed on the rack that sustained the column, were utilised to support the poles and consequently the filter pack.

Figure 2.7: Filter pack

2.1.4.1 Collection of the powder

After a certain amount of time, the synthesis had to be stopped because the last filter, the one with the finer mesh spacing, occluded. The majority of the catalyst that was produced could be scraped from the surface of the filters because a layer of powder deposited on them. These particles, removed directly from the filters, could be tested in the catalytic reactor without any further treatment.
After the scraping, some powder still remained embedded in the meshes of the filters; therefore, to recover those particles, it was necessary to place them in a beaker full of deionized water which was then put in the ultrasonic bath (Figure 2.8).

To be cleaned by means of ultrasonic cleaning, an object is immerged in a bath of distilled water, where a transducer produces high frequency sound waves. The compression waves create many microscopic cavitation bubbles, which immediately collapse resulting in a local increase of the temperature up to 5000 K and of the pressure up to 135 MPa. Moreover, when the bubbles close to the object surface collapse, a jet of liquid impacts with the surface, with the result of a deep cleaning of all its surfaces, even those inside the finest slits.

Figure 2.8: Ultrasonic bath

After the ultrasonic cleaning, the catalyst, that had been embedded into the meshes, was dispersed in the water which had to be evaporated in order to collect the dry powder. Therefore, the beaker was placed in a muffle at 180 °C and when the dried catalyst was recovered, this could too be tested.

2.1.5 The blower

The blower, utilised during this thesis project, is marked Mapro, CL 34/1 (Figure 2.9).
This apparatus was utilised to create the depression that conveyed the powders, produced in the hot zone at the top of the column, down at the bottom to the filter pack where they were collected.
The blower was controlled by an inverter from which it was possible to regulate the frequency. The inverter acted on the blower by modulating the engine frequency that is related to its rotational speed. Each rotational speed is associated to a specific flowrate of air aspired by the blower which would remain constant if the pressure drops along the system did not change during the synthesis. Instead, if the pressure drops increased, the flow of air aspired would decrease and therefore not the same amount of air would be conveyed from the coned shape junction with the risk of letting gases that were too hot in the blower.

It is important that the temperature of the gases entering the blower is not superior to 125 °C, as specified by the manufacturer, otherwise there is the risk of damaging the internal components of the blower or the rubber gaskets. This is the reason why it was important to have a consistent flow of air at ambient temperature entering from the aperture before the filter pack. The filter pack was connected to the blower with a flexible metallic tube. At the entrance of the blower, there was another metallic filter to ensure that the least amount of powder possible entered the body of the blower. The gas exiting from the blower was conveyed under hood with a flexible metallic tube not to disperse the nano powders which were not blocked by the various filters in the environment.

Figure 2.9: Blower

2.2 New experimental set-up

One of the aims of this thesis work was to improve the initial experimental set-up in order for it to become more reliable and to optimise the production of perovskites and their collection. While constructing a new experimental set-up, it is crucial to make it reliable; the equipment has to function properly and it has to perform consistently throughout the same synthesis and all syntheses conducted at different times.

Figure 2.10 is the schematic representation of the experimental set-up after its optimisation; while in the next paragraphs, the improvements executed on the experimental set-up are listed.

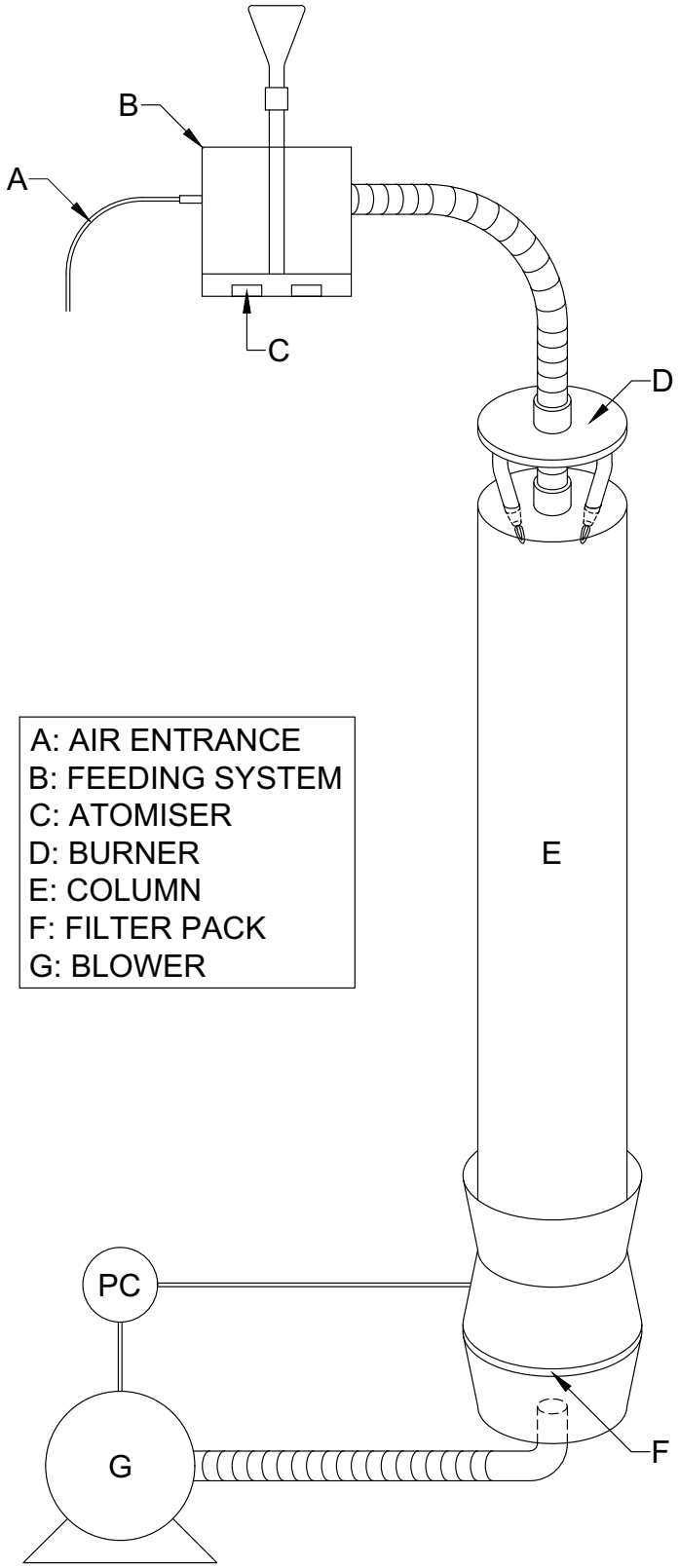

Figure 2.10: Schematic representation of the optimised experimental set-up

2.2.1 Pressure control

In order to improve the existing flame synthesis set-up and to obtain a better control on the quantity of air that was sucked in by the blower, a pressure control was programmed on the inverter that regulated the blower.

It was crucial to have a constant amount of air sucked in by the blower from the coned shape junction to assure the cooling of the flow of gases going inside the blower at the proper temperature, which must be less than 125 °C. Moreover, a proper amount of air sucked in by the blower prevented the powder that was produced to be dispersed in the room. This is why it was important for the blower to aspire a consistent amount of air and to keep it constant even after the clogging of the filter pack.

The inverter, connected to the blower, had the option to set up a pressure control, therefore it was only necessary to program it with the right parameters and be able to feed a voltage signal to it so that it could be used as the setpoint. This signal was obtained from a pressure transducer connected to the inverter which detected a difference in pressure between two points and converted it in an electric analogical signal.

To obtain the desired difference in pressure for the inverter setpoint, a restriction was created before the entrance of the filter pack by partially obstructing the tube between the coned shape junction and the first filter as it can be observed in Figure 2.11.

Figure 2.11: Restriction before the filter pack for the pressure control

When air was aspired by the blower, the restriction created a pressure drop whose value would be utilised for the setpoint for the inverter. A pressure tapping point was arranged downstream the restriction to detect the pressure in that specific point in order to feed it to the pressure transducer.

The pressure transducer utilised in the set-up is shown in Figure 2.12 where it is possible to observe the two tubes that measured the difference in pressure. The right tube was connected to the pressure tapping point so that the sensor was able to detect the pressure in that point and calculate the difference with the atmospheric one measured by the tube on the left.

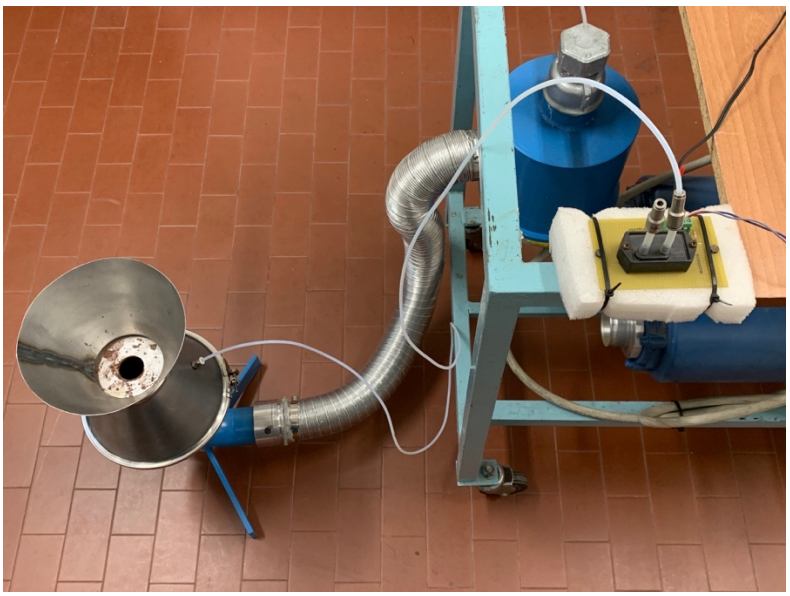

Figure 2.12: Pressure transducer connected to the filter pack

The difference in pressure, detected by the transducer while the blower was working, was converted in an electric signal which was transferred to the inverter that utilised it as a setpoint for the pressure control.

In order to keep the pressure drop constant, the blower had to aspire always the same flow of air; therefore the inverter had to increase the frequency at which the blower engine was working in order to counteract the clogging of the filters to maintain the same flowrate of air aspired and the same pressure drop as a consequence. The whole aspiration system is portrayed in Figure 2.13.

With the introduction of the pressure control, it was possible to have a constant flowrate of air aspired and therefore a more reliable system.

Figure 2.13: Aspiration system

2.2.2 Quartz tube set-up

During the first few syntheses, many discrepancies were encountered regarding the quantity of nano powders that was collected from the filters at the end of every synthesis. Certain times this quantity was substantial in comparison to the theoretic value that had to be collected and other times the deposited amount was too low to even be tested. The problem of the inconsistent collection of particles was not given by their variable production rate, but rather to a possible deviation of the solution spray that led to the particle depositing on the walls of the tube.

At first, it was thought that this problem could be related to the direction at which the atomiser was aiming when mounted on the set-up and that if it was not pointing exactly straight down, it could spray the solution on the wall instead of down and that would compromise the collection of the powders on the filter because these would stop on the wall of the tube instead of travelling downwards.

Then, it was thought that the problem could be related to the obstruction of the tip of the atomiser caused by the formation of solid residue of the solution at high temperatures during the synthesis. In fact, during one of the synthesis which had a very low powder collection from the filters, the OPC mounted at the bottom of the column at first registered the passage of particles, but after a few minutes it could not detect any particles.

Another indication of a possible obstruction of the tip of the atomiser during the synthesis was the decrement of the solution flowrate sucked in by the tube connected to the atomiser. In fact, the velocity at which the solution would be sucked in by the atomiser to be sprayed would decrease enormously during the synthesis. Because all the other parameters were fixed, the only aspect that could be changing was the tip opening. The probable obstruction of the tip of the

atomiser could lead to a subsequent deviation of the spray of solution directing it towards the walls and not downwards anymore.

Therefore, in order to understand how the fluid dynamics inside the column worked, the metallic tube was substituted with a quartz one in order to be able to see inside the tube during the synthesis and therefore have a better understanding of how the direction of the solution spray was influenced by the external factors.

The quartz tube was smaller than the metallic one, therefore some modifications had to be made to the burner structure for it to be able to fit in the new column. The nozzles' plate was reconstructed; the narrower tube attached to it had to be removed because it did not fit in the quartz column and it was substituted with a coned shape piece to guide the positioning of the burner after the ignition of the flames. With this new configuration, the gap between the column and the nozzles' plate was not present anymore. In Figure 2.14 it is possible to observe the modifications that were carried out on the burner structure, while in Figure 2.15 the quartz tube set-up is represented.

Figure 2.14: New burner structure realised to adapt it to the quartz tube

Figure 2.15: Quartz tube set-up

At first, a test in “cold conditions” was conducted in order to analyse the direction of the spray without flames. For this type of test, the atomiser was fed with distillated water and the nozzles with just air instead of the flammable mixture of hydrogen and oxygen. The quantity of air fed was comparable to the one used during the syntheses. In order to have the closest conditions to the ones experienced inside the tube during a real synthesis, also the blower was switched on.
As soon as the spray started, it was possible to notice that it was deviated towards one side of the tube and that the water droplets were wetting the surface and that they were not able to travel straight down as they were supposed to do. Through the transparent tube, it was possible to check that the tip of the atomizer was pointing correctly downwards. Therefore, the conclusion that was acquired from this cold experiment was that the direction of the spray could be influenced also by the position of the needle inside the atomiser.
After the cold experiment, a real synthesis was conducted with the quartz tube set-up. The flame synthesis of perovskite using the quartz set-up was a very delicate operation because the tube was much narrower than the metal one and therefore there was a higher chance of the flames touching the walls of the column.
As soon as the synthesis started, it was possible to notice that some powder was depositing on the surface instead of travelling down to the filter pack. The particles deposited only on one side of the tube near the atomiser as it is possible to observe from Figure 2.16. Because of the

transparency of the quartz, it was possible to check the position of the tip of the atomiser, which was pointing straight down. Therefore, it was possible to conclude that the deviation of the particle spray was most likely given by the bad positioning of the needle inside the atomiser.

Figure 2.16: Catalyst depositing unevenly on the walls of the quartz tube

However, even if some particles deposited on the tube, a good quantity of perovskites was recovered from the filter pack after the synthesis with this set-up.
The synthesis conducted with the quartz tube led to the collection of a satisfying amount of powder; but the spray gun was nevertheless depicted as unreliable because of the many factors related to it that could jeopardise the outcome of a synthesis.
Therefore, a new feeding system was assembled and utilised in the experimental set-up to substitute the spray gun.

2.2.3 Ultrasonic membrane atomiser

The quantity of nanoparticles recovered with the old set-up was very dependent on uncontrollable circumstances, such as the possible obstruction of the tip of the spray gun and other factors, such as the position of the needle inside the spray gun which gave the direction to the solution spray. If a substantial quantity of solution was sprayed against the walls of the tube, not enough perovskites would be recovered from the filter pack.
All these aspects caused the system to become unreliable and therefore it was decided to implement a new system to feed the solution into the flame cone in order to synthesise the perovskites.

The new feeding system was composed by an atomiser (Figure 2.17) that utilised an ultrasonic membrane to nebulise the solution.

Figure 2.17: Ultrasonic membrane atomiser

The atomiser was placed in a closed container with two openings (Figure 2.18); one was necessary to let in a flow of air that had to transport the mist out of the other aperture through the flexible tube that connected the container to the opening above the flame cone. The air to move the mist came from a compressor and its flow rate was regulated by a tap put on the line, while to visualise its value a digital flowmeter was used. The flow of air was of about 8 l/min, equal to the one fed to the spray gun in the old set-up.

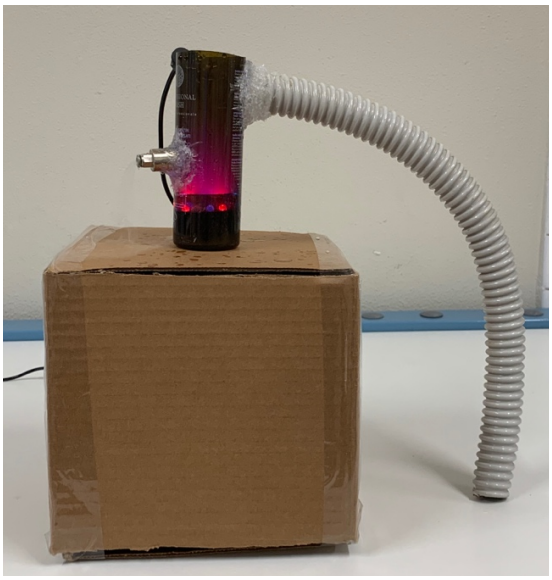

Figure 2.18: New feeding system with one atomiser

In addition to the mist, the atomiser produced some squirts in correspondence of the membrane; therefore, a piece of plastic was put above the atomiser in order to block all drops of water from going into the tube that transported the mist.

The flowrate of liquid nebulised by the atomiser is dependent on the height of liquid above it: the shorter the column of liquid, the quicker the nebulisation. Therefore, it was important to keep a constant and low level on top of the atomiser to maximise the nebulisation. To accomplish this without constantly adding solution manually, a system to keep the desired level constant was implemented. A flask was positioned upside down, closed on top and connected to a plastic tube so that the liquid inside could go down. The height, at which the end of the tube connected to the flask was positioned above the atomiser, gave the setpoint for the level. In fact, when the liquid level in the container went down and the end of the tube was not submerged anymore, the air that entered in the tube allowed some liquid in the flask to go down and therefore the level above the atomiser returned to the setpoint.

Before testing the new feeding system in a real synthesis, a test in cold conditions was conducted nebulising water and feeding air to the burners, instead of H_2 and O_2, in order to maintain the same fluid dynamics inside the tube as of when the flames were lit. The flowrate of air, fed inside the container to transport the mist, was kept equal to the one fed to the spray gun which was 8 l/min.

At first, the set-up was tested in the quartz tube. It was possible to observe the formation of condensation in some points of the tube where the mist was depositing. Because the tube carrying the mist was directed straight down and therefore also the flow of mist was going downwards, it was thought that the mist was depositing on the wall because the tube was too narrow.

Therefore, the quartz tube was discarded and the reacting column was switched back to the metal one and in order to examine the direction of the mist and where it would deposit, the inside of the tube was covered with aluminum foil and coloured water was nebulised. With the wider tube, coloured water did not deposit on the tin foil and therefore it was decided to perform a real synthesis to examine if more or less nanoparticles would be recovered from the filter pack and if some of them would still deposit on the walls of the tube.

The metallic tube was covered with aluminum foil in order to quantify the amount of powders that would deposit on the tube walls. The quantity of catalyst recovered from the aluminum was negligible, which meant that the particles did not deposit on the walls.

Therefore, the new feeding system was considered satisfactory and some improvements were made on it. In fact, while working with just one atomiser, a synthesis lasted almost an hour. This implied a very high consumption of hydrogen and oxygen which resulted in high costs of production of the catalyst.

This happened because one atomiser was capable of nebulising almost 1.4 ml of liquid per minute. Therefore, in order to be able to nebulise the same flowrate per minute as the spray gun, four atomisers should have work at the same time. This is why a new apparatus was constructed to host four atomisers working simultaneously.

A picture and a schematic representation of the new feeding set-up are respectively reported in Figure 2.19 and Figure 2.20.

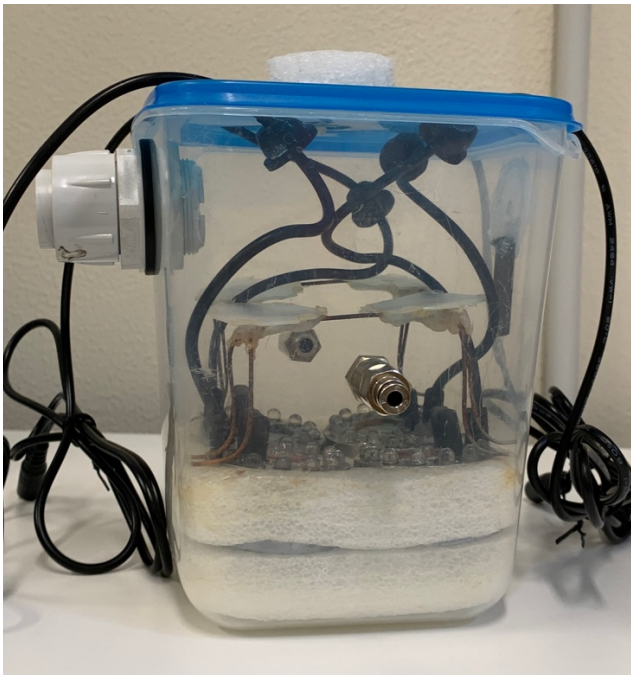

Figure 2.19: New feeding system with four atomisers

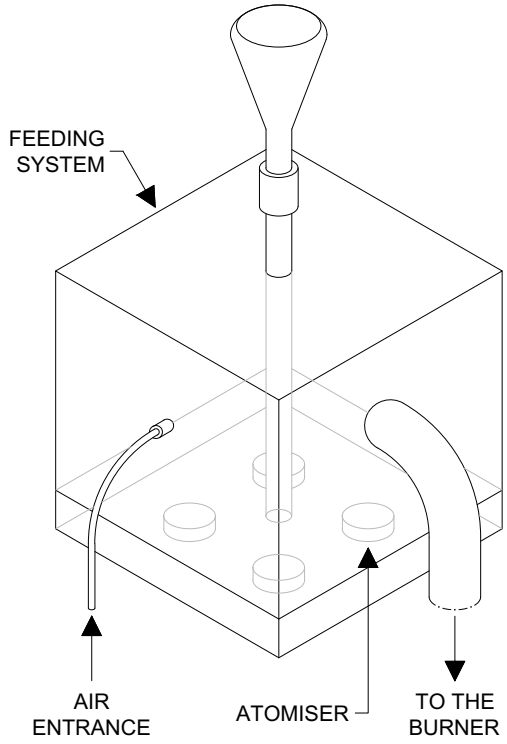

Figure 2.20: Schematic representation of the new feeding set-up

The improved feeding system was built with a larger box. In order to avoid the stagnation of the mist in the corners of the container, the air, necessary to transport the mist, entered from two points on opposite sides of the box, while the mist still exited from just one opening. A tube, connected to the container, transported the mist at the centre of the nozzles so that it could pass through the cone of flames.
The four atomisers needed a certain level of liquid above them to function. Therefore, not to waste much solution to fill the container at an appropriate level, a housing for the four atomisers was constructed in order to occupy all the empty space underneath and around the atomisers.
As it happened with the previous set-up, the atomisers produced some squirts of solution together with the mist. To avoid the drops reaching the tube that transported the mist, a structure to block them was placed on top of the atomisers.
The system to keep the level constant was utilised also in this scale-up version because it proved to be very effective in the previous set-up.
As it is possible to observe from Figure 2.21, the container was placed on a shelf mounted at the top of the rack that sustained the column.

Figure 2.21: System to keep the level constant

2.2.4 New collection system

The particle size of the powder synthesised with the new feeding system was much smaller than the one of the powder produced with the old one. As it is possible to observe from the image taken at the ESEM (Figure 2.22), the catalyst obtained with the new system had a particle size ranging from the nanometers to a few microns.

This could be considered as one of the many advantages of nebulising the precursor solution via atomisers that utilise an ultrasonic membrane rather than employing a spray gun, because obtaining a powder with a smaller particle size implicates having a catalyst with a greater specific surface area and therefore a greater catalytic activity.

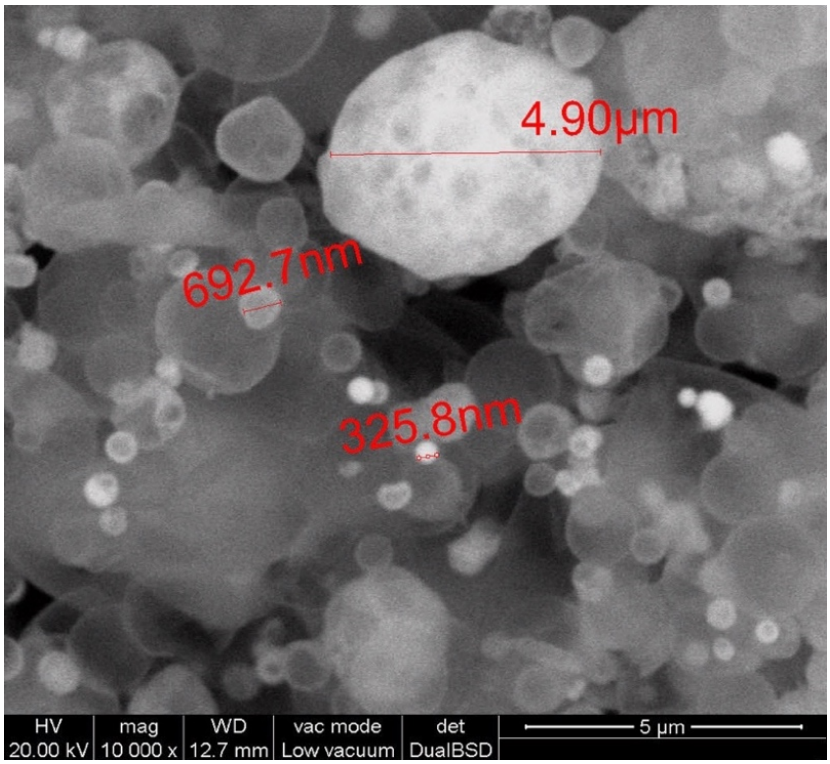

Figure 2.22: ESEM image of $LaFeO_3$

The old filtration unit was not able to collect the powder because the spacing of the meshes utilised was not tight enough.

Therefore, instead of utilising a sequence of five meshes with a decreasing grade of aperture, only the filter with the smallest aperture available (52 µm) was utilised. Three layers were put in place so that there was a higher chance of recovering the powder. It still was not the ideal collecting system because many particles could pass through those grids, but the collection percentage of catalyst improved from the older set-up.

To recover a higher percentage of powder produced, filters with thinner mesh aperture were required. It was decided to work with filters composed of various layers of stainless steel meshes that provided an aperture of 5 µm. This type of filter is displayed in Figure 2.23.

The finer the mesh of the filters, the more particles they stop, but also the higher the pressure drop they create if the gas velocity remains the same. Therefore, it was necessary to construct a new housing for the filters to increase the collecting surface in order to lower the pressure drop. In fact, while the meshes had to have a diameter of 9 cm to fit in the old compartment, the diameter of the new one widened up to 17 cm to host filters with a larger surface area.

Figure 2.23: Filter utilised in the new experimental set-up

The new compartment, shown in Figure 2.24, was composed of an inlet cone to collect a great flux of air so that the powder coming down from the tube was not dispersed in the surrounding environment, but it was channeled into the filter pack. Then, the main body of the housing was built with two other cones so that the section could widen up to the required diameter and then tighten up again to the diameter of the tube that connected the filter pack to the blower. Two filters were fixed in between the two bigger cones.

Figure 2.24: New filter pack

To recover the particles from the filters, they had to be put in a container, with distillated water, which was then placed in the ultrasonic bath. Then, the beaker with the catalyst dispersed in water was placed in the muffle at 180 °C to evaporate all the liquid and obtain dry powder.
This solution, for the recovery of the catalyst, was the most successful because it allowed to recover more than the 90% of the powder produced. The small percentage of powder which was not recovered was deposited of the walls of the tube or the walls of the cones.

2.3 Precursor liquid solution

The liquid solution, which was nebulised into the flame in order to produce the solid nanoparticles with the perovskite structure, was prepared with the same procedure of the solution utilised for the citrate sol-gel method by the IMPACT Group at the Department of Chemistry at the University of Padova.
The metallic precursors, needed for the preparation of $LaFeO_3$, were lanthanum oxide (La_2O_3) and metallic iron (Fe). Nitric acid helped the dissolution of the precursors in the solution and it influenced the successive combustion of the solution, since it participated in the formation of ammonium nitrate, which is explosive. The IMPACT group demonstrated that the correct quantity of nitric acid to be added to the solution to provide a complete combustion had to be more than 4.5 ml per gram of perovskites to be synthesised. In fact, the solution produced for the flame synthesis contained 5.6 ml/g.
Moreover, another essential component of the liquid solution was citric acid, that ensured the complete complexation of the metallic ions and avoided the precipitation of solids. The quantity of citric acid to be added to the solution was related to the quantity of metallic ions. Therefore,

the molar ratio between citric acid and the metallic precursors ions had to be greater than 1 for the reasons reported above, but it also had to be smaller than 2 to avoid crystallisation and the precipitation of the excess of acid. In this case the ratio had a value of 1.9.
Then, the last two components of the solution were ammonia (with a concentration of 30%) to neutralize the pH of the final solution and deionized water to help the dissolution of the solids. To be able to synthesised 5 g of $LaFeO_3$, each precursor and the acid were weighed in the quantities shown in Table 2.1 and placed in a dedicated beaker.

Table 2.1: Quantity of precursors for the preparation of the solution

Compound	Mass [g]
La_2O_3	3.36
Fe	1.15
Citric acid	16.45

In each beaker, the distilled water was added in a quantity sufficient to completely submerge the precursor. Then, the nitric acid was poured in each beaker with a graduated pipette: 16 ml in the La_2O_3 and 12 ml in iron. The lanthanum and iron were difficult to dissolve, and for this reason their beakers were placed on a heating plate. The temperature required for the iron dissolution was 100°C, to be maintained for approximately 20 minutes, while the lanthanum oxide dissolution was carried out with the mixing provided by a magnetic stirrer. In the meantime, the citric acid was weighed in a beaker, where successively the other solutions were poured. Finally, the beaker, containing the citric acid and all the metallic precursor dissolved, was placed on a heating plate at the temperature of 80°C with a magnetic stirrer; ammonia was slowly added until the pH, measured by means of litmus paper, reached the value of 7-8. The final product is displayed in Figure 2.25.

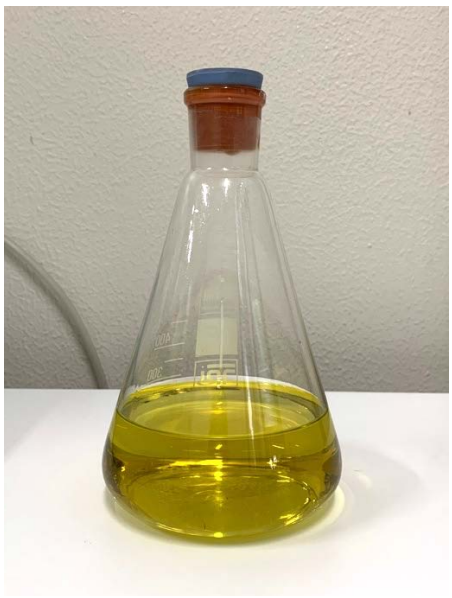

Figure 2.25: Solution to be synthesised to produce $LaFeO_3$

In order to have a 100% carbon free synthesis, a precursor solution without the addition of citric acid was produced to understand if this component was necessary to successfully synthesised metal oxides with perovskites structure able to catalyse a specific reaction. To produce this type of solution, all the steps reported above were followed except for the addition of citric acid.
As it is possible to observe in Figure 2.26, the solution obtained had a brick red colour instead of the yellow colour of the solution with citric acid. Moreover, in the solution without citric acid, the solid started to precipitate if not constantly mixed. With the new feeding system, it was possible to utilise this solution even if the solid deposited at the bottom of the container because the atomisers with the ultrasonic membrane, while working, generated a spray that kept the layer of liquid mixed when falling back down.

Figure 2.26: Segregation of the $LaFeO_3$ solution made without citric acid

Chapter 3

Materials and methods

In the previous chapter, the experimental set-up utilised for the flame synthesis of $LaFeO_3$ was described. In this chapter, the descriptions of all the apparatuses utilised for the catalytic testing of the perovskites and of all the instruments necessary for the analysis of the gas mixture are reported. Moreover, the methods for the characterisation of the solid nanoparticles are also described.

3.1 Set-up for the catalytic analysis

The $LaFeO_3$ synthesised was tested to determine if it was effective in the catalysis of a model reaction. The reactor utilised to test the catalytic properties of the powder, and all the instruments associated to its functioning, will be described in the next paragraphs.

3.1.1 Vibratory sieve shaker

The vibratory sieve shaker is an apparatus utilised to sift the $LaFeO_3$ powder synthesised in order to divide the particles in the appropriate size classes.

The vibratory sieve shaker is composed of multiple sieve trays, stacked one on top of the other. The trays with the larger meshes are positioned at the top of the pile, while the ones with finer meshes are arranged at the bottom. The separation in different size classes is obtained through the vibration of the plate present at the bottom of the pile. It is possible to regulate the oscillation frequency and the working time. Based on the type of particles that require separating, it is possible to choose the mesh spacing of the trays and also the number of trays needed. In Figure 3.1, it is possible to observe the structure of a vibratory sieve shaker.

The particles were cohesive and they formed clusters kept together by weak forces such as the electrostatic force and the Van der Waals force. These clusters had a lower specific surface area with respect to the single particles and for this reason it was preferable not to utilise them during the catalytic tests. Therefore, the $LaFeO_3$ synthesised was always sieved to separate the bigger clusters from the single particles. In order to do this, the 200 μm tray was utilised and only the single particles or smaller clusters that passed through the sieve were catalytically tested.

Figure 3.1: Vibratory sieve shaker

3.1.2 Gas distribution system

The gases are stored in cylinders externally to the laboratory, where the pressure is up to 200 bar. Each cylinder is provided with a pressure reducer that decreases the pressure to 8 bar, before the gas line enters the laboratory. There, other pressure reducers are used to provide the distribution pressure of 5 bar for each gas. Successively each gas is sent to a distributor, which is equipped with up to 8 taps that allow more people to use that gas simultaneously.

A gas mixture with a specific composition had to be fed to the reactor during the catalytic tests; therefore, the flowrates of each component of the mixture had to be regulated to assure their value was the required one. The flowrates were controlled by Brooks and Bronkhorst mass flowmeters, whose functioning is based on the calorimetric principle. When the flow crosses the electrical resistance, it heats up bringing its temperature to a known value. The flowrate is proportional to the temperature variation of the fluid between two probes.

The flowmeters had to be calibrated before being employed and this operation was executed by utilising a single reference gas (N_2). Afterwards, the setpoints, to ensure the desired flowrates for the different gases, were obtained by means of corrective factors, related to each gas.

In the laboratory, there are twelve electronic flowmeters and the ones employed for these catalytic tests were chosen based on their flow range. In fact, different flowmeters could modulate different flow ranges varying from 0-10 ml/min to 0-2000 ml/min.

The setpoint linked to each flowrate was calculated by an Excel sheet based on the type of gas and the flowmeter employed. These setpoints were inserted in a software that communicated directly with the flowmeter.

The composition of the gas mixture fed to the reactor had to be extremely precise; therefore, the setpoints, given by the Excel sheet, were checked manually by means of a bubble flowmeter before starting the tests to assure that they were associated to the correct flowrate.

3.1.3 Catalytic reactor

The catalytic tests were carried out in a tubular reactor which consisted of a quartz tube inserted into a programmable temperature furnace that heated up through an electrical resistance.
The flowrate and composition of the reacting gas mixture, introduced into the reactor, were regulated by the flowmeters described above; while the composition of the gas mixture exiting the reactor was analysed by means of a gas chromatograph (GC 7820) and a Fourier transform infrared spectrometer (FT-IR), which will be described later. The complete configuration of the setup is displayed in Figure 3.2.

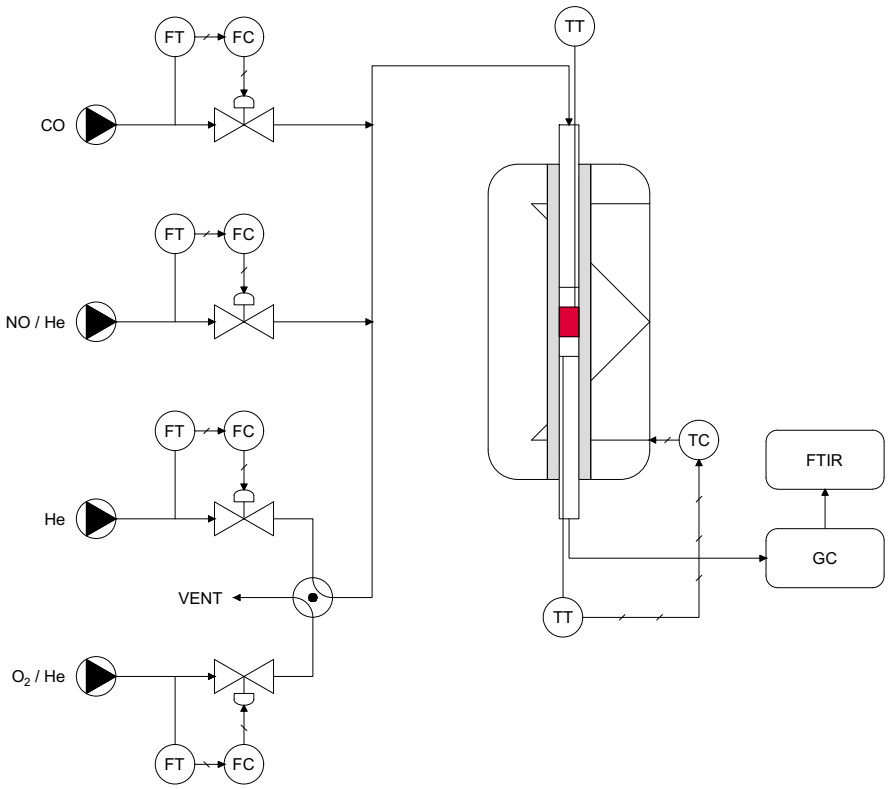

Figure 3.2: Schematic representation of the set-up configuration for the catalytic tests

The $LaFeO_3$, which catalysed the reaction between the components of the reacting gas mixture, was contained in the quartz tube, that had an internal diameter of 8 mm. Quartz glass was chosen as the material for the reactor because it is characterised by an excellent chemical inertia, a high melting temperature (1400 °C) and the ability to tolerate high temperature changes over time.

The catalytic powder, in the form of a fixed bed, was positioned in the middle of the quartz tube and it was kept in place by two layers of quartz wool, placed above and below it as it can be observed in Figure 3.3.

Figure 3.3: Catalytic bed held in place by quartz wool

Two thermocouples were inserted in the quartz reactor; the one to monitor the temperature inside the reactor was mounted at the top, while the one inserted at the bottom was part of the temperature control loop.

The two extremities of the quartz tube were closed with two junctions which consisted of a steel cube welded with a steel thread cylinder. The cube was perforated and the three holes were joined in a T shaped cavity: the opening orthogonal to the tube was utilised for letting the gas in the tube, the other ones were aligned to the cylinder and allowed the passage of the thermocouple. On the face opposite to the gas hole, the cube presented a small thread that allowed the attachment of the device to the support by utilising a screw. The quartz tube was inserted inside the steel cylinder and was joined with a hex nut. Between the nut and the thread, a Teflon O-ring was inserted to guarantee the mechanical seal.

It could have been necessary to change the level at which the two thermocouples were inserted inside the quartz tube based on the position of the catalytic bed inside the rector, the height of the bed or the length of the tube. This could have been done by varying the portion of the thermocouple that went inside the tube by loosening the hex nut that kept the thermocouple at a fixed level and adjusting it as desired.

In order for the quartz tube to be positioned at the right height, so that the catalytic bed could be at the centre of the furnace not to be subjected to thermal fluctuations, its top closing part was screwed to a support. This support had various holes that could be used to regulate the position of the tube inside the furnace at different heights depending on the situation.

Furthermore, with the purpose of minimising the thermal disturbances and avoiding heating loss, some compact quartz wool was placed at the top and bottom extremities in the empty space left between the quartz reactor and the furnace walls.

The catalytic reactor is displayed in Figure 3.4.

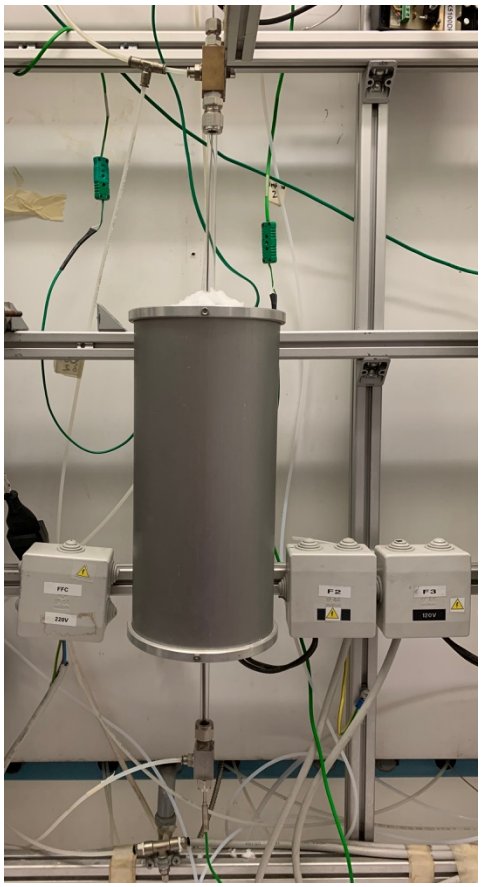

Figure 3.4: Catalytic reactor

3.1.4 Temperature control

In order to control and monitor the temperature inside the reactor, two thermocouples were positioned in the quartz tube. The first one was placed below the catalytic bed and it was utilised for the reactor thermal control, while the second one was located above the catalytic bed in order to measure a temperature as close as possible to that of the powder so to monitor it. The tips of the two temperature transducers were placed as close as possible to the catalytic bed, touching the layer of quartz wool in order to obtain the more truthful reading possible of the temperature of the catalytic bed.

The furnace was heated with an electrical resistance and the power was controlled by an Omron controller. The related software, CX-Thermo, allowed the implementation of the desired temperature policies via computer, while the monitored temperature, at the catalyst inlet, was read by a Measurement Computing data acquisition device via a Matlab code.

The thermocouple, inserted at the bottom of the quartz tube, together with the software that regulated the electric resistance responsible for the heating of the reactor formed the temperature closed loop control. The thermocouple, acting as the temperature transmitter,

communicated directly with the software CX-Thermo which, based on the temperature signals received and the setpoint inserted in the program, gave a specific input to the electric resistance of the furnace.

In the course of every catalytic test, two temperature cycles were performed; during each temperature cycle, the reactor was heated up to 600 °C and it was kept in isotherm for two hours when the maximum temperature was reached. After the isotherm, the reactor was cooled down to 90 °C and this temperature was kept for 30 minutes before the second cycle began. The heating and cooling rate were equal to 2 °C/min.

During each test, two temperature cycles were performed so that the composition of the gas reacting mixture could be varied between the two cycles.

It is possible to observe the temperature protocol adopted during the catalytic tests in Figure 3.5.

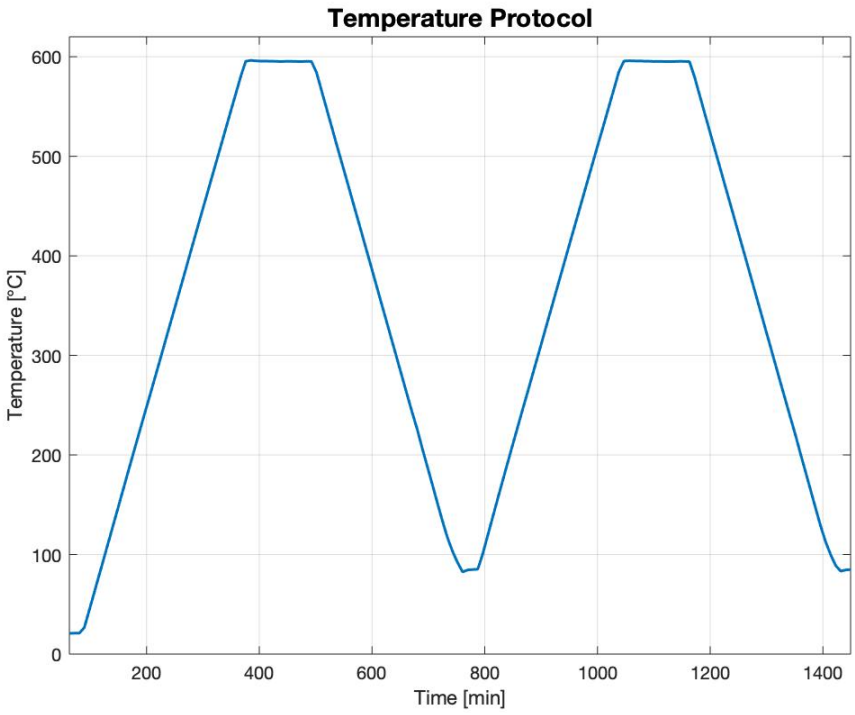

Figure 3.5: Temperature protocol

3.1.5 4-way Valve

The catalytic tests conducted were dynamic ones, which means that the composition of the reacting gas mixture changed during the test and, to be able to accomplish that from remote overnight, a 4-way valve was utilised.

This type of valve has two inlets and two outlets and therefore it is possible to switch just one particular component of the mixture with another one that needs to be added while the test is already running or to entirely change the composition of the mixture that is being fed to the reactor. The outlet that was connected to the reactor was the number 2, while the outlet 4 released the gas into the hood. When the valve was in the OFF position, inlet 1 was connected

to the outlet 2, which went to the reactor. Instead, in the ON position, inlet 3 was connected to outlet 2. Based on which gas had to go into the reactor, the position of the valve was switched. In order to switch its position, the valve utilised pulses of air coming from a compressor which were regulated by a computer program.
Figure 3.6 is the schematic representation of the two possible positions that the 4-way valve can assume. On the left, the valve is in the OFF position, while on the right it is in the ON position.

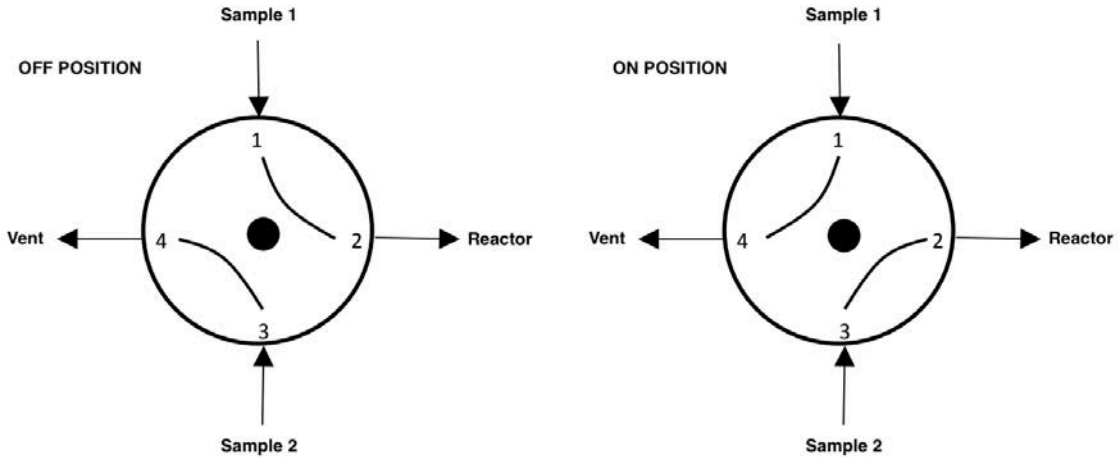

Figure 3.6: Schematic representation of the 4-way valve OFF and ON position

3.2 Analytical instruments

In this paragraph, the instruments utilised for the analysis of the gas mixture composition exiting from the catalytic reactor are described. Two different instruments were employed so that the results from one instrument could verify the accuracy of the outcome of the other machinery. Moreover, it was necessary to utilise both the FT-IR and the gas chromatograph because some components of the gas mixture, such as N_2 and O_2, could not be detected by the FT-IR, while the gas chromatograph had difficulties in identifying others.

3.2.1 FT-IR IRTracer 100 Shimadzu

FT-IR stands for Fourier transform infrared and it is the preferred method of infrared spectroscopy which is an analytical technique based on the interaction of electromagnetic radiation with matter. When a molecule is hit by an infrared radiation, the energy is converted into vibrational one. The molecules absorb only the frequencies that are characteristic of their structure. Therefore, the frequency of the vibrations is associated with a particular normal mode of motion and a particular bond type. The intensity at a given wavelength depends on the value

of the dipolar moment of the bond and therefore on the relative electronegativity of the atoms involved in the bond.
The FT-IR spectrometer, with which the analyses of the gas mixture exiting from the reactor were conducted, is an IRTracer-100 Shimadzu (Figure 3.7).

Figure 3.7: IRTracer-100 Shimadzu

This type of FT-IR spectrometer has a Michelson type interferometer and the gas mixture is conveyed to a sample cell (Figure 3.8), crossed by the infrared radiation, that is equipped with infrared-transparent windows, made in KBr, at both ends of the tube. At the end of the IR source, there is a detector that analyses which frequencies have been absorbed by the mixture components over time. The IR analysis is almost continuous and therefore allows precise indications on the characteristics of the mixture.

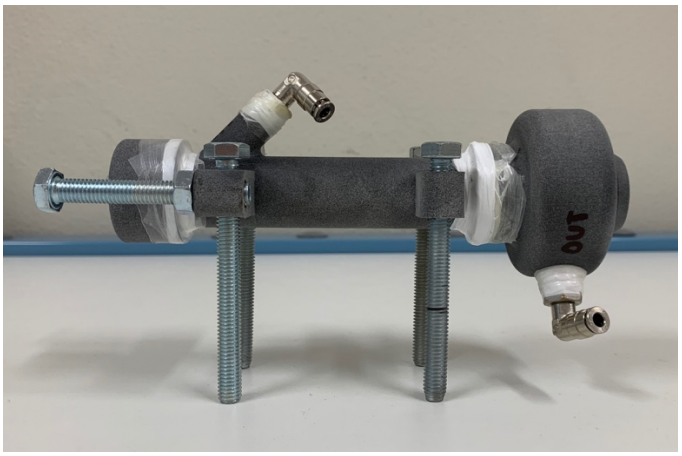

Figure 3.8: FT-IR sample cell

A FT-IR spectrometer produces an infrared spectrum that can be visualised in a plot of absorbance intensity as a function of wave number (cm^{-1}), usually in the interval between 4000 and 400 cm^{-1}. The infrared spectroscopy is often used to identify the structures (qualitative analysis) because functional groups give rise to characteristic peaks both in terms of intensity

and position. It is possible to identify the structure of the molecule analysed thanks to the reproducibility of these peaks and the characteristic values of absorption intensity.
However, in this thesis project, the FT-IR spectrometer was employed to perform a quantitative analysis of specific known species in the product mixture. In fact, apart from identifying unknown components of a mixture, it is also possible to assign a corresponding concentration to a particular component by monitoring the intensity value of peaks properly identified within the spectrum.
The FT-IR was utilised to detect the concentration of the reactants, CO and NO, and of some of the products CO_2, N_2O and NO_2. By means of infrared spectroscopy, it was not possible to identify the concentration in the mixture of some components, such as O_2 and N_2, because symmetrical diatomic molecules do not absorb infrared radiation.
A characteristic wave number was associated to each component of the gas mixture exiting the reactor. The instrument was programmed to register the absorbance values referred to each characteristic wave number over time. The program that communicated with the FT-IR did not register only the characteristic wave numbers, but also the intervals around it. The characteristic wave numbers and intervals monitored with this instrument are reported in Table 3.1.

Table 3.1: Range and characteristic wave number of each monitored species

Species	Characteristic wave number [cm^{-1}]	Wave number interval [cm^{-1}]
CO	2073.3	2072.31 / 2074.27
NO	1900.2	1898.76 / 1901.66
CO_2	2334.16	2333.19 / 2335.12
N_2O	1298.95	1285 / 1319
NO_2	1630.2	1629.71 / 1631.16

The volumetric concentrations of the components are proportional to the absorbance values registered by the FT-IR program. The concentrations were calculated with calibration lines obtained by analysing gas mixtures with known compositions.

3.2.2 Gas chromatograph GC-7820

The principle of gas chromatography consists in the chemical-physical separation of a gaseous mixture, based on the adsorption equilibrium of distinct species partitioning between a mobile and stationary phase. In gas chromatography, the mobile phase is a carrier gas which could be an inert gas such as helium or an unreactive gas such as nitrogen; while the stationary phase is a polymer on an inert solid support, inside a piece of glass or metal tubing called a column. The gaseous compounds interact with the walls of the column coated with the stationary phase. This causes each compound to elute at a different time, known as the retention time of the compound. The comparison of retention times is what gives gas chromatography its analytical

usefulness. Some parameters that could be used to alter the order or the retention time of the gases are the carrier gas flow rate, the column length, the temperature or the pressure.
The instrument used to perform gas chromatography is called a gas chromatograph. The one employed for these analyses is an Agilent GC-7820 (Figure 3.9) where the gas sample is injected through a six-way valve and two columns are equipped for the separations of all the various components.

Figure 3.9: Agilent GC-7820

The two columns are a Porapak Q (PPQ), able to separate CO_2, H_2O and light hydrocarbons (up to C_6) and a Molsieve (Molecular Sieve 5 Å, MS5A), capable of separating permanent gases, such as O_2 and N_2. This instrument has a switching valve to isolate the MS5A from species, such as CO_2, which would be adsorbed irreversibly, depleting the performances of the column.
Figure 3.10 shows the sequence of elements inside the gas chromatograph that allows the separation of the components of the gas mixture.

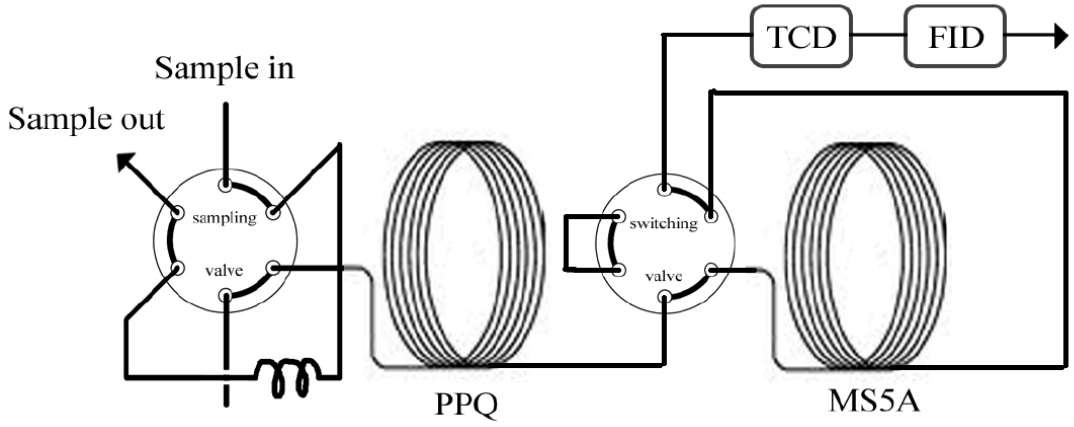

Figure 3.10: Schematic representation of element inside the Agilent GC 7820

After the separation, two detectors in series quantify the chemical species: a thermal conductivity detector (TCD) and a flame ionisation detector (FID). Among these two, only the TCD was utilised to carry out the tests because it detects all the species.

The choice of the carrier is very important because, in order to have a good detection of each components, the difference between its thermal conductivity and the one of the species to measure has to be as high as possible. For the analyses of the gas mixture exiting from the catalytic reactor, He was chosen as carrier. As it is possible to observe from Table 3.2, CO, CO_2, O_2 and N_2 have a much lower thermal conductivity compared to He, therefore these components were well visible with the TCD. All the values of thermal conductivity reported in Table 3.2 were calculated at the temperature of the TDC which is 250 °C.

Table 3.2: Thermal conductivity of the analysed gases at 250 °C

Gases	**Thermal conductivity [W/(m·K)]**
He	0.2606
CO	0.03957
NO	0.189
O_2	0.0432
CO_2	0.03464
N_2	0.04035
N_2O	0.10112

As it was mentioned before, by varying the temperature and pressure inside the chromatograph, it is possible to alter the time of retention of the various components in order to obtain distinct and clear peaks that could be quantified easily. The values of temperature and pressure and the hold time for each of them were specifically chosen for a good separation of the components that were expected to be present in the gas mixture exiting the reactor. These protocols were adopted for all the analyses and they are reported in Figure 3.11.

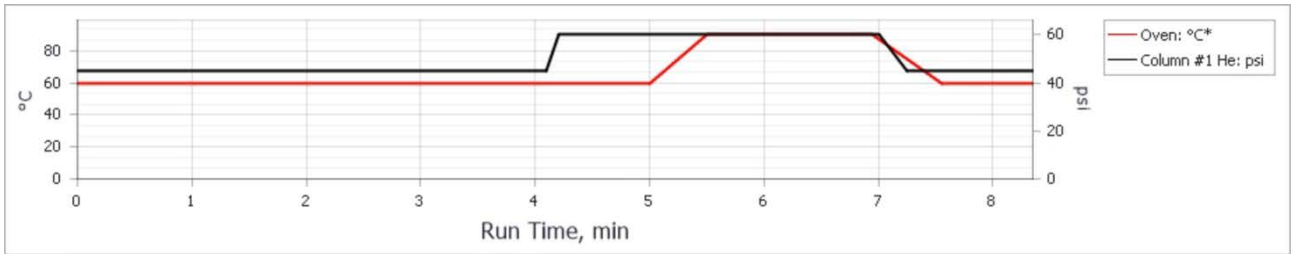

Figure 3.11: Temperature and pressure protocols adopted for the separation

The software connected to the chromatograph produces a chromatogram were each component is associated to a peak based on its retention time. The areas of these peaks are directly proportional to the concentration of the compounds in the mixture.
In this thesis project, the gas chromatograph was used mostly to detect O_2 and N_2 which could not be identified by the FT-IR. Moreover, CO_2 and CO were also detected in order to cross check the data obtained with the other analytical instrument and verify that the results were accurate. NO and N_2O were also detected by the gas chromatograph, but because the N_2O and the NO peaks did not show properly on the chromatogram, the concentrations associated to those could not be quantified.
The first phase of the concentrations quantification involved the determination of calibration lines of the gaseous compounds, obtained by analysing a mixture with a known composition.
Then the areas obtained by OpenLab were exported and elaborated by a Matlab code which utilised the calibration lines to obtain the volumetric concentration of the compounds in the product mixture.

3.3 Instruments for particle characterisation

In the next paragraphs, the techniques for the characterisation of solid particles are described. These instruments were utilised to study the particle size, the composition and the phase of the $LaFeO_3$ synthesised via flame synthesis with the experimental set-up that was described previously.

3.3.1 Optical particle counter

The optical particle counter (OPC) is an instrument that detects and counts physical particles. The OPC employed in this set-up was the Alphasense OPC-N3 that, to determine the particle size and particle number concentration, measures the light scattered by individual particles carried in an air stream through a laser beam. This type of OPC uses an elliptical mirror and dual-element photodetector to create a ‘virtual sensing zone’ in free space at the centre of an open scattering chamber. All particles, regardless of their shape, are assumed to be spherical and are assigned a ‘spherical equivalent size’. This size is related to the measurement of light scattered by the particle as defined by Mie theory, an exact theory to predict scattering by spheres of known size and refractive index (RI).

In order to function, the OPC had to be connected to a computer and communicate with its software that classified each particle size and recorded it to one of the twenty-four “bins” covering the size range from 0.35 to 40 µm. In Figure 3.12 an example of the software interface is shown while the OPC is sampling.

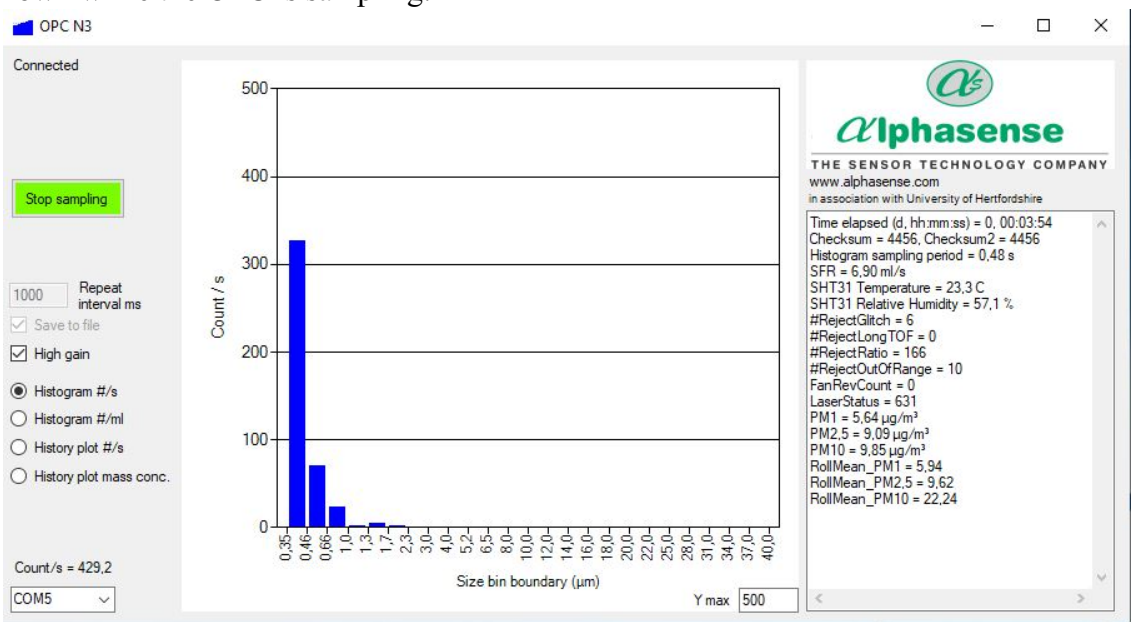

Figure 3.12: OPC software interface

The optical particle counter utilised for this thesis project is displayed in Figure 3.13 and, as it is possible to notice, a metallic tube was attached to the body of the OPC to be able to detect the particles inside the column in a high temperature environment.

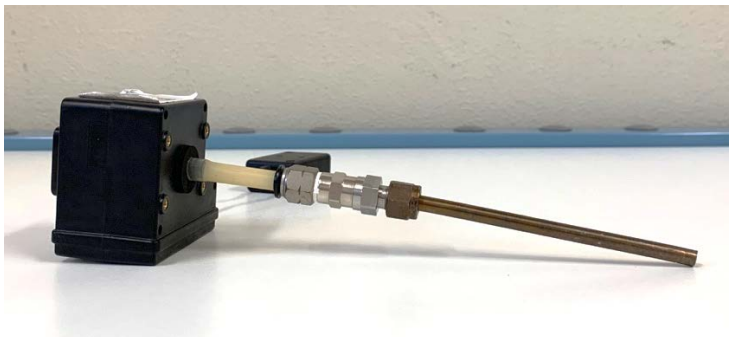

Figure 3.13: Optical particle counter (OPC) and sampling probe

3.3.2 Environmental scanning electron microscope

The environmental scanning electron microscope (ESEM) is a direct descendant of the conventional scanning electron microscope (SEM). The two instruments function utilising the same basic technology but have also some differences.

Environmental and conventional scanning electron microscopes, unlike the optical ones, do not employ photons as a source of radiation, but they use a beam of electrons that collides against

the sample and their resolution power is definitely superior with respect to the one of optical microscopes. These instruments allow to enlarge an image up to ten thousand times and they could be utilised both for qualitative and quantitative analyses.
A filament of tungsten, lanthanum hexaboride (LaB_6) or cerium hexaboride (CeB_6), positioned at the top of the column in the gun chamber, generates the electrons by thermionic effect. The electron beam is accelerated by an anode located underneath the filament and it is focalised by a series of electromagnetic lenses.
The SEM and the ESEM work by scanning this electron beam across the sample; the primary electrons penetrate into the sample and the energy that they lose is emitted back in the form of various signals such as other electrons or X-rays. These signals, transferred on a fluorescent screen, produce the image of the sample scanned.
Typically, the emitted electrons fall into two categories: low-energy secondary electrons (with energies inferior to 50 eV) produced by inelastic collisions of the incident beam with the sample and backscattered electrons (with energies greater than 50 eV) that arise from elastic collisions in the sample leading to scattering through angles approaching 180°.
With equal accelerating voltage, the electron beam penetration is superior in lighter materials and inferior in heavier ones. Therefore, the quantity of backscattered electrons emitted back by the sample and measured by a specific detector will be proportional to the molecular weight of the sample analysed. The lighter materials will produce darker images because the penetration of electrons is greater and therefore less of them are emitted back; in contrast to this, heavier materials will give lighter images because many more electrons are emitted back.
In conventional scanning electron microscopy, the whole column of the microscope operates under high vacuum to prevent air scattering of either the incident beam or the subsequently produced electrons. Instead, in environmental scanning electron microscopy a gaseous environment is maintained around the sample while imaging is carried out, although the electron gun itself is kept at the standard pressures of around 10^{-6} to 10^{-7} torr. This is achieved with the use of differential pumping down the column, so that there is a series of different pressure zones, with increasing pressures until a pressure of about 10 torr is reached in the sample chamber. Figure 3.14 is a schematic illustration of an environmental scanning electron microscope with a distinction of all the different pressure zones.

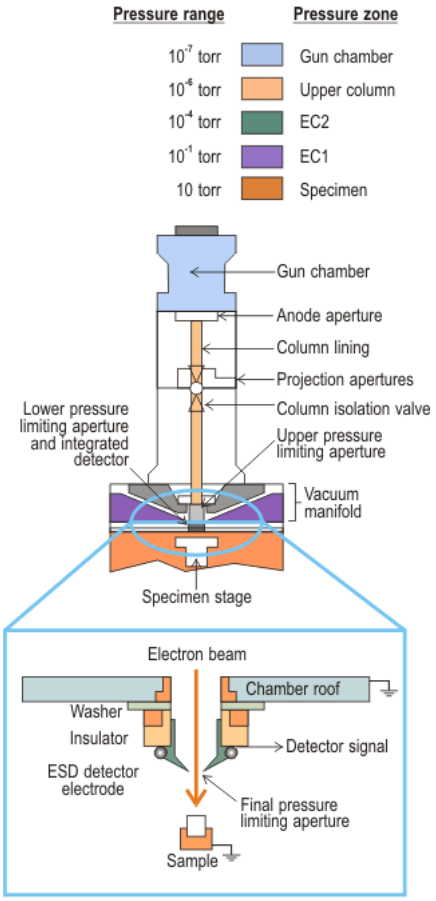

Figure 3.14: ESEM schematic representation

In environmental scanning electron microscopy, it is possible not to have high vacuum around the sample and still obtain an image with good resolution because the total distance through which electrons travel with a significant presence of gas is kept as short as possible, so that most incident electrons do not undergo any large-angle collisions.

The second major difference between ESEM and conventional SEM is that insulators do not need to be coated with a metallic layer before imaging in the ESEM thanks to the gas in the chamber that helps dissipate the build-up of charge, injected by the incident electron beam.

In fact, the gas is not simply a passive participant in the imaging process, but it plays a key role in signal detection. It can be observed that as electrons (secondary or backscattered) are emitted, they also have to travel through the gas. The secondary electrons in particular, because of their low energies, have a high collision cross section with the gas molecules and the ionisation of the molecules has a significant probability of occurring. Each ionising collision leads to the generation of an additional electron, so that a cascade amplification occurs. All the electrons produced are drawn towards the positively biased detector.

In the ionising collisions, positive ions are also produced which move towards the sample and serve to compensate the charge build-up at the surface of insulators. It is for this reason that

insulators do not need to be coated to prevent charging artefacts and consequent loss of image quality [16].

The cascade amplification process and the ionisation of molecules is represented in Figure 3.15.

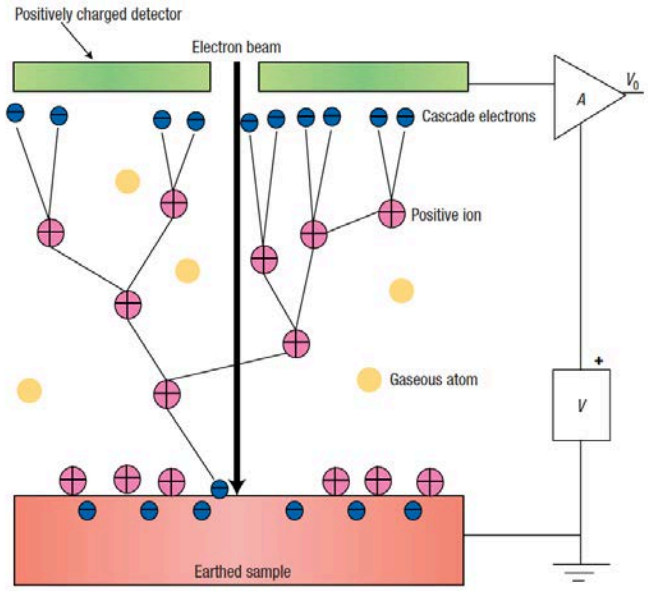

Figure 3.15: Cascade amplification process and molecules ionisation

3.3.3 Energy dispersive X-rays spectroscopy

As it was mentioned before, an environmental scanning electron microscope could be utilised also for qualitative and quantitative analyses. In fact, the chemical characterisation of a sample could be conducted with this instrument by means of energy dispersive X-ray spectroscopy (EDS).

This analytical technique relies on the interaction between a source of X-ray excitation and the sample. Its characterisation capabilities are due in large part to the fundamental principle that each element has a unique atomic structure allowing a unique set of peaks on its electromagnetic emission spectrum where the peak positions are predicted by the Moseley's law.

To stimulate the emission of characteristic X-rays from a sample, a beam of X-rays is focused into it. At rest, an atom within the sample contains unexcited electrons in discrete energy levels or shells bound to the nucleus. The incident beam may excite an electron in an inner shell, ejecting it from the shell while creating an electron hole where the electron was. An electron from an outer, higher-energy shell then fills the hole, and the difference in energy between the higher-energy shell and the lower energy shell may be released in the form of an X-ray. The number and energy of the X-rays emitted from a sample can be measured by an energy-dispersive spectrometer. As the energies of the X-rays are characteristic of the difference in

energy between the two shells and of the atomic structure of the emitting element, EDS allows the elemental composition of the specimen to be measured.

3.3.4 X-rays diffraction analysis

X-rays diffraction analysis (XRD) is an analytical technique used to determine the crystallographic structure and the chemical composition of a material by irradiating it with incident X-rays and then measuring the intensities and scattering angles of the X-rays that leave it.

A primary use of XRD analysis is the identification of materials based on their diffraction pattern. As well as phase identification, XRD also yields information on how the actual structure deviates from the ideal one, owing to internal stresses and defects.

Crystals are regular arrays of atoms; these atoms scatter the incident X-rays primarily through the interaction with the atoms' electrons. This phenomenon, represented in Figure 3.16, is known as the elastic scattering and the electrons are known as scatterers.

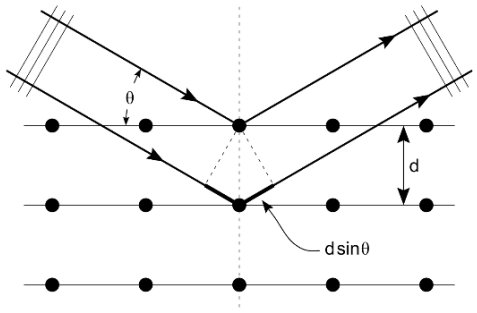

Figure 3.16: Representation of the interaction between a beam of X-rays and a lattice of scatterers

A regular array of scatterers produces a regular array of spherical waves. In the majority of directions, these waves cancel each other out through destructive interference, however, they add constructively in a few specific directions, as determined by Bragg's law:

$$2 \cdot d \cdot \sin\theta = n \cdot \lambda \tag{3.1}$$

where d is the spacing between diffracting planes, θ is the incident angle, n is an integer and λ is the beam wavelength.

X-rays are used to produce the diffraction pattern because their wavelength, λ, is often of the same order of magnitude as the spacing, d, between the crystal planes (1-100 Å).

Using Bragg's law, it is possible to determine the reticular distance. During an XRD analysis the wavelength of the beam is kept constant, while the incident angle θ is varied measuring the intensity of the deflected waves. The result is a diffractogram, where in the x axis the double of the incident angle is reported and in the y axis the intensity of the deflected waves. A diffractogram presents peaks at different incident angles that depend on the substance in

analysis and its crystalline structure. Usually, the diffractogram obtained is compared with a database of known substances to find the match.

Figure 3.17 are examples of two diffractograms obtained from the analysis of two different samples. As it is possible to notice, if the analysed material has a crystalline structure, sharp peaks are produced; while if it is amorphous, sharp peaks are not present.

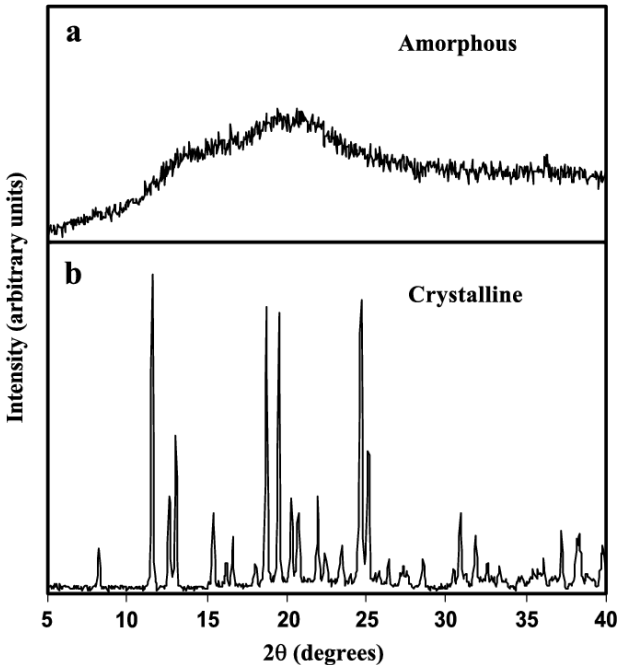

Figure 3.17: Examples of diffractograms

The main components of the experimental apparatus for an XRD analysis are the source of the X-rays (X-ray tube) the detector and the sample holder. The X-rays are generated inside a glass tube containing a low-pressure gas and two electrodes. When a potential difference is applied to the electrodes, the cathode starts to emit electrons directed to the anode. The anode is made of tungsten, molybdenum or copper and its electrons and ions are accelerated when hit by the electrons coming from the cathode. A small fraction of the energy received is reemitted as X-rays perpendicular to the electrons beam. The X-rays are then filtered to obtain only a precise wavelength and collimated towards the sample.

The geometry of an X-ray diffractometer is such that the sample rotates in the path of the collimated X-ray beam at an angle θ while the X-ray detector is mounted on an arm to collect the diffracted X-rays and rotates at an angle of 2θ. The instrument used to maintain the angle and rotate the sample is called a goniometer and a schematic representation is shown in Figure 3.18. As the sample and the detector are rotated, the intensity of the reflected X-rays is recorded [17].

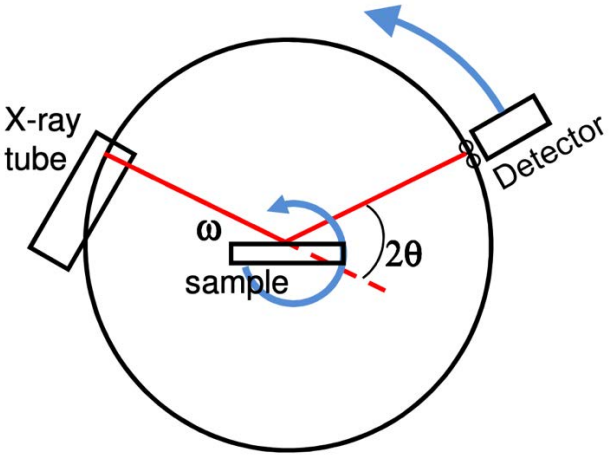

Figure 3.18: Schematic representation of an X-ray diffractometer

Chapter 4

Synthesis and characterisation of $LaFeO_3$

$LaFeO_3$ was the oxide with perovskite structure chosen to be synthesised and then tested in this thesis project, whose main goal was to understand which are the best synthesis conditions for the production of perovskites with great catalytic activity towards a specific reaction. Therefore, a basic perovskite, without the addition of dopants, extensively investigated and promising for non-PGM automotive application was selected, synthesised, characterized and tested for activity (next Chapter).
In the following, all the various parameters that were individually varied during the flame synthesis process of $LaFeO_3$ are described, applied to the synthesis, and all the $LaFeO_3$ characterisation of the catalyst are reported, except for the catalytic testing, specifically described in Chapter 5.

4.1 Synthesis of $LaFeO_3$

A great part of the work done during this thesis project was focused on the optimisation of the flame synthesis of $LaFeO_3$. In order to optimise the process, the first thing that had to be improved was the production plant, as explained in Chapter 2.
After all the improvements were implemented in the reactor for the synthesis of $LaFeO_3$, the focus shifted on all the various parameters that influenced the synthesis and in understanding which process conditions provided the catalyst with the best activity.
In the next paragraphs, all the various parameters considered will be described.

4.1.1 Flowrate of the combustible and oxidising gas

In the old thesis project, the quantities of hydrogen and oxygen utilised for the synthesis of $LaFeO_3$ were substantial. Therefore, the aim was to reduce the amounts of combustible and oxidising gas used in order to have an economically sustainable process.
While varying the flowrate of H_2 and O_2, the equivalence ratio (ϕ) was kept around a certain value to obtain flames with the required characteristics. It was not possible to keep ϕ constant because of the limitations imposed by the instruments utilised to feed the two gases.
For this type of synthesis and process reactor, it was chosen to keep a fuel-lean mixture for multiple reasons. First, an excess of oxygen was required because the oxidant was needed in the reaction that led to the formation of perovskite. Moreover, the flames were in a confined

environment, that limited the availability of air for the combustion, and there could have been safety problems if the flames accidentally extinguished inside the steel tube. But the flowrate of oxygen could not have been increased too much with respect to the one of hydrogen because this would have caused the narrowing of the flames, an undesired effect because it would have increased the probability that part of the precursor solution sprayed would not have crossed the flames.

The flowrate of hydrogen and oxygen determined the length of the flames which could not be too short because that would have prevented the closing of the flame cone, leaving a hole in the centre without flames. While reducing the flowrate of the combustible and the oxidant gas, it was important to assure the crossing of the sprayed solution through the flames; therefore, the flowrates of the feeding gases could not have been decreased below a certain value.

In the previous study, the flowrates adopted were 12 l/min for H_2 and 9 l/min for O_2, quite large, causing an impressive gas consumption at each single test, that lasts 15 min on average. Instead, in this thesis project all the various flowrates investigated are reported in Table 4.1.

Table 4.1: Flowrates of combustible and oxidising gas utilised to feed the flames

H_2 flowrate [l/min]	**O_2 flowrate [l/min]**	ϕ
9	8	0.56
8	7	0.57
7	6	0.58

As it is observable from Table 4.1, the equivalence ratio, between the flowrates of combustible and oxidising gas utilised, was not kept to a fixed value in the various syntheses because it was difficult to regulate the exact flowrates required on the manual rotameters. The values of the flowrates, required to keep a constant equivalence ratio, were approximated to the closer whole numbers which were easier to set on the manual rotameter. Therefore, it was not possible to keep the equivalence ratio constant, but only around the required value.

All the catalysts synthesised with the various combinations of flowrates were tested in the catalytic reactor to identify the catalyst with the better catalytic activity.

4.1.2 Dilution of the precursor solution

Another factor that was considered while analysing all the parameters that could have influenced the production of $LaFeO_3$ and its catalytic activity was the dilution of the precursor solution.

As it was explained in Chapter 1, the concentration of the metal precursors in the solution could have an effect on the size of particles, their SSA and consequently on their catalytic activity.

The amount of liquid (deionised water and nitric acid) present in the initial solution was the one required for the optimal complexation of the metallic ions. To obtain a less concentrated

solution, a certain quantity of deionised water was added in the atomisers' container before the start of the synthesis.
$LaFeO_3$ particles synthesised starting from solutions at different level of dilution (no dilution or 50% dilution) were analysed via ESEM imaging and tested catalytically to observe the differences induced by the variation of the metal precursor concentration in the solution.

4.1.3 Recovery method of $LaFeO_3$ from the filters

As it was explained in Chapter 2, the powder was recovered from the filters in two different ways. A certain amount of powder formed a layer on top of the filters and therefore it could be scraped directly from their surface and tested without further treatment.
Instead, part of the catalyst was embedded in between the meshes and therefore the filters had to be placed in the ultrasonic bath to release the powder. The following step was to evaporate the deionised water, utilised to submerge the filters, in which the $LaFeO_3$ was released during the ultrasonic cleaning by placing the beaker in the muffle at 180 °C. The dry powder recovered could then be tested.
Both the $LaFeO_3$ recovered directly from the filters and the one retrieved from the deionised water were tested to understand if the different methods of recovery would impact on its structure and its catalytic activity.

4.1.4 Synthesis of $LaFeO_3$ solution without citric acid

Other than the standard one, a precursor solution without the addition of citric acid was produced to understand if it was possible to synthesise the catalyst via FASP, nebulising this type of solution in order to have a 100% carbon free synthesis.
This solution was synthesised with the same technique as the standard one, but it did not provide the results that were expected. The problems, encountered while trying to synthesise this type of solution, were caused by the precipitation of the metal precursors that occurred as soon as the suspension was not mixed properly.
The two syntheses that were conducted utilising this solution were deemed unsuccessful because the quantity of catalyst recovered from the filters was extremely modest.
At the beginning, it was thought that the mixing provided by the falling back of the squirts produced by the membranes would have been enough to mix the solution properly and as a consequence keep the solid phase dissolved, but that was not the case. In fact, the mixing was not sufficient to keep the metal precursors dissolved in the solution and therefore, the ultrasonic membranes of the atomisers were able to nebulise only the liquid part, such as water, nitric acid and ammonia, while the solid phase remained at the bottom of the container. Most likely, this was the reason for the poor collection of powder from the filters.

As it is possible to observe from Figure 4.1, the metal precursors deposited around and on the ultrasonic membranes caused an interference with the nebulisation process. In fact, the nebulisation of the solution did not start as soon as the atomisers were turned on, as it usually did with the standard solution, but it took around 10 minutes to obtain a decent amount of nebulised solution. This led to an unnecessary waste of combustible and oxidising gas because the synthesis lasted twice the usual time (about 15 minutes with the standard solution, with citric acid).
These were the reasons that led to discard the idea of synthesising $LaFeO_3$ by utilising a solution without citric acid.

Figure 4.1: Deposition of metal precursors on the atomisers

4.2 ESEM imaging of $LaFeO_3$

In this thesis project, ESEM imaging was utilised to obtain a better understanding of how the size of the particles synthesised varied as a function of the various parameters considered. It was important to examine how the particle size was influenced by these variables because the particle size and consequently the specific surface area of $LaFeO_3$ have an effect on its catalytic activity. Perovskites are not very porous and therefore the geometry of the particles already gives a good idea of their specific surface area.
Through ESEM imaging, it was studied how the variation of the flowrate of combustible and oxidising gas, the concentration of the metal precursors in the solution and the method of recovery of the powder from the filters influenced the particle size.

The effects that these variables had on the morphology of the particles are reported in the next paragraphs, while the effects on the catalytic activity of $LaFeO_3$ will be discussed in the next chapter.

4.2.1 Flowrate of the combustible and oxidising gas

The first parameter that was investigated was the variation of the flowrates of hydrogen and oxygen that were fed to the burner. The ESEM images reported in Figure 4.2 and Figure 4.3 are respectively of particles produced in a flame fed with 8 l/min of H_2, 7 l/min of O_2 and 7 l/min of H_2, 6 l/min of O_2. In both cases, the initial solution was not diluted and the powder was scraped directly from the filters.

There are not any significant differences between the size distribution of the particles in the two images. In both cases, there are agglomerates and the diameters of the particles are comparable and they range from less than 1 μm to a few microns.

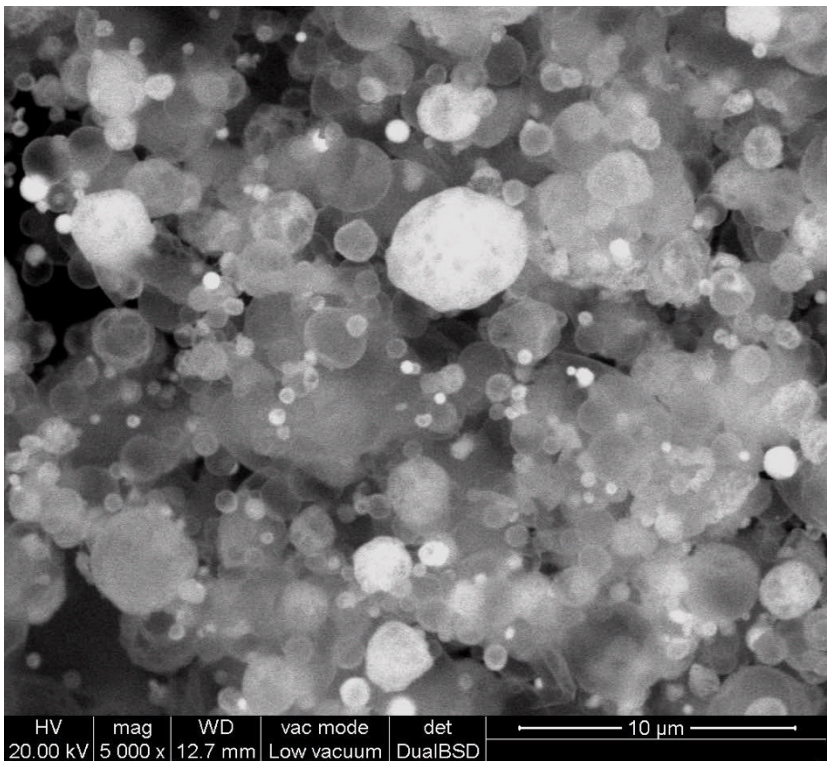

Figure 4.2: ESEM image of $LaFeO_3$ synthesised with 8 l/min of H_2 and 7 l/min of O_2

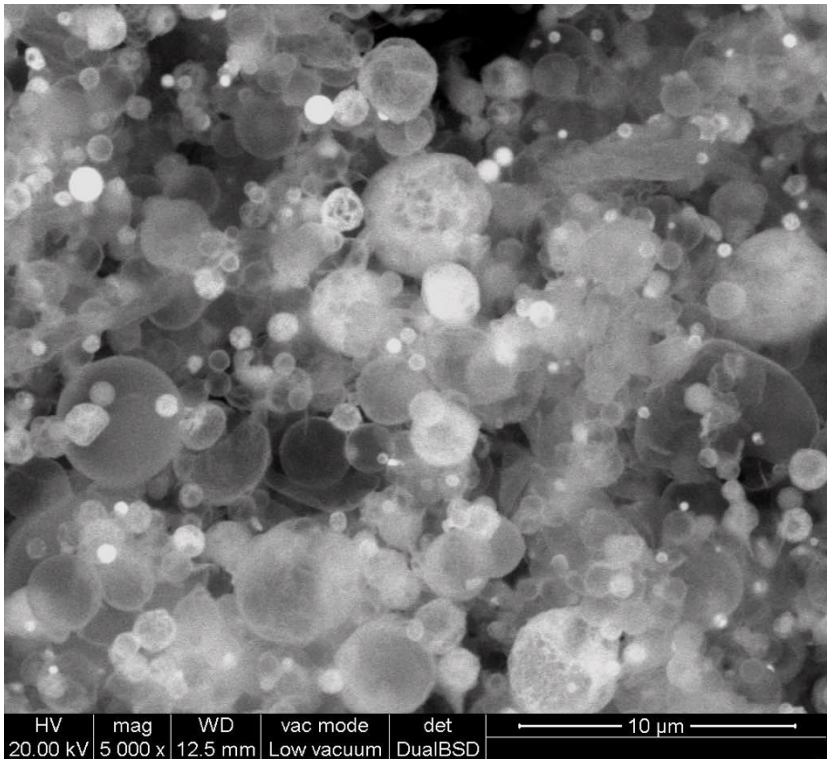

Figure 4.3: ESEM image of $LaFeO_3$ synthesised with 7 l/min of H_2 and 6 l/min of O_2

A more precise idea of the actual diameters of the particles was provided by the optical particle counter (OPC) mounted at the bottom of the column, before the filter pack.

From the particle size distributions (PSD) reported in Figure 4.4 and Figure 4.5, of the powder produced in a flame fed with 8 l/min and 7 l/min of H_2, respectively, it is noticeable that in both synthesis the majority of the particles detected by the OPC was catalogued in the bins that had a mean particle diameter ranging from 2.65 to 11 μm. The OPC detects particles with diameters up to 30 μm; it suggest that quite large ones, up and above 10 µm, are present in the flame products; those are not observed in the ESEM images because they might not have been included in the limited quantity of particles analysed.

However, in both images it is noticeable that many particles with a diameter below approximately 2 μm are present, contrary to the PSD from the OPC. These particles were not reported in the PSD plots because they might not have been detected properly by the OPC since the optical particle counter utilised during the syntheses did not operate through isokinetic sampling, which would have been the optimal method for the proper detection of the particles.

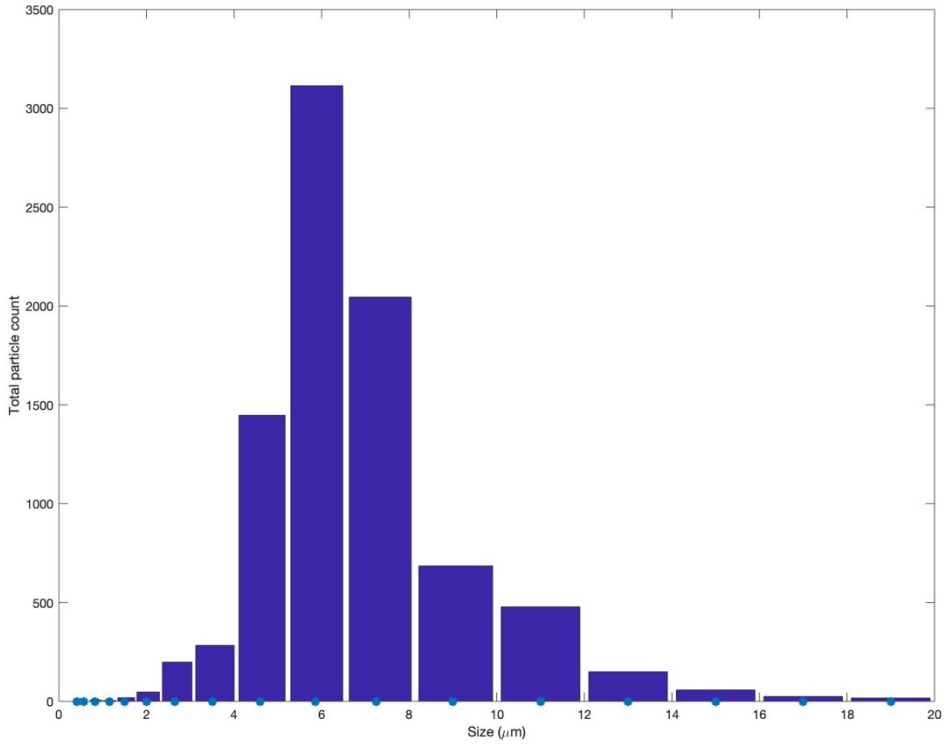

Figure 4.4: PSD of the powder synthesised in flames fed with 8 l/min of H_2 and 7 l/min of O_2

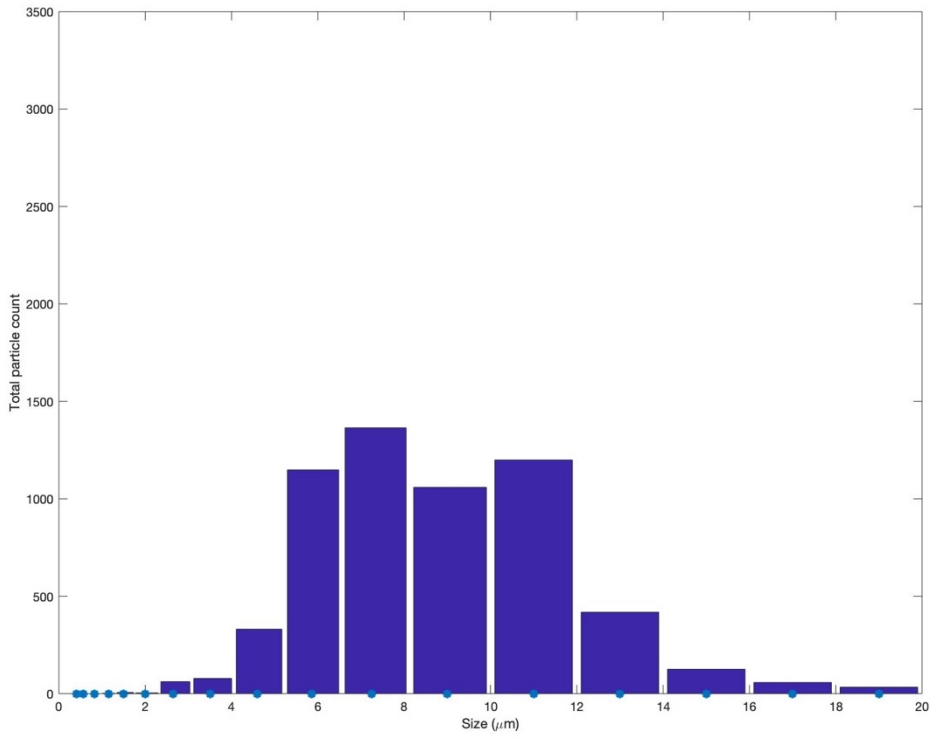

Figure 4.5: PSD of the powder synthesised in flames fed with 7 l/min of H_2 and 6 l/min of O_2

To explain the PSD from the OPC, it is possible to conclude that the particles, synthesised in flames fed with a lower flowrate of H_2, tended to form aggregates, kept together by the electrostatic force, which had larger diameters with respect to the single particles. These

aggregates were made of particles which had comparable sizes to the ones synthesised in flames fed with a higher flowrate of H_2.

Therefore, if the variation of the flowrates is not substantial, increasing or decreasing the flowrates of combustible and oxidising gas fed to the burner does not have a significant impact on the particle size of the $LaFeO_3$ produced, but it has an effect on the particle size distribution. However, the variation of the flowrates of H_2 and O_2 could have an effect on the catalytic activity of the particles as it will be discussed in the next chapter.

4.2.2 Dilution of the precursor solution

The images obtained via ESEM of the $LaFeO_3$ were utilised to examine how the different levels of concentration of the metal precursors in the solution would influence the particle size.

The ESEM images reported in Figure 4.6 and Figure 4.7 are of particles synthesised from the initial solution, and the one using a 50% dilution, respectively. In both cases, the catalyst was produced through a synthesis where the burner was fed with 7 l/min of H_2 and 6 l/min of O_2 and the deposited powder was recovered directly by scraping the filters.

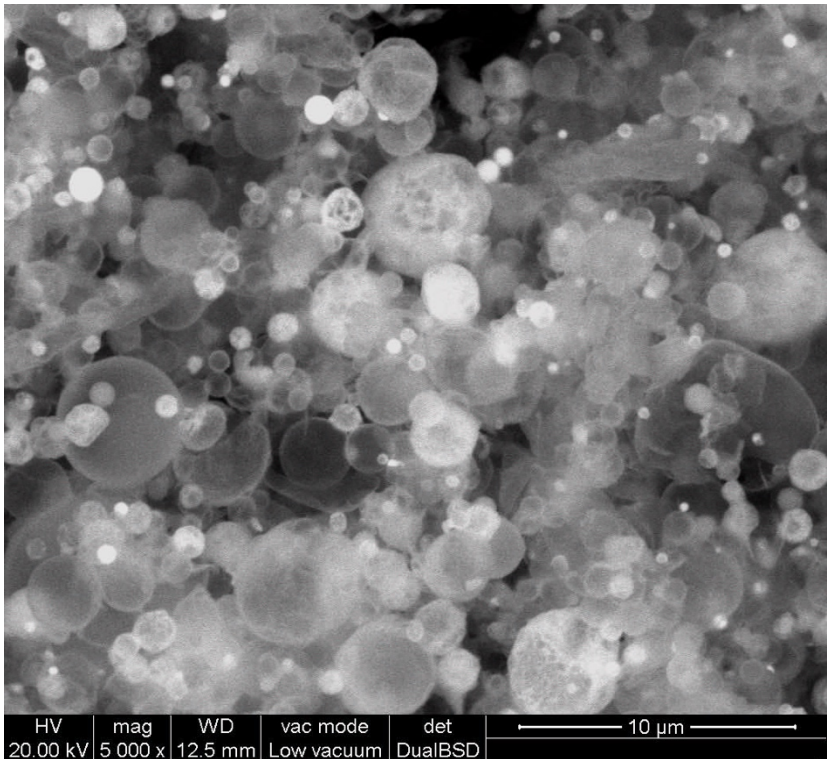

Figure 4.6: ESEM image of $LaFeO_3$ synthesised with a non-diluted solution

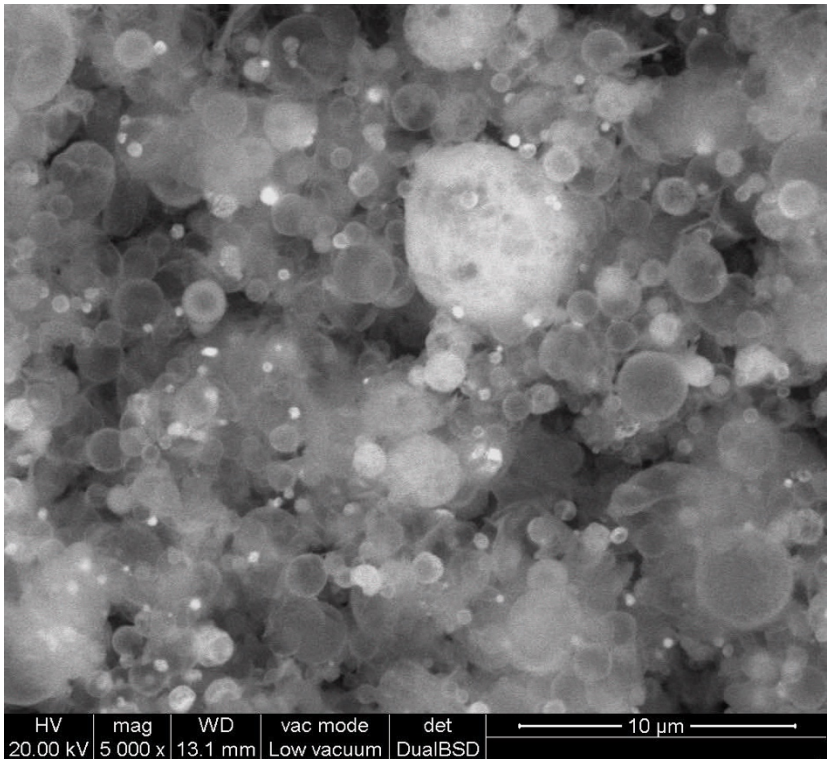

Figure 4.7: ESEM image of $LaFeO_3$ synthesised with a precursor solution with a 50% concentration

It is noticeable how in both cases, there is a broad range of particle sizes and that the diameter of the smallest particles is less than 1 μm.

By analysing the data registered by the OPC, reported in the PSD plot in Figure 4.8, to have a more precise idea of the actual diameters of the particles, it was observed that the average size of the particles detected in the two syntheses had different values, with the ones synthesised with the more concentrated solution being much larger.

In fact, as it was mentioned before, the majority of the particles detected by the OPC, from the synthesis which utilised the more concentrated solution, was catalogued in the bins that had a mean particle diameter ranging from 2.65 to 11 μm.

Instead in the synthesis which used the less concentrated precursor solution, the majority of the particles detected by the OPC were catalogued in the bins that had a mean particle diameter inferior to 2.65 μm.

In fact, comparing the two ESEM images, the more concentrated solution produced a larger number of bigger particles which had a greater tendency to agglomerate.

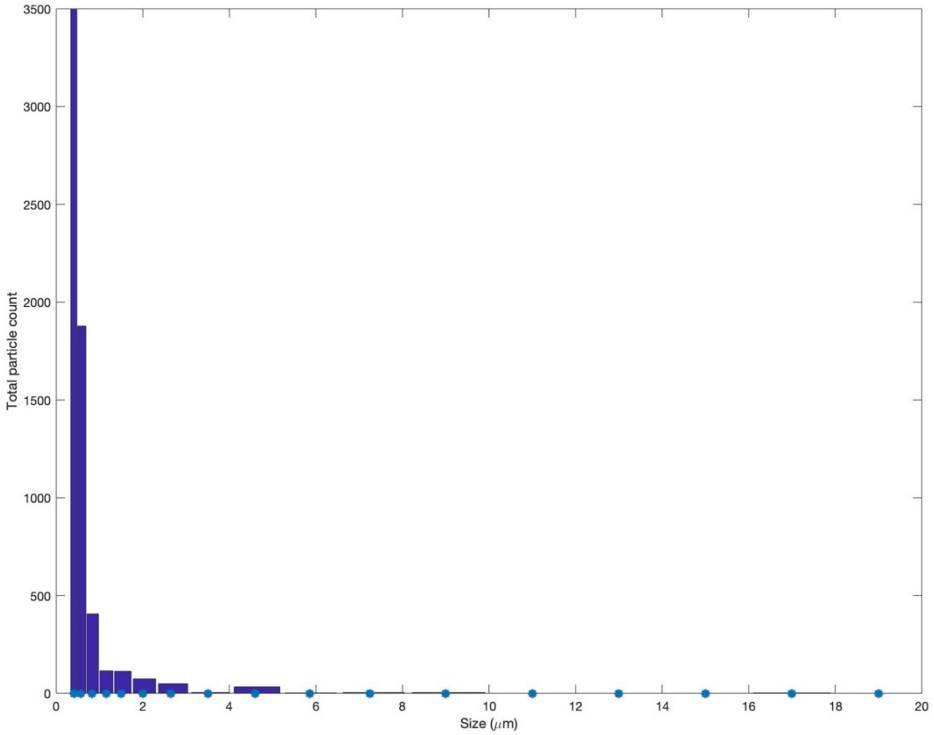

Figure 4.8: PSD of the powder synthesised with a 100% diluted

These were the most significant morphological differences between the $LaFeO_3$ synthesised with solutions with different concentration of metal precursors.

4.2.3 Recovery method of $LaFeO_3$ from the filters

The last parameter that was analysed was the recovery method of the powder from the filters. In fact, the impact that a different recovery method could have on the size of the particles was examined via ESEM imaging. In particular, the effects that a possible hydration and the permanence of $LaFeO_3$ at 100 °C for several hours could have on the particles were investigated.

Figure 4.9 and Figure 4.10 are images of particles obtained from the same synthesis, in which the burner was fed with 7 l/min of H_2 and 6 l/min of O_2 and the precursor solution was not diluted. The only difference between the two samples was the method of recovery of the powder; in Figure 4.9 the catalyst was directly scraped from the surface of the filters, while in Figure 4.10 the $LaFeO_3$ was released from the filters after the ultrasonic cleaning.

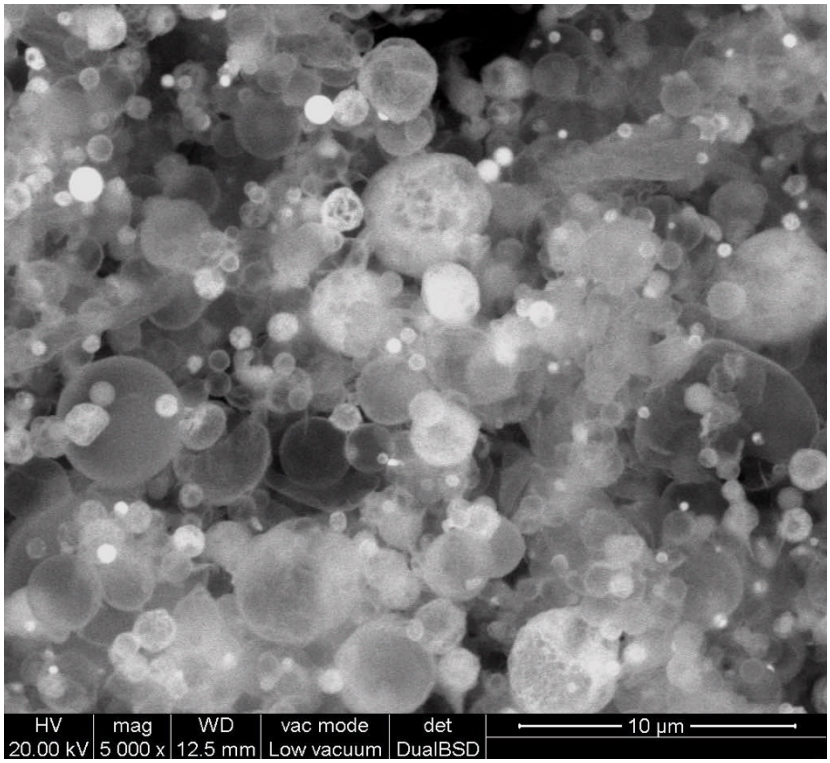

Figure 4.9: ESEM image of $LaFeO_3$ recovered by directly scraping the filters

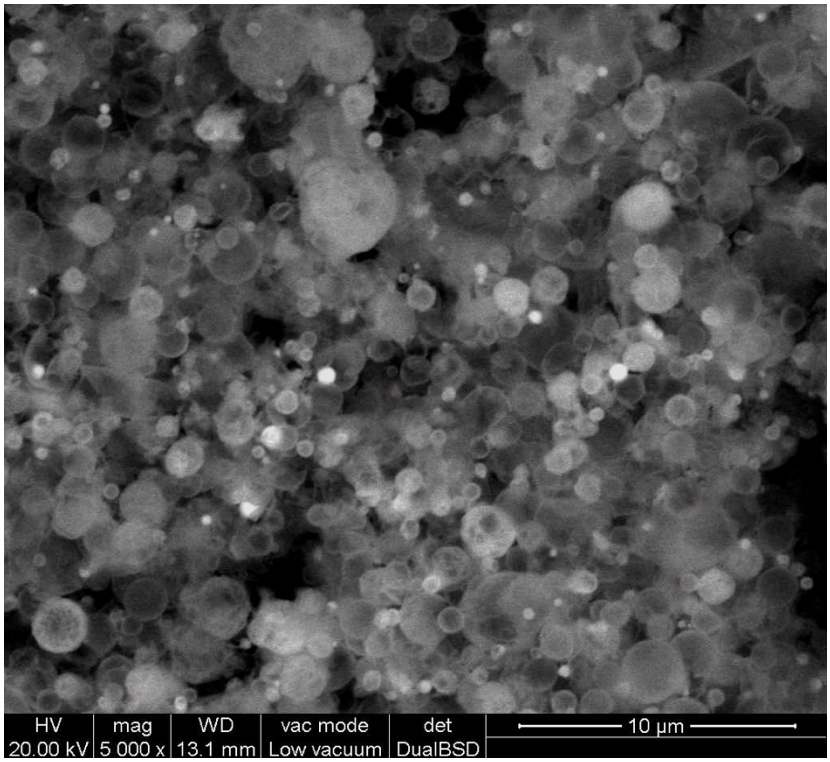

Figure 4.10: ESEM image of $LaFeO_3$ recovered from the ultrasonic cleaning of the filters

The significant difference noticeable between the two samples analysed is that the average particle size of the powder of particles recovered by ultrasounds, Figure 4.10, is much lower than the one from the filters, Figure 4.9. In fact, while the $LaFeO_3$ that was scraped had a higher

percentage of agglomerates and larger particles, the other sample had a greater number of particles with a diameter of 1 μm or less.
The powder that was retrieved by means of ultrasonic cleaning was the one embedded in the meshes of the filters and therefore composed of particles with a smaller diameter. In fact, not many particles with a large diameter were present in that sample because they could not pass through the layer of powder that had previously deposited on the surface of the filters. Therefore, only the particles with a small enough diameter could pass through the layer of deposited powder and get embedded in the filter meshes. The reasoning presented for the lack of large particles in the sample represented in Figure 4.10 is also valid for explaining the reduction of the number of agglomerates in the same sample.
The lower average particle size could result in a higher catalytic activity of the perovskite recovered by means of ultrasonic cleaning.
Comparing all four samples together, it is possible to affirm that the particles retrieved with the ultrasonic cleaning (Figure 4.10) had the most homogeneous diameter sizes and the least number of agglomerates. Instead, the two batches synthesised with the non-diluted initial solution and scraped directly from the filters (Figure 4.2 and Figure 4.3) had the higher percentage of larger particles and aggregates.
Therefore, based on the information acquired from the ESEM images, the $LaFeO_3$, recovered after the ultrasonic cleaning of the filters, should have the best catalytic activity because it was the powder with the lowest average particle size and therefore the greatest SSA. Instead, the perovskites in Figure 4.2 and Figure 4.3 should not be as catalytically active because of the larger average particle size and the abundance of agglomerates. All these perovskites were catalytically tested and the results will be reported in the next chapter.

4.3 Characterisation of $LaFeO_3$

The characterisation of the catalysts synthesised was executed via EDS and XRD analysis. EDS analysis was carried out on various samples to detect the possible presence of any residue of the acids and ammonia utilised in the precursor solution. XRD analysis was necessary to confirm that the $LaFeO_3$ had a crystalline perovskite structure right after coming out of the flame, without the need of any further treatment.
In the next paragraphs, the results obtained through these analyses will be reported and commented to draw some conclusion that will help to better understand the results of the catalytic tests that will be described later on.

4.3.1 EDS analysis

EDS analysis allows to measure the elemental composition of a sample. In this thesis project it was utilised to examine the composition of the $LaFeO_3$ synthesised, to understand if any of the

components of the precursor solution were present as residues, such as the citric acid, nitric acid or the ammonia.

The spectrums were obtained by analysing only a restricted area and not the whole sample. Therefore, the height of the peaks and the weight and atomic percentages of each element might slightly differ from the average values, based on the area of the sample that was analysed.

Two samples, synthesised with decreasing flowrates of hydrogen, were characterised through EDS analysis. The batches were tested to examine if producing the catalyst in flames fed with different amounts of hydrogen and oxygen would lead to having more or less residues.

The first sample that was tested was the $LaFeO_3$ synthesised with the non-diluted solution in a flame fed with 8 l/min of H_2 and 7 l/min of O_2. As it is noticeable from the peaks in Figure 4.11, the most substantial presences of elements in the perovskite were of lanthanum, iron and oxygen as it should have been. But, other elements, such as carbon and nitrogen were detected in non negligeable quantities; while others were identified but only in traces, such as copper, zinc and chlorine.

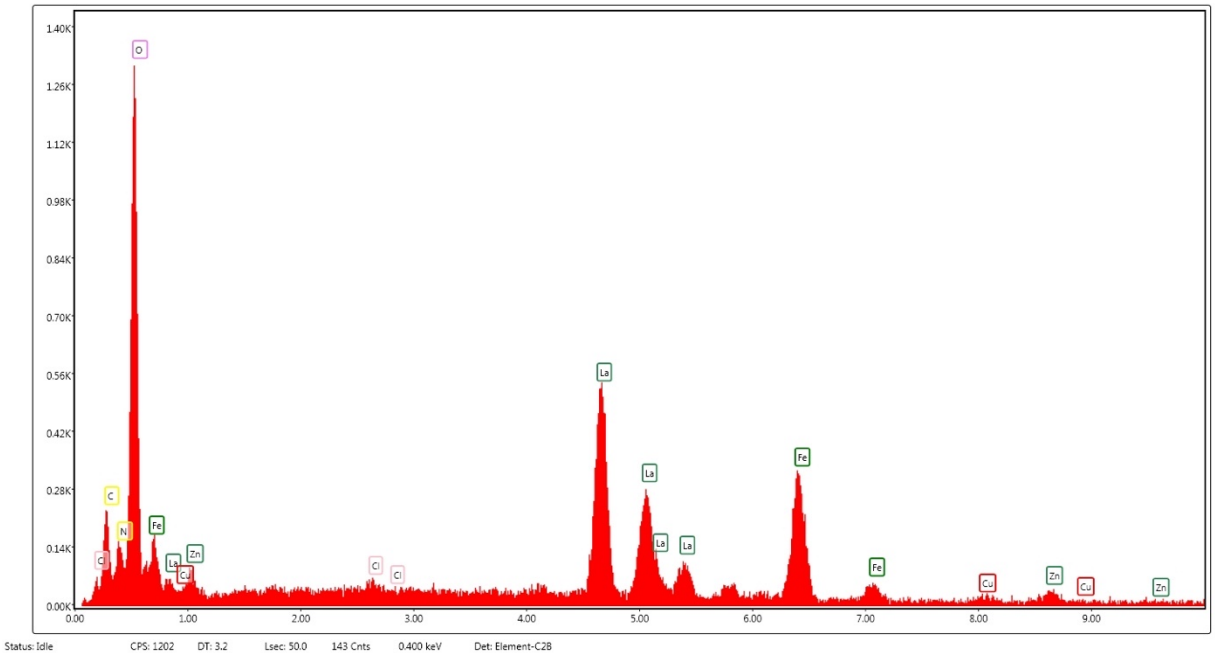

Figure 4.11: EDS spectrum of $LaFeO_3$ synthesised with 8 l/min of H_2 and 7 l/min of O_2

The composition of the analysed sample is summarised in Table 4.2 where both the weight and atomic percentages of each element are reported together with the error in the measurement.

When utilising EDS for quantitative analyses, it is important to remember that this type of analysis is intrinsically unprecise; in fact, some of the measurements have considerably high errors. Moreover, it is also difficult to obtain correct values for the measurements of the element percentages when two or more peaks overlap.

Table 4.2: Composition of the $LaFeO_3$ synthesised with 8 l/min of H_2 and 7 l/min of O_2

Element	Weight %	Atomic %	Error %
C	6.71	17.7	11.49
N	4.26	9.63	14.01
O	25.76	51.03	8.57
Cl	0.26	0.23	63.84
La	41.29	9.42	5.1
Fe	17.37	9.85	5.19
Cu	1.42	0.71	38.52
Zn	2.93	1.42	24.72

From Table 4.2, it is observable that the atomic percentages of lanthanum and iron were perfectly consistent because they match the 1:1 proportion that the atomic percentages of the two elements had to follow according to the perovskite formula $LaFeO_3$.

The atomic percentage of oxygen should have been three times the one of lanthanum or iron; instead, its value was more than five times the percentage of the two other elements. This excess could have derived from the residues of the acids that did not decompose completely.

From the atomic concentrations reported in Table 4.2, it is also noticeable that significant amounts of carbon and nitrogen were present in the perovskite. This is an indication of the fact that the citric and nitric acid and the ammonia did not decompose completely during the flame synthesis.

In this specific case, the presence of a residue of carbon was more consistent than the one of nitrogen. However, the percentage value of carbon might have been compromised by the presence of carbon on the support on which the sample was placed inside the ESEM. Therefore, that value might not be truthful.

Furthermore, traces of copper and zinc were reported. These might derive from the junctions utilised in the flame synthesis plant which are made of brass. However, the error percentage on these measurements was particularly high, therefore these values might not be truthful.

Chlorine was also detected. But, because the atomic percentage value was extremely low and the error on this measurement was very high, there might not have actually been any chlorine present in the sample.

The second sample that was characterised was the $LaFeO_3$ synthesised with the non-diluted solution in a flame fed with 7 l/min of H_2 and 6 l/min of O_2. The peaks present in the spectrum of the second sample, reported in Figure 4.12, are the same ones that appeared also in the spectrum of the first sample apart from the ones characteristic of chlorine which are not present.

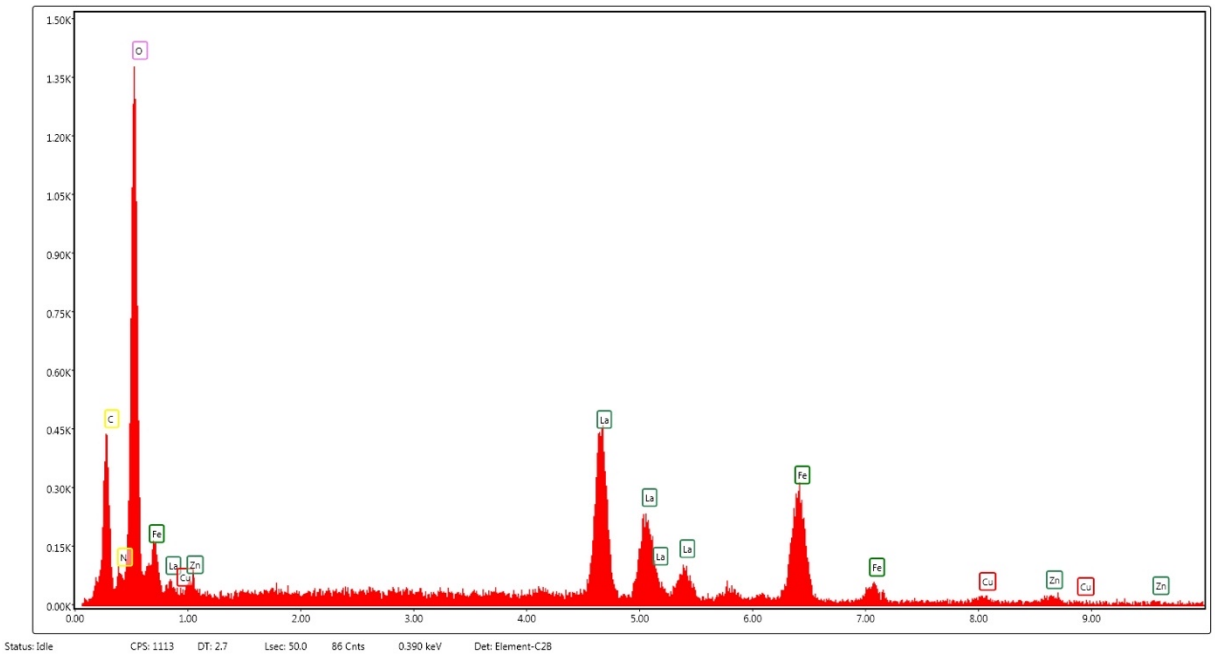

Figure 4.12: EDS spectrum of $LaFeO_3$ synthesised with 7 l/min of H_2 and 6 l/min of O_2

The composition of the analysed sample is summarised in Table 4.3 where, as before, both the weight and atomic percentages of each element are reported together with the error in the measurement.

Table 4.3: Composition of the $LaFeO_3$ synthesised with 7 l/min of H_2 and 6 l/min of O_2

Element	Weight %	Atomic %	Error %
C	14.78	32.43	9.47
N	2.16	4.07	20.88
O	29.08	47.91	8.77
La	34.27	6.5	5.85
Fe	16.43	7.75	4.97
Cu	1.43	0.59	33.47
Zn	1.85	0.74	31.87

Taking into considerations the lack of precision of EDS for quantitative analyses, the atomic percentages of lanthanum and iron, from Table 4.3, could be considered coherent with each other because they almost respected the 1:1 proportion that the atomic percentages of the two elements had to follow according to the perovskite formula $LaFeO_3$.

Also in this case, as it happened before, the atomic percentage of oxygen was more than three times the percentage of lanthanum and iron. This excess could have derived from the residues of the acids that did not decompose completely during the synthesis of the perovskite.
In this case, the atomic percentage of carbon almost doubled its value with respect to the sample synthesised in a flame fed with 8 l/min H_2, while the percentage of nitrogen halved its value. By analysing the data, it is affirmable that the residues of nitric acid or ammonia decreased in comparison to the first sample, while the residue of citric acid increased.
Therefore, it is possible to assert that increasing the flowrate of combustible and oxidising gas fed to the burner, which should create better conditions for the synthesis of $LaFeO_3$, does not assure an improvement in the decomposition of all the citric acid, nitric acid and ammonia present in the precursor solution. In both samples, there were residues of carbon and nitrogen, but they did not decrease in the sample synthesised in a flame fed with a higher flowrate of hydrogen and oxygen; in fact, while the atomic percentage of carbon decreased, the one of nitrogen doubled.
Therefore, it is important to consider that in all the $LaFeO_3$ samples that will be catalytically tested there will be residues of citric acid, nitric acid and ammonia.

4.3.2 XRD analysis

In this thesis project, XRD analysis was mostly utilised to prove that the $LaFeO_3$ produced via flame synthesis had a perovskite structure already after being recovered from the filters without the need of any additional thermal pre-treatment.
During the catalytic tests, temperatures up to 600 °C were reached. The permanence of the catalyst at such high temperatures could have caused a variation in the crystalline phase of the perovskite. Therefore, XRD analysis was also utilised to be assured that the $LaFeO_3$ structure was not altered during the catalytic tests.
Two amounts of $LaFeO_3$ from the same synthesis were analysed: one was considered “fresh” because it was composed of powder recovered directly from the filters, while the other one had been utilised during a catalytic test.
The diffractogram reported in Figure 4.13 was obtained from the analysis of the fresh $LaFeO_3$. The baseline presents a slight curvature, but it is also possible to observe various sharp peaks which corresponds to the characteristic peaks of the $LaFeO_3$ perovskite structure.
Therefore, it could be stated that the powder presented almost entirely a perovskite crystalline phase, but also a small percentage of amorphous phase which was probably given by the residue of the nitric and citric acid and ammonia that had not been decomposed entirely during the synthesis as it was also observed from the EDS analysis.

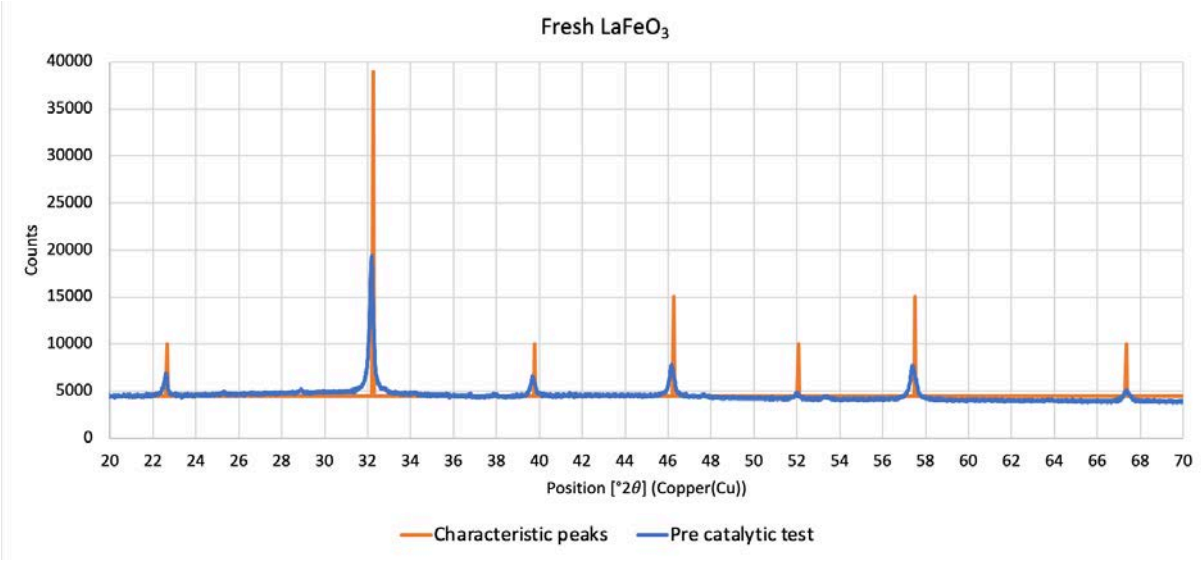

Figure 4.13: Diffractogram of the "fresh" $LaFeO_3$ (pre-catalytic test)

In Figure 4.14, the diffractograms of the fresh and utilised $LaFeO_3$ were superimposed to examine if there were any changes in the $LaFeO_3$ perovskite structure before and after the catalytic tests.

As it is noticeable, the baseline of the diffractogram of the $LaFeO_3$ analysed after being utilised during the catalytic test has no curvature. This difference between the two diffractograms is caused by the fact that the residues of nitric and citric acid and ammonia were decomposed during the catalytic test and therefore the powder did not present a percentage of amorphous phase anymore, but it presented entirely a crystalline phase.

Moreover, all the peaks present in the two diffractograms perfectly overlap, meaning that the $LaFeO_3$ perovskite crystalline structure was not altered during the catalytic test.

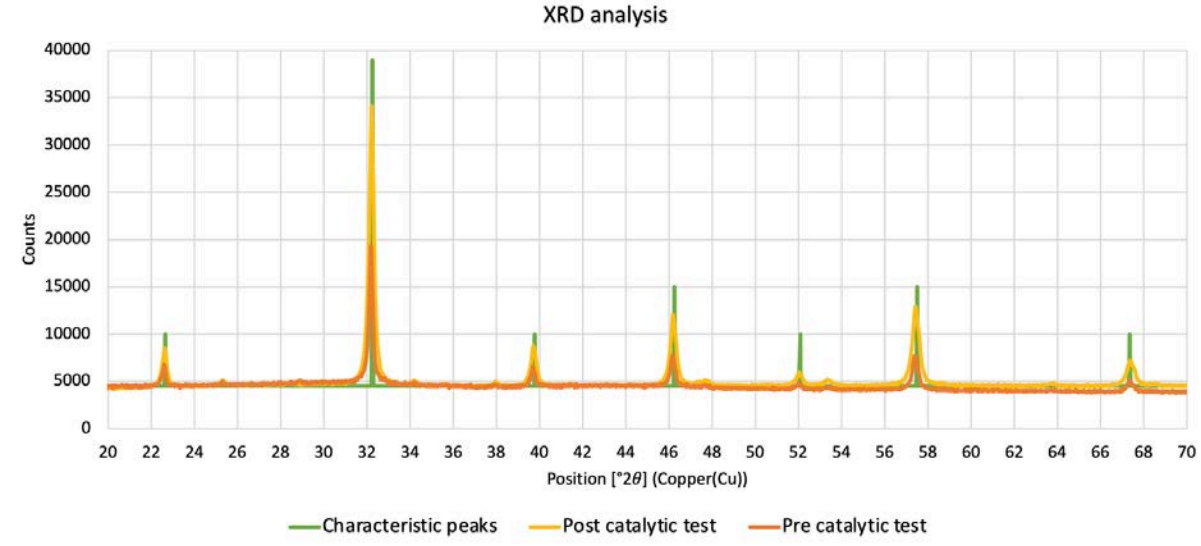

Figure 4.14: Diffractograms of the $LaFeO_3$ pre- and post-catalytic test

Therefore, it is possible to affirm that the $LaFeO_3$ that is produced via flame synthesis does not require any additional treatments because it already has a crystalline structure which is not altered by the processes taking place during the catalytic tests.

Chapter 5

Catalytic testing of $LaFeO_3$

All the variants of $LaFeO_3$ synthesised were catalytically tested to understand the influence that all the various synthesis parameters, such as the flowrates of combustible and oxidising gas fed to the burner, the precursor solution concentration and the powder recovery method, had on the catalytic activity of the perovskite.
ESEM imaging and the characterisation analyses carried out on the samples allowed to obtain a better understanding of the structure and composition of $LaFeO_3$ which could help predict some of its possible behaviours during the catalytic tests.

5.1 Model reaction and mechanism

The reaction model considered was the reduction of NO with the simultaneous oxidation of CO, according to the following reaction:

$$2\,CO + 2\,NO \rightarrow 2\,CO_2 + N_2$$

The catalytic activity of $LaFeO_3$ was tested for this reaction because this is the model reaction for TWC and $LaFeO_3$ is one of the materials which has been investigated to reduce the amount of PGMs utilised in catalytic converters.
The reaction mechanism on $LaFeO_3$ was supposed in a collaboration between the University of Padova and the University of Lille for the European Project "Partial PGMs" through microkinetic modeling with detailed superficial chemistry and it allowed the identification of the gases to be monitored during the reaction [3]. The experimental validation of this mechanism has been carried out through the catalytic tests of this thesis work. The reaction model is reported below.

1)	$CO + * = CO*$	*CO adsorption on active sites (Fe atoms) (*)*
2)	$CO* + O_{(l)} = CO_2 + *V$	*CO_2 formation with lattice O ($O_{(l)}$) and vacancy formation*
3)	$NO + * = NO*$	*NO adsorption on active sites*
4)	$NO + *V = NO*V$	*NO adsorption on active sites with neighboring vacancy*

5)	$NO * V = N * + O_{(l)}$	*NO decomposition to reform $O_{(l)}$*
6)	$NO * + N * = N_2O * + *$	*N_2O formation*
7)	$N * + N * = N_2 + 2 *$	*N_2 formation and desorption*
8)	$H_2O + * = H_2O *$	*H_2O adsorption on active sites*
9)	$O_2 + * V = O * + O_{(l)}$	*O_2 adsorption on active sites with neighboring vacancy*
10)	$CO * + O * = CO_2 + 2 *$	*CO_2 and vacancies formation from CO and O on active sites*
11)	$N_2O * = N_2O + *$	*N_2O desorption*
12)	$O_2 + * = O_2 *$	*Molecular O_2 adsorption on active sites*
13)	$O_2 + 2 * = 2\,O *$	*Atomic O_2 adsorption on two active sites*

This reaction model went up against the oxidation of CO by means of O_2, when the oxidant was added to the gas reacting mixture as it will explained later.

The information obtained through the FT-IR and the gas chromatograph concerned the quantitatively trend of the species in gas phase over time; the compounds that were detected by these instruments were CO, CO_2, NO, N_2O, NO_2, N_2 and O_2. Instead, the set-up was not predisposed for in-situ analysis and it was not possible to obtain information on the chemical species adsorbed on the catalyst's surface.

5.2 Reacting gas mixture

The catalytic tests carried out on $LaFeO_3$ were dynamic ones because the temperature and the composition of the gas mixture fed to the catalytic reactor changed over time. In order to be able to change the composition of the gas reacting mixture while the catalytic test was running, a 4-way valve was utilised.

As it was mentioned in Chapter 3, each catalytic test carried out was composed of two temperature cycles. Each of these two cycles was fed with a gas reacting mixture with a different composition. The gas mixture fed to the reactor during the first temperature cycle was composed of CO, NO and He as an inert. The volumetric concentrations are reported Table 5.1.

Table 5.1: Composition of the gas reacting mixture for the first temperature cycle

Component	Volumetric fraction [%]
CO	1.52 ± 0.03
NO	0.96
He	97.52 ± 0.03

CO and NO were not fed in stoichiometric quantities to the reactor, but the CO was in excess because the aim was to understand if it was possible to obtain a complete conversion of nitric oxide with a lean NO reacting mixture.

In the second temperature cycle, O_2 was added to the reacting mixture in order to understand if, with the presence of O_2, the simultaneous reduction of NO and oxidation of CO would still take place or if the oxidation of CO would prevail over the first reaction.

During this cycle, the concentration of O_2 in the mixture was augmented to understand if the reactants would have behaved differently with an excess of O_2 in the mixture. The stoichiometric value of the volumetric concentration of O_2, considered as the one necessary to completely oxidise the CO, was 0.775 %.

It was possible to change the concentration of the O_2 within the same cycle because, as it will be explained in the paragraph 5.4, the behaviour of the components in the heating and cooling ramp was identical; therefore, it was not necessary to record the data of both ramps for each concentration.

The composition of the O_2 lean gas mixture fed to the reactor is reported in Table 5.2.

Table 5.2: Composition of the O_2 lean gas reacting mixture

Component	Volumetric fraction [%]
CO	1.52 ± 0.03
NO	0.96
O_2	0.25 ± 0.01
He	97.27 ± 0.04

At the beginning of the second temperature cycle, O_2 was introduced into the reacting mixture via the 4-way valve. During the first temperature cycle, in addition to the flowrates of CO and NO/He, the valve was feeding the reactor a flowrate of helium, equal to the one of O_2 that would have been introduced, in order to maintain constant the total flowrate after the valve switch.

The reacting mixture with the composition reported in Table 5.2 was fed to the reactor for half the temperature cycle and then, during the isotherm, it was switched to the gas mixture with the O_2 in excess with the composition reported in Table 5.3. The composition of the gas reacting mixture was switched during the isotherm to have a constant initial value of the volumetric concentrations of all the components.

Table 5.3: Composition of the gas reacting mixture with excess of O_2

Component	Volumetric fraction [%]
CO	1.43 ± 0.02
NO	0.89 ± 0.01
O_2	0.85 ± 0.03
He	96.83 ± 0.06

However, with the reacting mixture reported in Table 5.3, the total flowrate was slightly augmented. This small variation in the total flowrate fed to the reactor did not cause significant variations to the catalytic activity.

In order to have a better understanding of when the O_2 was inserted in the gas reacting mixture during the catalytic test, the temperature profile of the catalytic tests is reported in Figure 5.1.

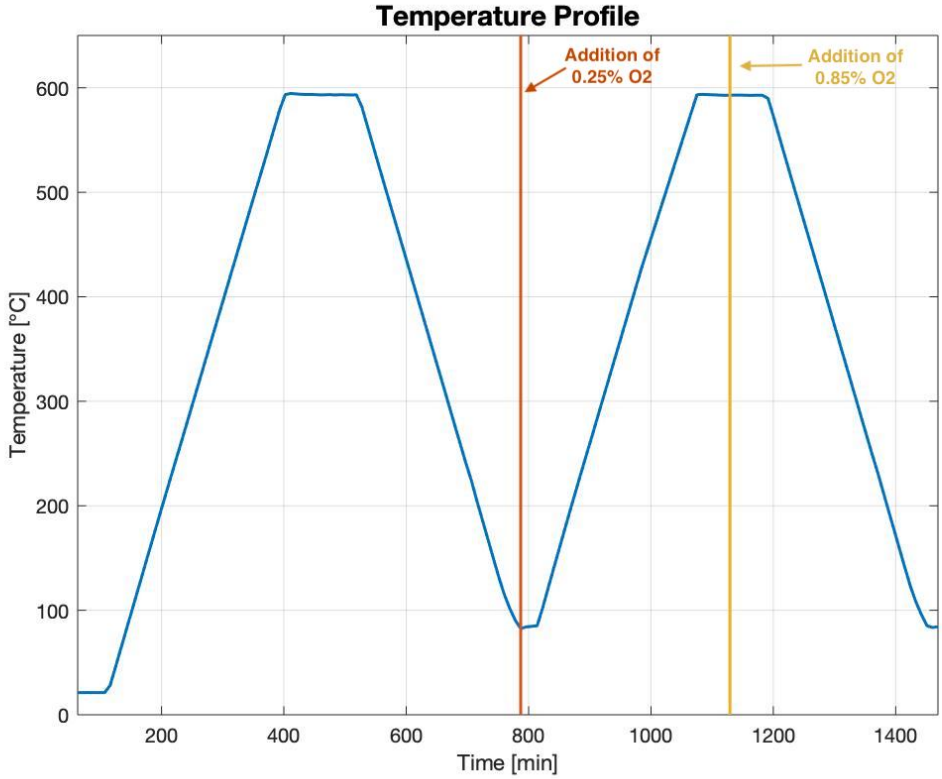

Figure 5.1: Temperature profile of the catalytic tests

The mass of catalyst loaded in the reactor changed with every test based on the quantity of powder that was available. The total flowrate of reacting gas mixture fed to the reactor changed accordingly to the mass of catalyst because the aim was to keep the weight hourly space velocity (WHSV) at a fixed value. The WHSV is defined as the flowrate of fluid flowing per unit weight of catalyst and it is calculated according to the following equation:

$$WHSV = \frac{\dot{V}}{m_{cat}} \tag{5.1}$$

where the volumetric flowrate of the reacting gas mixture is expressed in cm^3/h and the catalyst mass is expressed in g. The measurement unit of WHSV is $cm^3/g_{cat}h$.
The higher the value of the WHSV, at which the catalyst results having a satisfying performance in terms of catalytic activity, the better. In fact, the inversely proportional of the weight hourly space velocity is the contact time, which corresponds to how much time the gas is in contact with the catalyst under the conditions of operation. Therefore, if the value of the WHSV is high, the contact time between gas and catalyst will be short and if the powder is able to catalyse the reaction in such a short time, it means that it has a great catalytic activity.
In literature, the majority of the catalysts are tested at a WHSV of around $10{,}000 - 20{,}000\ cm^3/g_{cat}h$. Instead, in the European project "Partial PGMs", where alternative materials such as perovskites were tested to find possible substitutes to the commercial Platinum-Group Metal based catalysts utilised in the coating of DPF (Diesel Particulate Filter) and TWC, the catalysts were analysed at a WHSV of $60{,}000\ cm^3/g_{cat}h$.
For this thesis project, the tests were executed at a higher value of WHSV to emphasise the great performances of $LaFeO_3$ for the catalysis of a particular reaction in real industrial conditions and not "academic" ones. The first set of catalytic tests was carried out at a WHSV value of $150{,}000\ cm^3/g_{cat}h$; then tests in the same condition were repeated at a WHSV value of $170{,}000\ cm^3/g_{cat}h$. Tests in the same condition were executed at two different values of weight hourly space velocity in order to understand if the $LaFeO_3$ that had a great catalytic activity at a lower value of WHSV would still perform in a satisfying way at a higher value of WHSV.

5.3 Thermal pre-treatment

From the XRD analysis executed on the "fresh" $LaFeO_3$ recovered from the filters, it was observed that the powder synthesised already had a complete crystalline perovskite structure and therefore a thermal treatment (calcination) was not necessary. However, from the EDS analysis carried out on the powder, it was discovered that, apart from lanthanum, iron and O_2, also other elements were present in the powder, such as carbon and nitrogen. It was thought that some residues of nitric and citric acid and ammonia from the synthesis were still present on the powder.
Therefore, a thermal pre-treatment was executed on $LaFeO_3$ to understand how the residues of the acids and of ammonia would decompose at high temperature, which gases would be produced and to obtain a rough indication of the quantity of residues that were present in the sample based on the concentration of the gases released.
If one or more gases were to be produced in a significant amount during the thermal pre-treatment, it meant that the data obtained during the real catalytic tests would be distorted by

their presence. Therefore, this test was carried out preliminary to know if the data of the other tests needed to be corrected and in which way.

The set-up to carry out this test was mounted in the same way as the other catalytic tests and also the temperature protocol adopted was equal to the one which was utilised for all the catalytic tests. During the first temperature cycle, the thermal pre-treatment was carried out in an inert environment and helium was fluxed; while during the second one the pre-treatment was run in an oxidising atmosphere in which synthetic air was fed to the reactor.

The composition of the gas mixture exiting from the reactor after the thermal pre-treatment was analysed with the FT-IR and the volumetric concentration of the compounds detected during the first temperature cycle in an inert atmosphere are reported in the plot at Figure 5.2. In the plot, it is possible to observe the volumetric fractions of the various components in function of time, but it is also possible to associate the varying of the concentration to the varying of the temperature.

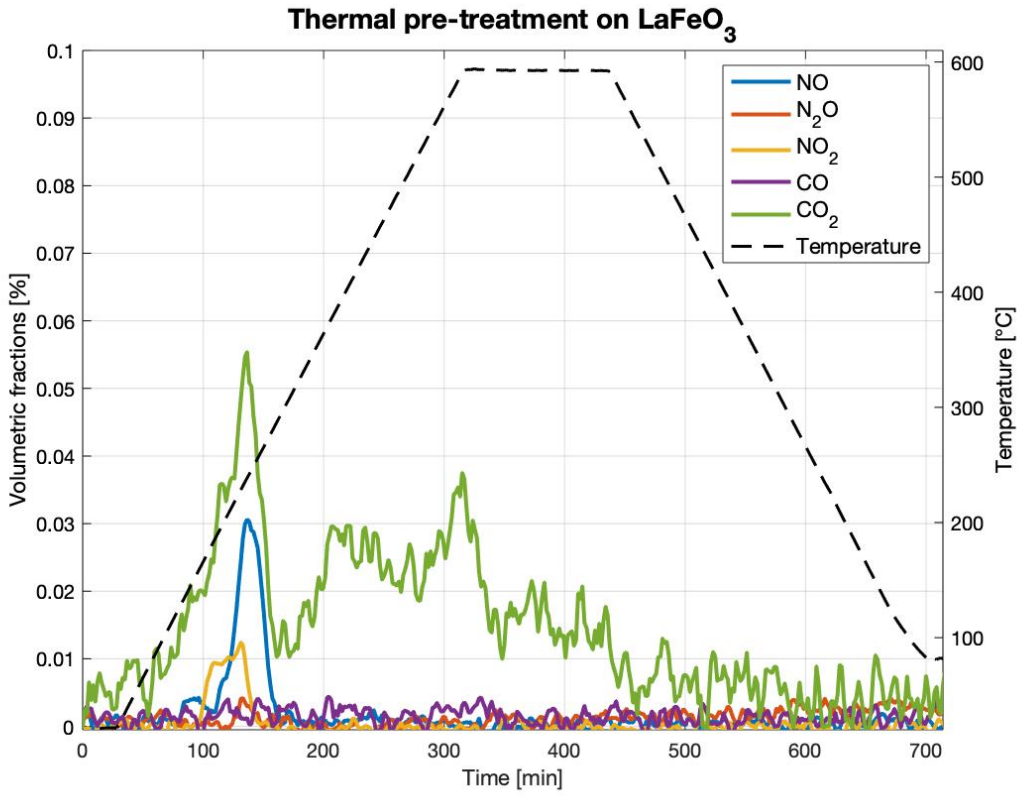

Figure 5.2: Thermal pre-treatment in inert atmosphere

It is noticeable that the only gas which was released consistently and in a considerable quantity by the powder was CO_2. The production of CO_2 is easily explained by the results of the EDS analysis which proved the presence of carbon and O_2 residues that reacted together when the temperature inside the reactor increased.

The other two compounds, that were emitted, were NO and NO_2, which had a peak in their production at the temperature of 235 °C during the heating ramp. Their release could also be explained by the residues of nitrogen and O_2 present in the powder.
In Figure 5.3, it is possible to observe the composition of the gas mixture exiting from the reactor after the thermal pre-treatment in oxidising atmosphere.
In this case, the amount of CO_2 being released from the $LaFeO_3$ is less than the cycle before and this could be because the majority of the residues had decomposed during the first cycle. All the other compounds behaved as they did in the first cycle apart for N_2O whose volumetric fraction was slightly higher with the presence of O_2. In the second cycle, there were not peaks in the production of NO and NO_2.

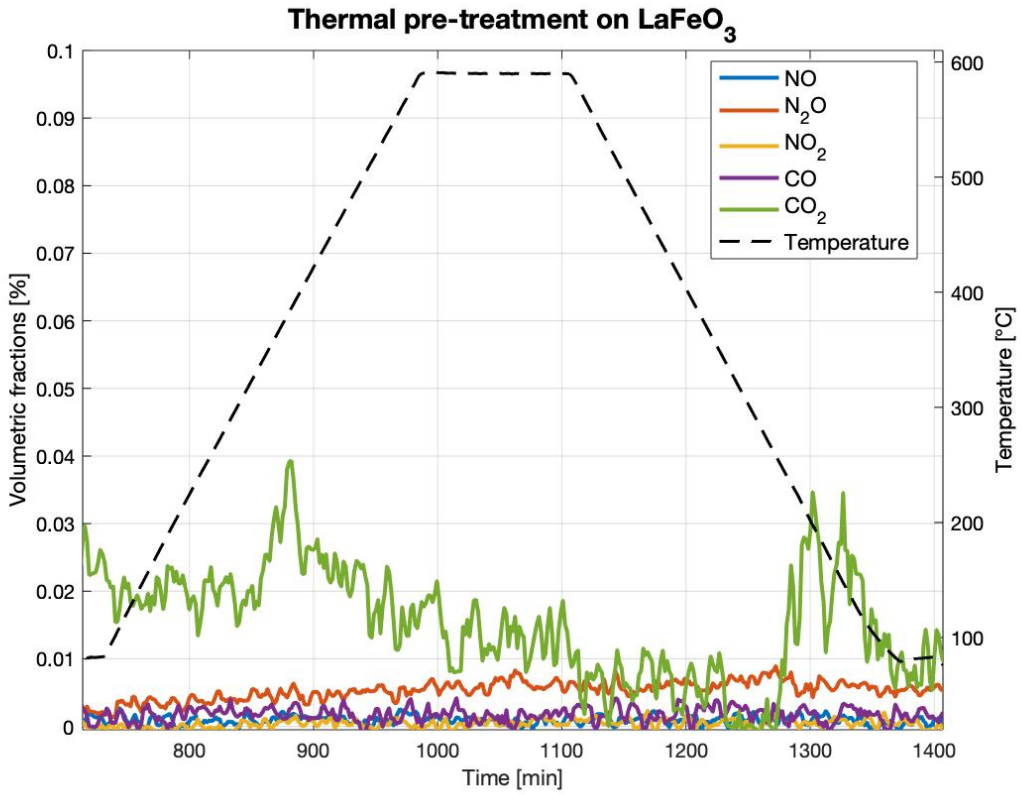

Figure 5.3: Thermal pre-treatment in oxidising atmosphere

By analysing the plots reported in Figure 5.2 and Figure 5.3, it possible to affirm that the only component, among the ones detected, whose release from the powder is not negligeable is CO_2. Therefore, this fact will have to be kept into consideration while analysing the data obtained from the catalytic tests.

5.4 Test reproducibility

In the first couple of catalytic tests, three temperature cycles were carried out, where in the first two cycles the composition of the gas mixture fed to the reactor was the one reported in Table

5.1, while in the third cycle O_2 was added to obtain the mixture with the composition reported in Table 5.2. The temperature profile of those first tests is reported in Figure 5.4.
In those catalytic tests, two cycles, feeding the same mixture, were executed to understand if the concentration's profiles of the component exiting from the reactor obtained in the first cycle were perfectly repeatable in the second cycle. Obtaining repeatable results in the catalytic tests is crucial because a catalyst, to be considered valid, needs to have a great catalytic activity, but it also must assure the reproducibility of results, which means that it must not lose activity or completely deactivate after one single temperature cycle.

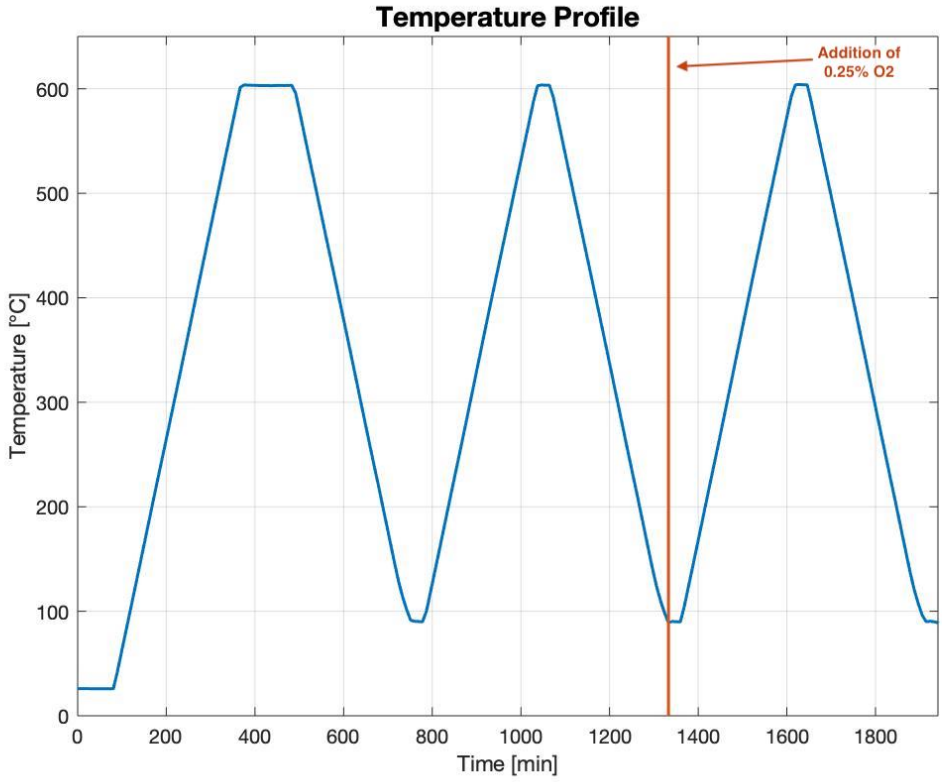

Figure 5.4: Temperature profile of the catalytic tests to study the reproducibility

From the plot reported in Figure 5.5, it is noticeable how the concentration profiles of the various components of the cooling ramp of the first cycle are equal to the ones of the heating and cooling ramps of the second cycle. The concentration profiles of the heating ramp of the first cycle are different from the others because the $LaFeO_3$ was stabilising its structure to obtain an entirely crystalline perovskite structure as it was shown in the XRD plot (Figure 4.14). This particular behaviour of the concentration profiles will be present in all the catalytic tests that will be studied in the paragraphs 5.6, 5.7 and 5.8.
Moreover, the concentration of CO_2 reached a higher value in the first temperature cycle because, as it was pointed out in the paragraph about the thermal pre-treatment, CO_2 is released from the powder and this will also be a recurrent behaviour in all the catalytic tests.

Form Figure 5.5, it is possible to observe a particular behaviour of the concentration profiles, which is more marked in the NO and N_2, but also in the CO and CO_2 profiles. This behaviour is perfectly reproduced in both cycles, in the cooling ramp of the first and both ramps of the second. As it is noticeable from the NO profile of the cooling ramp of the first cycle, around 400-450 °C the NO concentration stopped increasing, as it should have, and it suddenly dropped to a lower value. After the drop, the NO concentration started to increase its value again. This specific behaviour is present in all three ramps and also the CO had the same peak in its profile, at the same temperature. N_2 and CO_2 had specular trends with respect to the reactants.
This behaviour will be observed in all the plots that report the results of the various tests, making it characteristic of the concentration profiles of the tests catalysed by $LaFeO_3$ and not only of the test reported in Figure 5.5.
This trend for the concentration profiles was not expected and an explanation still has to be provided. Finding a cause for this trend was not an objective of this thesis work and therefore in the future, ad-hoc tests will have to be carried out to understand the reasoning behind this variation in activity.

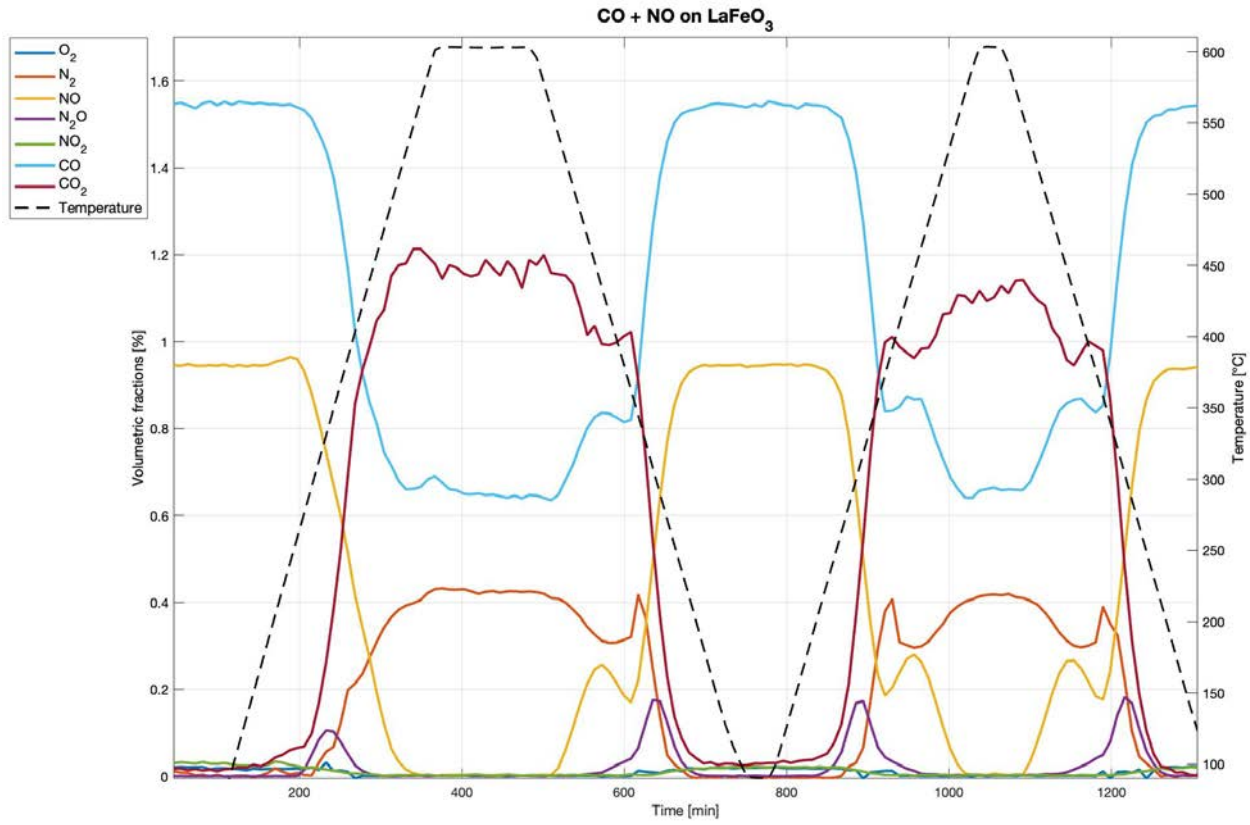

Figure 5.5: Repeatability of results in two temperature cycles of a catalytic test

In order to have a better understanding of how good the reproducibility of the results was for this catalytic test, in the plots displayed in Figure 5.6 and Figure 5.7 the concentration profiles

of the heating and cooling ramps of one reactant, CO, and one product, CO_2, have been overlapped.

In Figure 5.6 and Figure 5.7, it is even more noticeable how the concentration profiles of the two components superimpose perfectly, apart from the ones of the first heating ramp. These two images are reassuring of the fact that the results of these catalytic tests are reproducible.

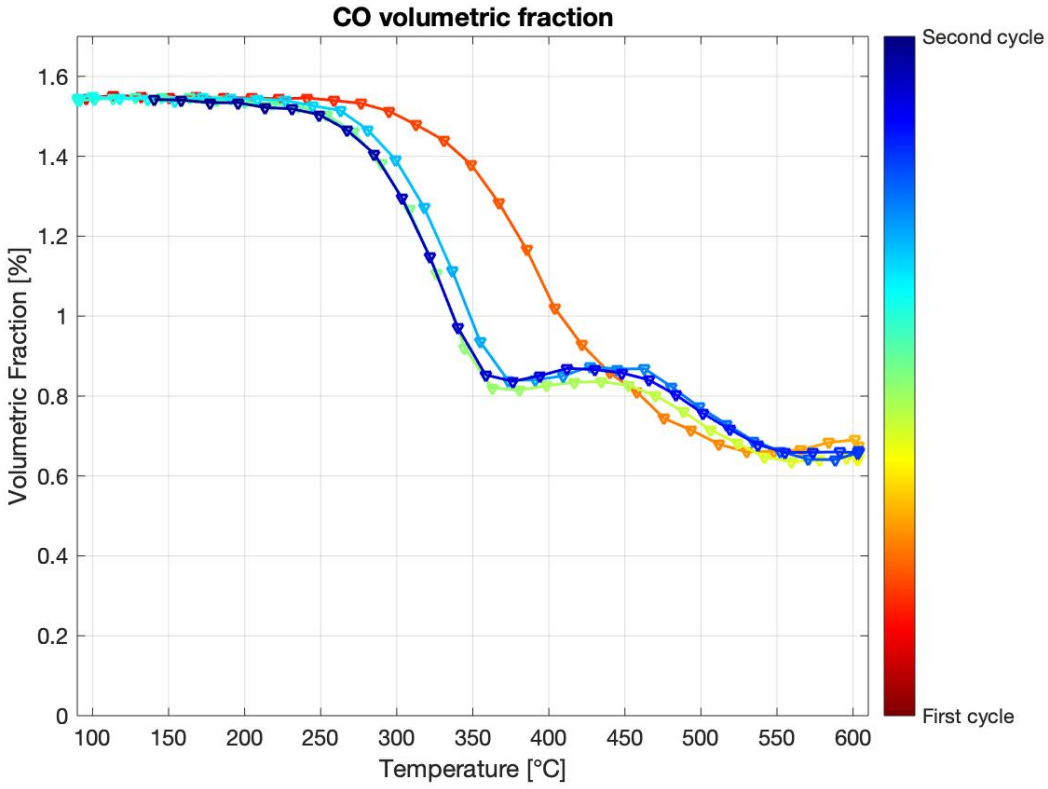

Figure 5.6: CO concentration profiles

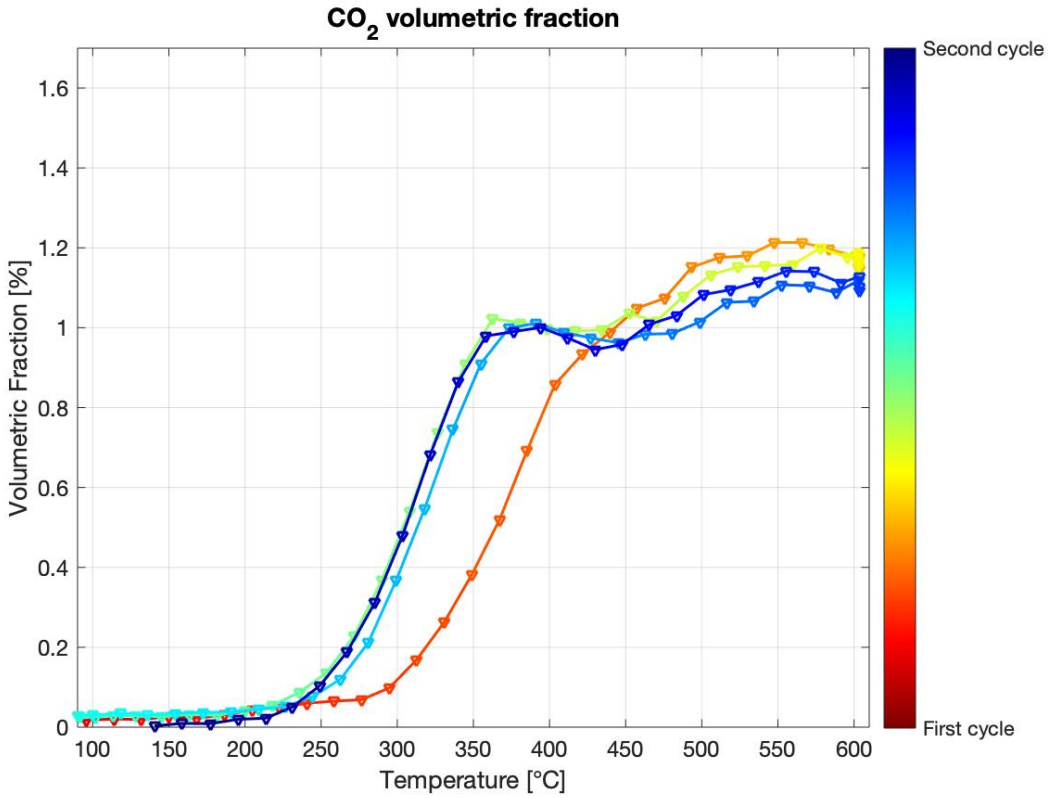

Figure 5.7: CO_2 concentration profiles

Apart from the test whose results are displayed in Figure 5.5, another catalytic test was carried out with three temperature cycles and also in that case there was the confirmation that the results were reproducible. Therefore, because the repeatability of the results was assured, it was decided to conduct the catalytic tests with only two temperature cycle in order not to waste the reactant gases and to shorten the duration of the test.

5.5 Catalytic test campaign

In the following, a detailed description of all the catalytic tests carried out is reported. The flame synthesis parameters that were investigated were the flowrate of combustible and oxidising gas fed to the burner, the precursor solution concentration and the recovery method, as reported in Table 5.4.

The catalytic tests were carried out without and with the presence of O_2 in the gas reacting mixture and at two different values of weight hourly space velocity (WHSV).

Table 5.4: Catalytic test campaign

WHSV [$cm^3/g_{cat}h$]	150,000			170,000				
H_2 flowrate [l/min]	7	8	9	7			8	9
Solution concentration	100%	100%	100%	50%	100%		100%	100%
Recovery method	Filters	Filters	Filters	Filters	Filters	Ultrasonic bath	Filters	Filters

For all the tests reported in Table 5.4, two temperature cycles were executed: one feeding to the reactor the mixture without O_2 and the second one feeding the mixture with O_2.
Each section in the following is dedicated to a specific synthesis parameter. The effect of WHSV and O_2 is separately discussed.

5.6 $LaFeO_3$ prepared with decreasing H_2 flowrates

In this paragraph, the comparison between the catalytic tests carried out with $LaFeO_3$ synthesised in flames fed with different quantities of H_2 and O_2 will be discussed.
The aim is understanding how much these flowrates could be decreased without negatively affecting the catalytic activity.
First, the results of the tests with a $WHSV = 150{,}000\ cm^3/g_{cat}h$ will be presented, then the ones at $WHSV = 170{,}000\ cm^3/g_{cat}h$. The $LaFeO_3$ used in all these catalytic tests was synthesised with a non-diluted solution and recovered by scraping the filters.

5.6.1 Reference WHSV

The first set of catalytic tests was executed at a WHSV value of $150000\ cm^3/g_{cat}h$ to understand how the catalytic activity of $LaFeO_3$ synthesised in flames fed with decreasing H_2 flowrates would be affected.

5.6.1.1 Mixture without O_2

Figure 5.8 and Figure 5.9 show the CO and NO conversion of $LaFeO_3$ with a reacting gas mixture composed of only CO and NO. The conversion of CO was calculated with respect to the CO stoichiometric composition relative to the limiting reactant (NO) as it is reported in the following equation.

$$X_{CO} = \frac{y_{CO}^{in} - y_{CO}}{y_{NO}^{in}} \tag{5.2}$$

In all three cases, the conversion of CO started approximately at 250 °C and very similar values were reached for the maximum conversion. In all three cases, the conversion reached a peak at around 400 °C to then decrease its value and go right back up and reach its maximum value around 600 °C. This peak was more prominent in the $LaFeO_3$ synthesised with the intermediate H_2 flow, i.e. 8 l/min, while in the other two cases the peak was less accentuated. As it was explained before in paragraph 5.4 the presence of this peak still has to be explained.
While the conversion profiles of the $LaFeO_3$ synthesised in flames fed with 8 and 9 l/min of H_2 are overlapping for the majority of the temperature interval, the profile of the $LaFeO_3$ synthesised in flames fed with 7 l/min of H_2 is a little different. The rate at which the conversion profiles of the tests, catalysed with $LaFeO_3$ synthesised in flames fed with 8 and 9 l/min of H_2, increase is greater than that of the blue profile. In fact, while during the tests, in which the reaction was catalysed by $LaFeO_3$ synthesised with 8 and 9 l/min of H_2, the maximum CO conversion value was reached at around 570 °C and then remained constant, the reaction catalysed by the $LaFeO_3$ synthesised with 7 l/min of H_2 reached the maximum CO conversion at 600 °C.

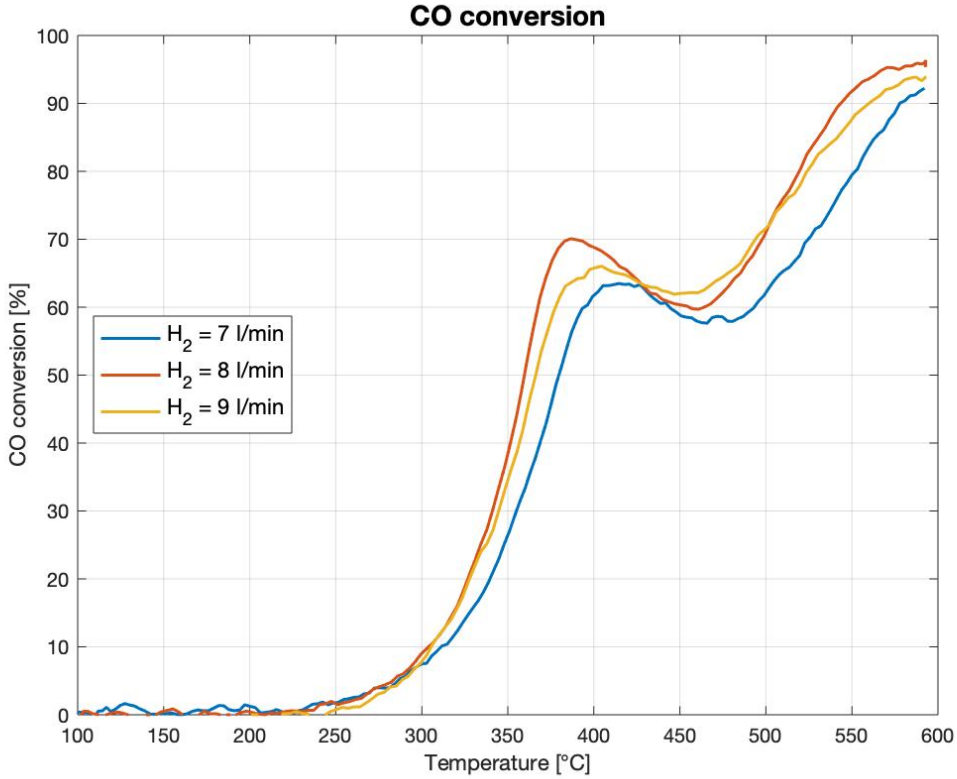

Figure 5.8: CO conversion on $LaFeO_3$ obtained using different H_2 flow rate at the flame

Overall, it could be affirmed that the CO conversion is satisfying in all three cases, reaching respectively the values of 92%, 96% and 94% for the test executed with $LaFeO_3$ synthesised in flames fed with 7 l/min, 8 l/min and 9 l/min.
In Figure 5.9, the NO conversion profiles have been superimposed. Many considerations about the CO conversion profiles are still valid. Also the NO conversion started at around 250 °C,

accordingly with the reaction mechanism which states that the CO and NO conversion evolve simultaneously.

The catalytic performances of the $LaFeO_3$ synthesised with higher flowrates of H_2 were better because a complete conversion for NO was reached and most importantly the conversion kept a constant value when the temperature was constant.

Instead, the $LaFeO_3$ synthesised with 7 l/min of H_2 was not able to catalyse properly the reaction because a complete conversion of NO was not reached and the conversion was not stable during the whole isotherm at 600 °C for 2 h. In fact, its value slightly decreased from 98% to 96%. The fact that the conversion was not stable during the whole isotherm was caused by the non-effectiveness of the catalyst at such a high value of weight hourly space velocity.

However, it is crucial to point out that even if the NO conversion decreased of 2% during the isotherm, that was still an excellent result for the $LaFeO_3$ synthesised in flames fed with 7 l/min of H_2 because the test was carried out with a weight hourly space velocity of $150{,}000\ cm^3/g_{cat}h$, which is ten times higher than the ones set for the tests cited in literature.

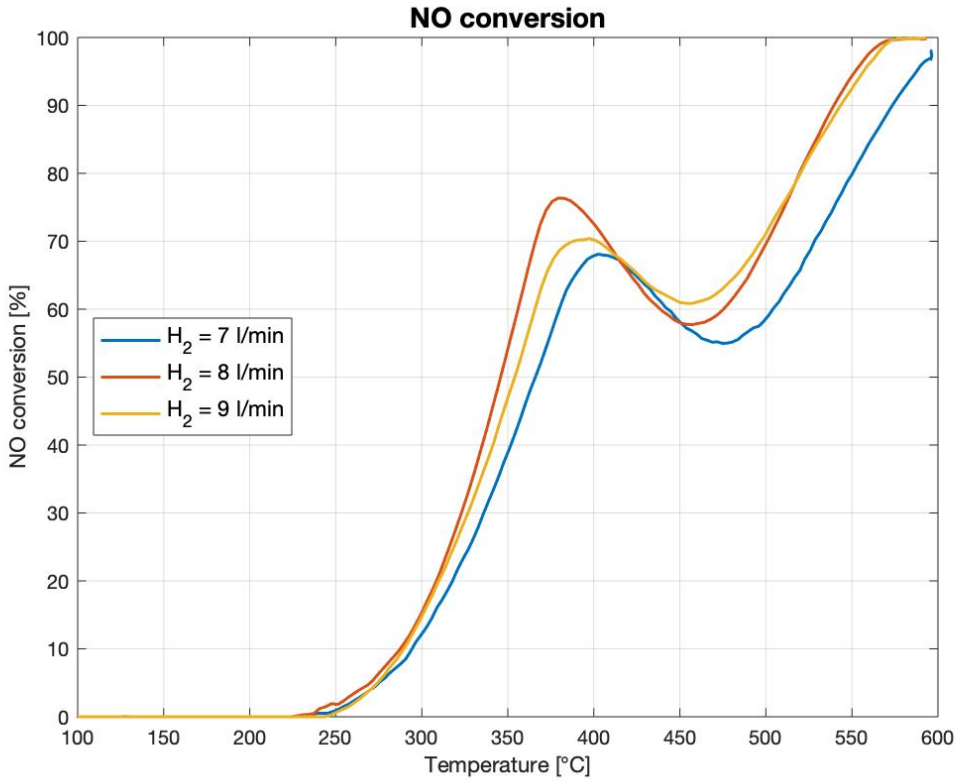

Figure 5.9: NO conversion on $LaFeO_3$ obtained using different H_2 flow rate at the flame

Therefore, it is possible to assert that the three types of perovskite, prepared with different H_2 flow rate at the flame, provided similar performances both in the dynamic and stationary part of the catalytic tests, and therefore the catalytic activity of $LaFeO_3$ is not significantly affected by the flowrates of fuel and oxidising gas that feed the flames, in which the powder is synthesised, if their variation is not substantial.

5.6.1.2 Mixture with O_2 in defect

The comparison between the catalytic performances of the three types of perovskites by means of the conversion profiles of the reactants was executed also for the second temperature cycle of the catalytic test, when O_2 was added to the reacting gas mixture; results are shown in Figure 5.10 and Figure 5.11.

In Figure 5.10, the comparison between the CO conversion profiles is displayed, where the conversion of CO was calculated with respect to the sum of the CO stoichiometric compositions relative to the first limiting reactant, NO and the second liming reactant, O_2 as it is reported in the following equation.

$$X_{CO} = \frac{\left(y_{CO}^{in} - y_{CO}\right)}{\left(y_{NO}^{in} + y_{O_2}^{in}\right)} \tag{5.3}$$

With a lean O_2 gas reacting mixture, the CO conversion started at a lower temperature (around 200 °C) with respect to first temperature cycle, when O_2 was not present in the mixture fed to the reactor. This change suggested a variation in the reaction mechanism, due to the presence of O_2. In fact, the conversions of CO and NO were not simultaneous, with CO reaching higher conversion values and NO stopping at lower values of conversion.

The three profiles did not follow exactly the same trend. In fact, the profile associated to the $LaFeO_3$, synthesised in flames fed with 7 l/min of H_2, presented a peak around 450 °C that was also observed in the plots referred to first temperature cycle (mixture without O_2); while the other two profiles did not have any peaks.

The two $LaFeO_3$ synthesised with the higher flowrates of H_2 provided full conversion of carbon monoxide, while the third one reached a maximum of 95%.

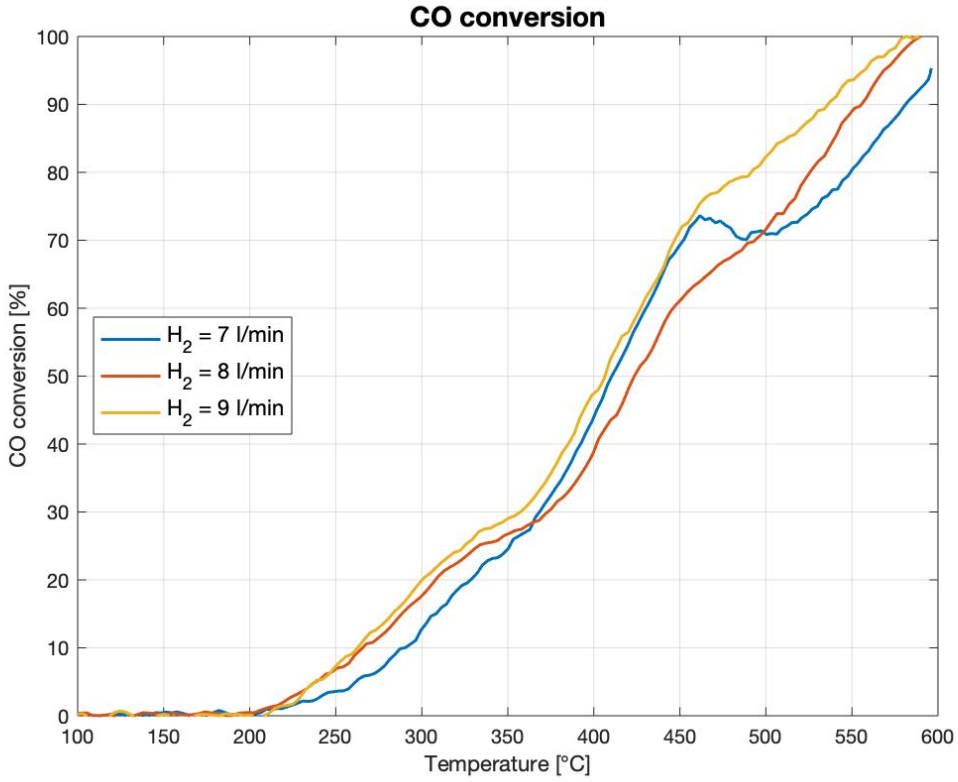

Figure 5.10: CO conversion in the presence of O_2 on $LaFeO_3$ obtained using different H_2 flow rate at the flame

In Figure 5.11, the NO conversion is reported. In all three cases, the conversion of NO at low temperatures is not precisely zero; in the presence of O_2, some NO converts to NO_2 even at ambient temperature.

Beside this, the reduction of NO did not begin before the reactor reached the temperature of 350 °C and in all three cases it reached similar values around 80-85%.

As it happened with the comparison of the CO conversion profiles, also in this case the three profile did not follow the same trend, but the one referred to the $LaFeO_3$ synthesised in flames fed with 7 l/min of H_2 presented a peak while the others did not.

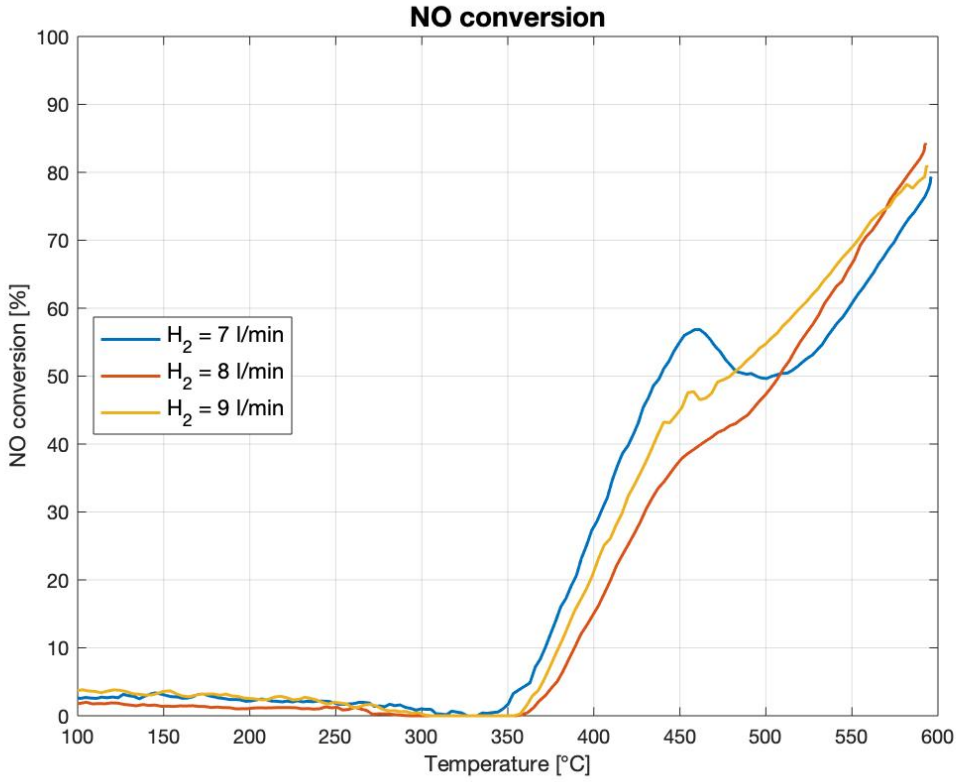

Figure 5.11: NO conversion in the presence of O_2 on $LaFeO_3$ obtained using different H_2 flow rate at the flame

With the presence of O_2, the three types of perovskite provided similar performances in the stationary part of the catalytic tests, but their catalytic activity was not as equal in the dynamic part of the tests. Despite, the small differences in the profiles' trend, it is possible to assert that also with this type of mixture the catalytic activity of $LaFeO_3$ is not strongly affected by the flowrates of combustible and oxidising gas utilised to feed the flame, in which the powder is synthesised, if their variation is not substantial.

After analysing the profiles of CO and NO conversion with a lean O_2 gas reacting mixture, it is possible to affirm that the reaction mechanism proposed in paragraph 5.1 changes with the presence of O_2 in the reacting mixture.

In fact, the CO reacts preferentially with the O_2 gas according to the reaction 1,10,12 and 13 and, because the O_2 present in the mixture is under stoichiometric, a certain quantity of the lattice O_2 still is involved into the mechanism, according to reaction 2, but only at higher temperatures (above 350 °C).

The NO reacts according to the reactions 3 and 4, the adsorption of NO on an inactive site and an active site, and according to reaction 5, which is the rate determining step because, from microkinetic calculations, it resulted as the reaction with the highest activation energy. A consequence of this is that the lattice O_2 is not completely restored by reaction 5 and therefore the higher conversion of CO is given by the lattice O_2 for the bulk of the perovskite which start to spread.

This is the reason why the conversion of CO and NO are not simultaneous and the one of CO reaches higher values when O_2 is present in the mixture.
This variation in the reaction mechanism, for the second temperature cycle when a lean O_2 gas reacting mixture is fed to the catalytic reactor, is also valid for all the other tests that will be reported in the next sections.

5.6.2 Higher WHSV

The second set of catalytic tests was executed with the same batches of $LaFeO_3$ used in the tests described in the previous paragraphs, but the value of the WHSV at which the tests were carried out was increased at $170{,}000\ cm^3/g_{cat}h$.
The value of the weight hourly space velocity was increased to understand how the catalytic activity of $LaFeO_3$ would be affected by this and to examine if the WHSV limit, at which the catalyst could perform well and assure to be able to keep a constant maximum conversion, had been passed or not.
It is crucial to remember that the higher the WHSV value at which the activity of a catalyst is great, the better; and the WHSV value of $170{,}000\ cm^3/g_{cat}h$, set for these catalytic tests, is extremely high in comparison to the values usually set for the tests cited in literature or even with respect to the value set for the tests of the European project "Partial PGMs".

5.6.2.1 Mixture without O_2

To study the differences in the performances of the $LaFeO_3$ synthesised in flames fed with decreasing H_2 flowrates, the conversion profiles correspondent to the cooling ramp of the first temperature cycle were compared. The purpose was to understand if the catalysts had comparable catalytic activities and provided the same performances.
In the plot reported in Figure 5.12, the profiles of the CO conversion, which were calculated with respect to the CO stoichiometric composition relative to the limiting reactant (NO), are shown.
As it is noticeable, in all three cases, the CO conversion reached the same maximum value which however was not kept constant during the isotherm at the maximum temperature. This is a clear sign that the upper limit of the WHSV has been reached and passed, which means that the mass of catalyst in the fixed bed cannot guarantee a satisfying catalytic performance with such a high total flowrate of reacting gas mixture.
The $LaFeO_3$, that had the worst performance, was the one synthesised with 8 l/min of H_2 because with this catalyst the conversion value decreased the most during the isotherm, going from 93% to 79%. For the other two perovskites, the decrease in conversion was not as substantial; for the $LaFeO_3$ synthesised in a flame fed with 7 l/min of H_2 there was a decrement of 3 % while for the one fed with 9 l/min of H_2 there was a diminution of just 1%.

Another noticeable difference between the profiles of the perovskites synthesised in flames fed with different flowrates of H_2 is the temperature at which they start to catalyse the reaction. The $LaFeO_3$ produced in flames fed with 7 and 9 l/min of H_2 started to catalyse the reaction between CO and NO at around 250 °C, while the one produced in flames fed with 8 l/min of H_2 began between 300 °C and 350 °C.

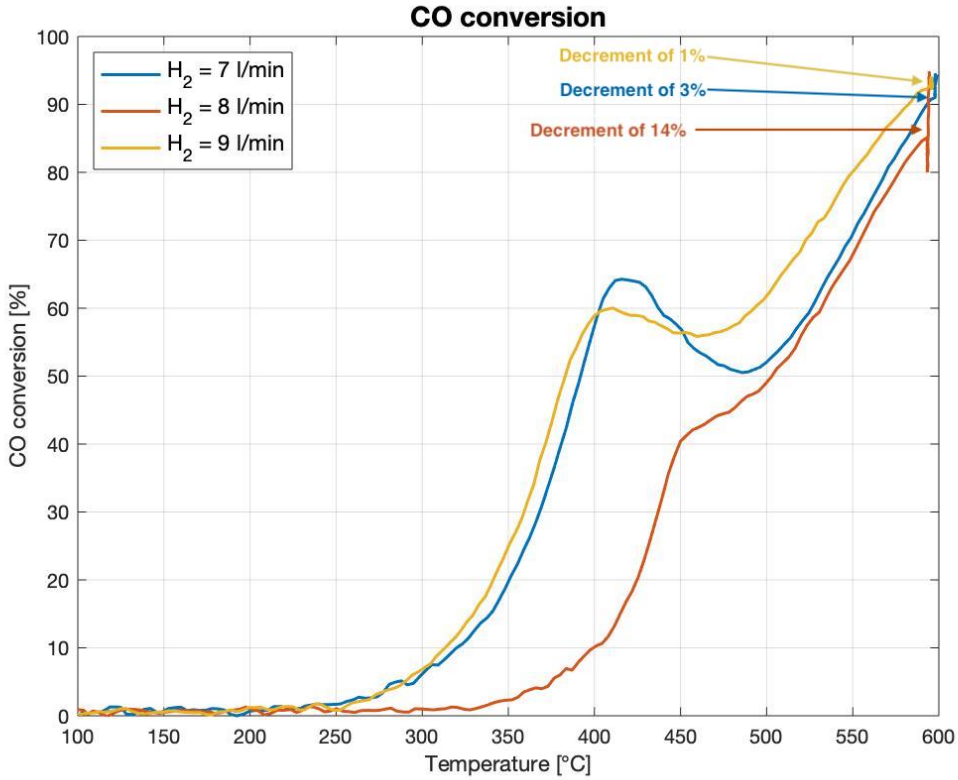

Figure 5.12: CO conversion on $LaFeO_3$ obtained using different H_2 flow rate at the flame

The decrement of the CO conversion during the isotherm is better portrayed in Figure 5.13, where the results are reported with respect to time. It is easier to observe that the concentration of the reactant is not stable during the isotherm.

This figure showcases very well the difference in the trends of the profiles obtained with $LaFeO_3$ synthesised in flames fed with 7 l/min or 9 l/min and the one synthesised in flames fed with 8 l/min. Such a substantial discrepancy between the behaviours of the various tests was not expected because the ESEM imaging reported in the paragraph 4.2.1 did not show any particular differences between the size of the particles.

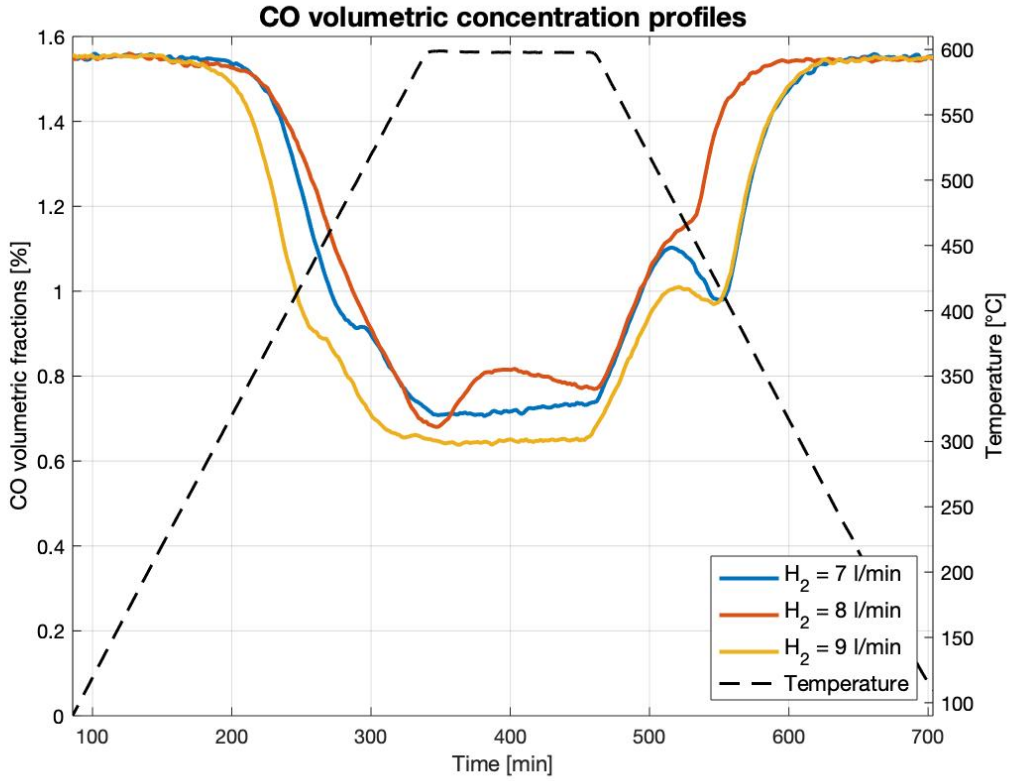

Figure 5.13: Comparison of CO volumetric concentration profiles

The majority of the comments asserted about the CO conversion profiles are valid also for the NO conversion profiles which are compared in Figure 5.14.

With all three types of $LaFeO_3$, nitric oxide is completely converted at the maximum temperature. However, the reduction of NO to N_2 was not constant during the isotherm and therefore the NO conversion value decreased.

The diminution of NO conversion is more accentuated than the one of CO conversion in all three cases; at the highest temperature of 600 °C, the decrement was respectively of 6%, 20% and 2% starting from the profile associated with the $LaFeO_3$ synthesised in the flames fed with the least amount of H_2.

In line with the reaction mechanism, nitric oxide started to be converted at the same temperature as CO did in all three cases. $LaFeO_3$ synthesised in flames fed with 7 or 9 l/min of H_2 began to catalyse the reaction at around 250 °C, while the one at 8 l/min in between 300 °C and 350 °C.

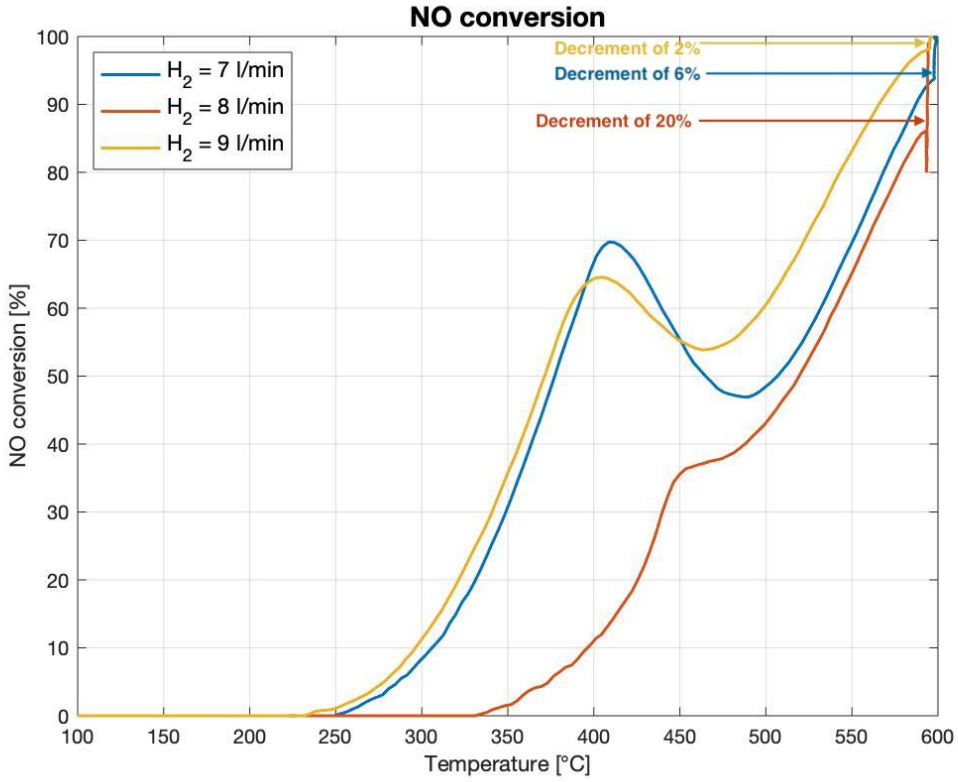

Figure 5.14: NO conversion on $LaFeO_3$ obtained using different H_2 flow rate at the flame

From Figure 5.14, the trend of the profiles is not clearly portrayed during the isotherm. To be able to examine better this aspect of the plot, in Figure 5.15, the NO volumetric concentration profiles of the first temperature cycle with respect to time are reported.

As it was anticipated by the NO conversion profiles, it is observable that for all the tests, the NO concentration did not result stable during the isotherm. The variation between the initial and final value of the concentration during the isotherm is less accentuated in the profile referred to the $LaFeO_3$ synthesised in flames fed with 9 l/min of H_2 and more accentuated in the profile referred to the $LaFeO_3$ synthesised in flames fed with 8 l/min of H_2.

Therefore, it is possible to affirm that carrying out the catalytic tests with a WHSV of 170,000 $cm^3/g_{cat}h$ is not ideal because the $LaFeO_3$ is not able to perform consistently during the isotherm at the maximum temperature of 600 °C. This means that the upper limit of the WHSV, for which the catalyst is capable of properly catalysing the reaction assuring a stable conversion of the reactants, has been passed.

However, the weight hourly space velocity of these catalytic tests was extremely high with respect to the values usually kept in the tests cited in literature; therefore, the results obtained in the tests, in which the $LaFeO_3$ synthesised in flames fed with 7 l/min and 9 l/min, in which the decrement in conversion during the isotherm was not substantial could still be considered satisfying with respect to the high value of WSHV set.

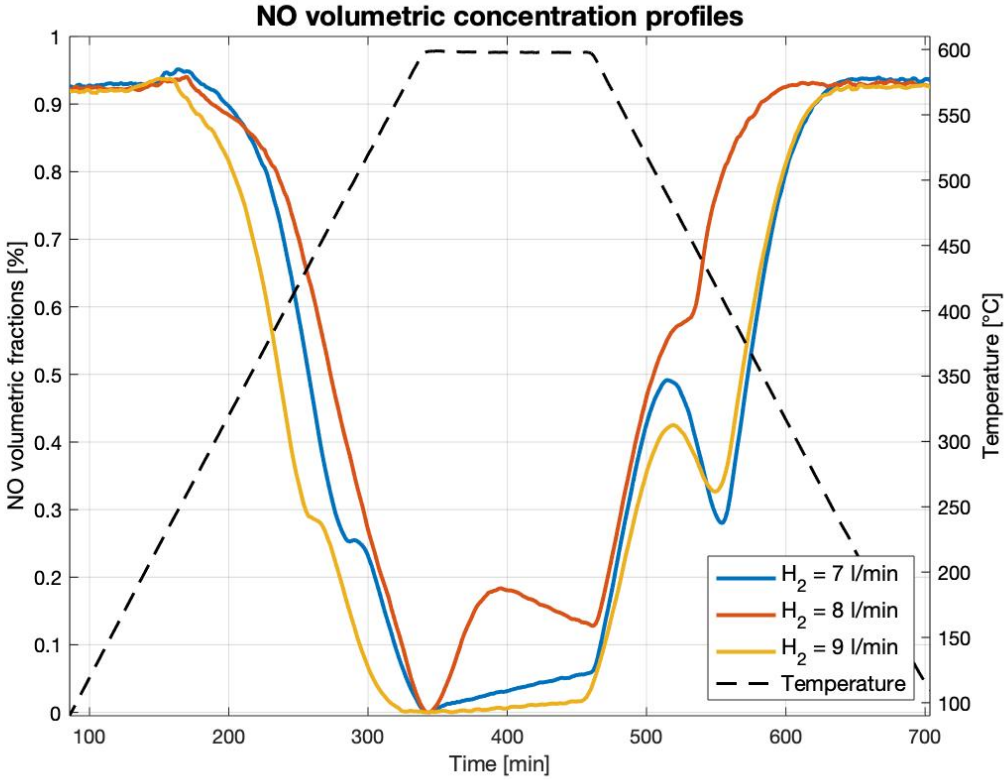

Figure 5.15: Comparison of NO volumetric concentration profiles

In Figure 5.12 and Figure 5.14, it is noticeable how the test, which was catalysed by $LaFeO_3$ synthesised in flames fed with 8 l/min of H_2, obtained worst results, both in the dynamic and stationary part of the test, with respect to the other two tests. Figure 5.16 represents the catalytic bed, made with the $LaFeO_3$ synthesised in flames fed with 8 l/min of H_2, at the end of the catalytic test. This could give an explanation to the particular behaviour of that test because that was the only test in which the catalytic bed shrunk. The shrinkage of the catalytic bed could have led to an increment of the WHSV value, consequently worsening the catalytic performance of $LaFeO_3$. The shrinkage might have been caused by the fact that more carbon residues were present in the catalyst and, when these were emitted from the catalyst during the heating ramp of the first temperature cycle as CO_2, the catalytic bed shrunk, and it lost mass. This could be corroborated by the results of the EDS analysis which showed that the sample of $LaFeO_3$ synthesised in flames fed with 8 l/min of H_2 had a consistent atomic percentage of carbon residues.

Figure 5.16: Shrinkage of catalytic bed

To have a better understanding of the effect of the WHSV at which catalytic tests are carried out, the CO conversion profiles of the tests, in which $LaFeO_3$ synthesised in flames fed with 7 l/min of H_2 was utilised and that were carried out with different WHSV, were compared (Figure 5.17). As it was predictable, the $LaFeO_3$ was more active at lower values of WHSV, when the contact time between the catalyst and the gas reacting mixture was longer. This is true also for the perovskites synthesised in flames fed with higher flowrates of H_2 and when in the gas reacting mixture O_2 is present.

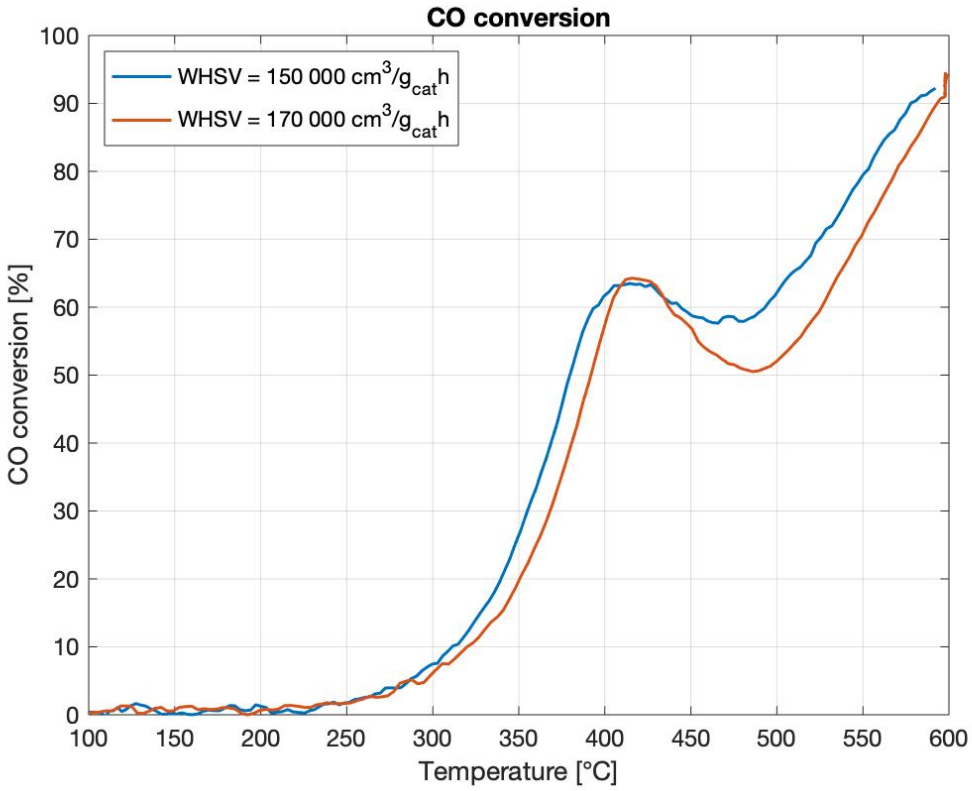

Figure 5.17: CO conversion on $LaFeO_3$ tested with different values of WHSV

5.6.2.2 Mixture with O_2

The comparison between the catalytic performances of the three types of perovskites by means of the conversion profiles of the reactants was executed also for the second temperature cycle of the catalytic test, when O_2 was added to the reacting gas mixture.

The comparison of the profiles referred to the CO conversion with a lean O_2 reacting gas mixture is reported in Figure 5.18.

It is observable how the CO did not reach complete conversion in any of the three cases. The CO conversion in the tests catalysed with $LaFeO_3$ synthesised in flames fed with 7 or 9 l/min of H_2 is constant during the isotherm, instead in the remaining test, the conversion value kept increasing during the isotherm because the stability had not been reached yet.

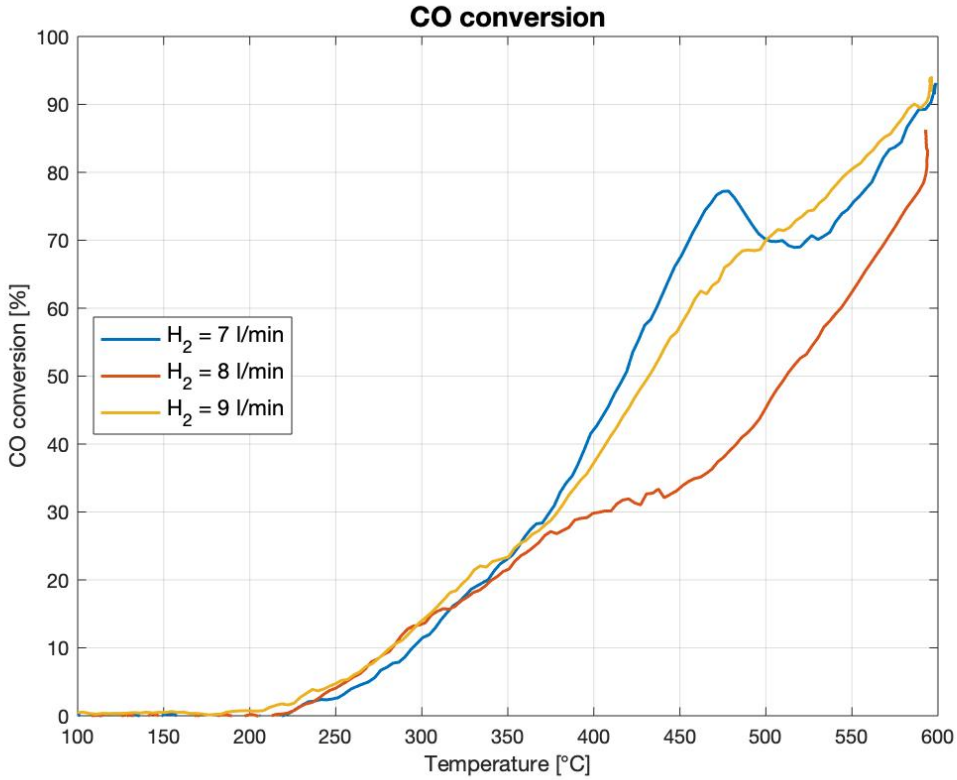

Figure 5.18: CO conversion in the presence of O_2 on $LaFeO_3$ obtained using different H_2 flow rate at the flame

To complete the analysis of the catalytic tests executed with a WHSV of 170,000 $cm^3/g_{cat}h$, the profiles referred to the NO conversion were compared as it can be observed in Figure 5.19. At low temperatures, the conversion of NO is not null because part of it present in the reacting mixture was oxidised to NO_2. In all three cases, the reduction of NO to N_2 is not satisfying, but the lowest conversion value was obtained in the test where the $LaFeO_3$, synthesised in flames fed with 8 l/min of H_2, was used.

As it was explained in the previous paragraph, the presence of O_2 in the reacting gas mixture changed the reaction mechanism, proposed at the paragraph 5.1. With the presence of O_2 in the gas reacting mixture, the oxidation of CO was favoured, and this is demonstrated by the fact

that the conversion of CO started at a lower temperature with respect to the first temperature cycle in which O_2 was not present. Instead, the reduction of NO was not as favoured as in the cycle without oxygen.

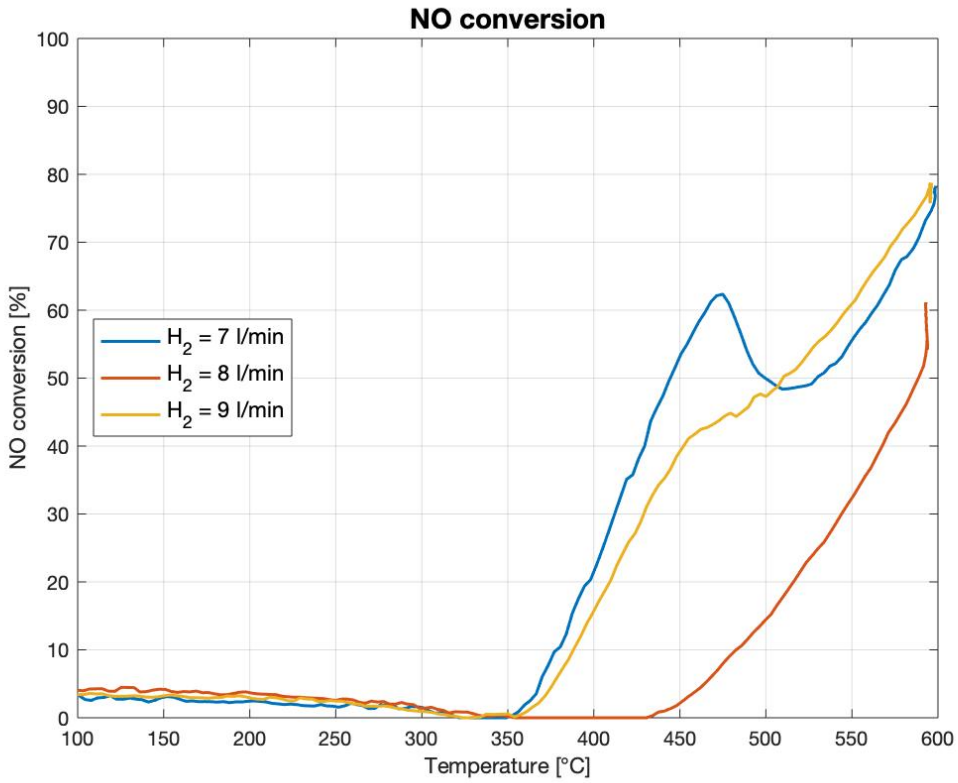

Figure 5.19: NO conversion in the presence of O_2 on $LaFeO_3$ obtained using different H_2 flow rate at the flame

5.7 $LaFeO_3$ prepared with different precursors' dilution

The effect on the catalytic activity of the concentration of the metal precursors in the solution, utilised to synthesise the perovskite, was also investigated.

In order to achieve this comparison, two batches of $LaFeO_3$ were synthesised in flames, obtained with the minimum H_2 flow rate (7 l/min of H_2 and 6 l/min of O_2), one utilising the initial non-diluted solution and the other one diluting the same solution of 50%. Both batches of catalyst utilised were scraped directly from the filters and both catalytic tests were carried out with a WHSV value of 170,000 $cm^3/g_{cat}h$.

For simplicity, the initial non-diluted solution will be considered to have a 100% concentration, while the solution in which the same quantity of initial solution and deionised water were added will be considered to have a 50% concentration.

5.7.1 Mixture without O_2

In order to fully understand which catalyst was the most active towards the simultaneous oxidation of CO and reduction of NO, and therefore which was the test with the highest values of conversion, the results of two tests, both the ones of the first temperature cycle without O_2 and the ones of the second temperature cycle with O_2, were compared.

Firstly, the conversion profiles of the cooling ramp of the first temperature cycle, when the gas reacting mixture did not contain O_2, were compared. As it is noticeable from the plot reported in Figure 5.20, the CO conversion profiles have very similar trends, but the maximum CO conversion value, reached in the test catalysed by the $LaFeO_3$ synthesised with the less concentrated solution, was lower. This is not the behaviour that was expected because, as it was observed from the ESEM images reported in Chapter 4, the batch produced with a less concentrated solution had a higher percentage of smaller particles and therefore it should have had a greater catalytic activity. Instead, from the profiles reported in the plot it resulted that the batch synthesised from a more concentrated solution resulted more catalytically active.

This could have happened because the size of the particles produced in every synthesis was not homogeneous and batches with a higher percentage of smaller particles still had bigger particles and vice versa. Therefore, the small amount of $LaFeO_3$ placed in the catalytic reactor could have had a different average particle size with respect to the one of the entire batch. This could explain the discrepancy between the expected results based of the ESEM images and the actual results obtained.

In both cases, the CO conversion was not constant during the isotherm, which is an indication of the fact that the WHSV value of these tests had pass the maximum value that would guarantee a good catalytic performance.

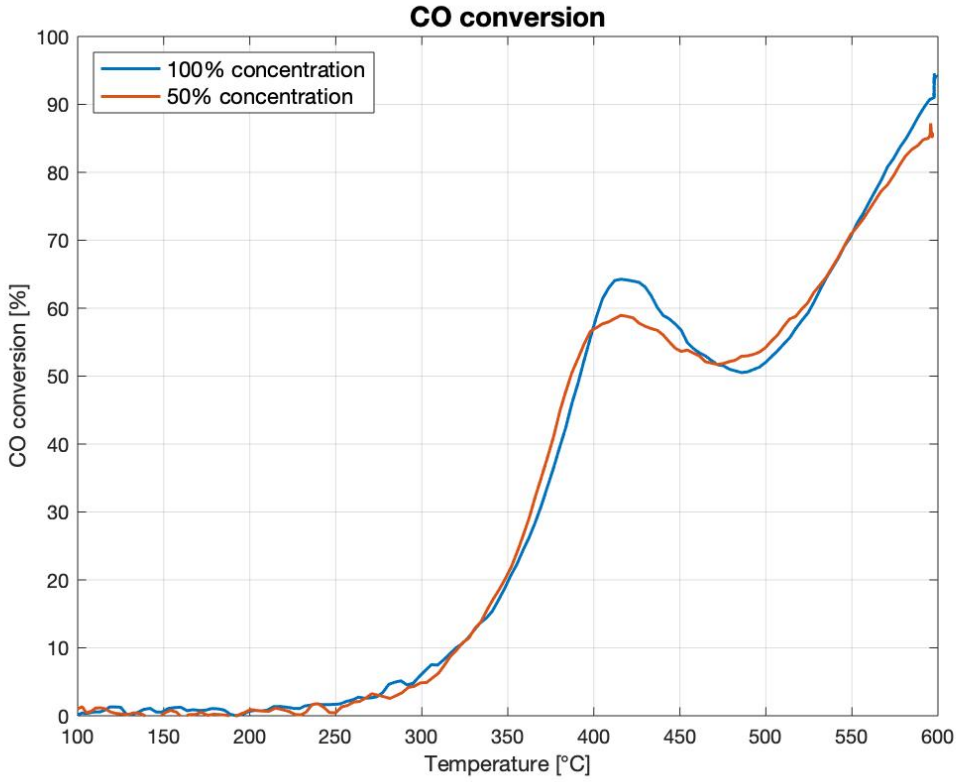

Figure 5.20: CO conversion on $LaFeO_3$ obtained using solutions with different concentrations

The NO conversion profiles had also very similar trends as it is observable from Figure 5.21. In both tests, NO started to convert at around 250 °C, but the maximum conversion values were slightly different. In the test that used the $LaFeO_3$ synthesised with the more concentrated solution, the NO fully reduced to N_2 at the highest temperature, but the conversion did not have a stable value during the isotherm. In the other test, NO converted only to a maximum of 90%, and still the conversion did not keep a constant value during the isotherm. As it was explained before, this was caused by the fact that a too high WHSV was chosen for the tests.

However, it is noticeable that the maximum value reached by the conversion profiles, both for the CO and NO, was more stable for the test in which the $LaFeO_3$, synthesised from the less concentrated solution, was utilised. In fact, in that test the maximum value decreased less during the isotherm.

Also in this case, there was a discrepancy between the expected and the actual behaviour. In fact, the $LaFeO_3$ synthesised with a more concentrated solution resulted more catalytically active even if it had a higher percentage of bigger particles.

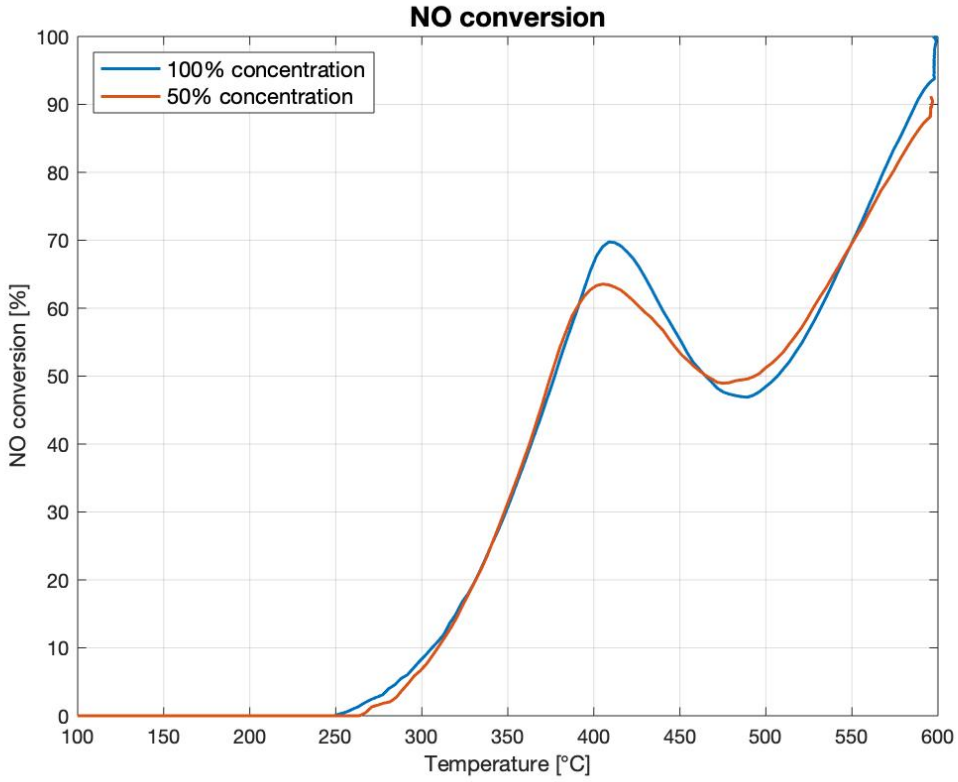

Figure 5.21: NO conversion on $LaFeO_3$ obtained using solutions with different concentrations

5.7.2 Mixture with O_2 in defect

After analysing the results from the first temperature cycle without O_2 in the gas reacting mixture, the conversion profiles of the heating ramp of the second temperature cycle were examined to observe the catalytic performance of $LaFeO_3$ with the presence of O_2 in the mixture fed to the catalytic reactor.

In Figure 5.22, the CO conversion profiles of the two tests are reported. In both cases, the carbon monoxide started to convert at around 200 °C and the maximum value of conversion reached by the profiles are close. The discrepancy that was detected in the previous comparisons is present also here because the $LaFeO_3$ synthesised with the more concentrated solution is the one with a slightly better catalytic activity.

A difference between the two profiles is that the one of the test, in which the $LaFeO_3$ synthesised with the fully concentrated precursor solution was utilised, presents a peak which is not there in the other one.

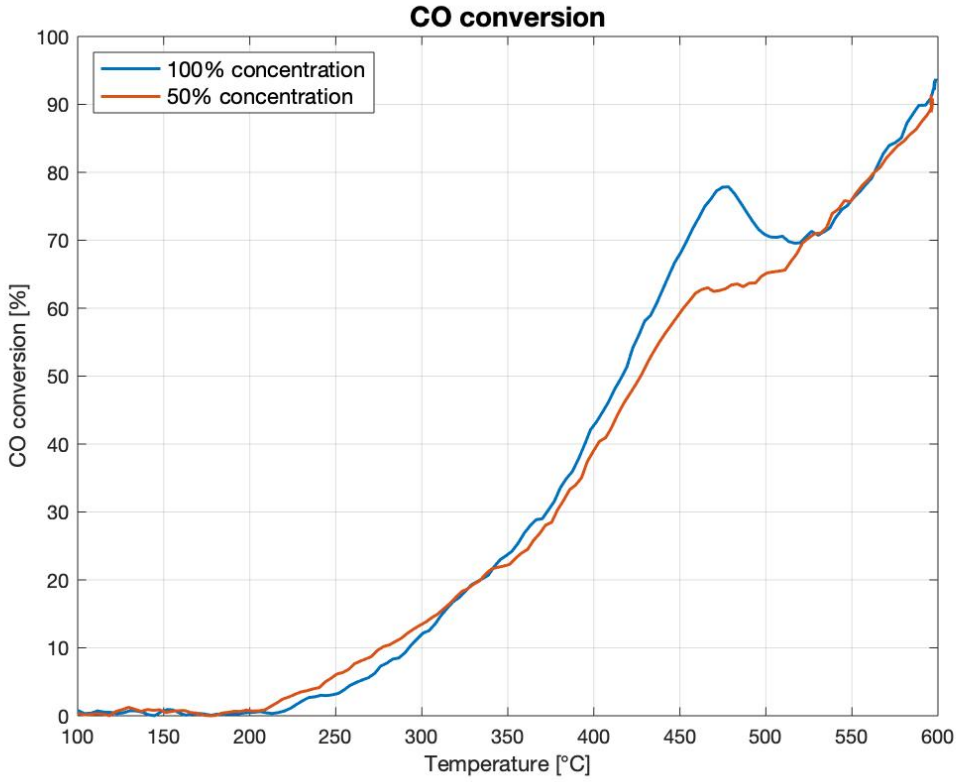

Figure 5.22: CO conversion in the presence of O_2 on $LaFeO_3$ obtained from solutions with different concentrations

As it happened for the CO, also the results related to the NO reduction, obtained from the two tests, are very similar as it is possible to observe from Figure 5.23.

In fact, in both cases NO started to reduce at around 350 °C and the maximum conversion values achieved were very close to each other. At low temperatures, the consumption of NO was given by its oxidation into NO_2 by means of O_2. It is noticeable that the conversion profile of the test, in which the $LaFeO_3$ synthesised with the less concentrated solution was utilised, has a lower value and therefore the formation of NO_2 was inferior in that case.

As it was observed with all the other types of $LaFeO_3$, the conversion of CO and NO was not simultaneous because of the variation of the reaction mechanism caused by the presence of O_2 in the mixture.

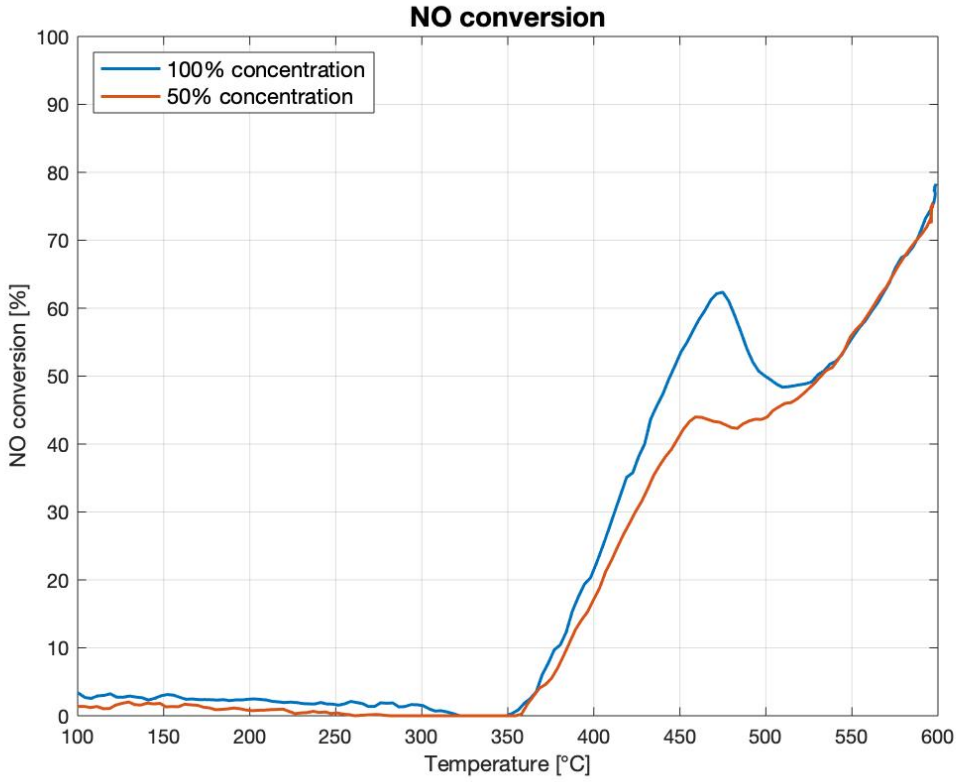

Figure 5.23: NO conversion in the presence of O_2 on $LaFeO_3$ obtained from solutions with different concentrations

After examining all the reactants' conversion profiles of the tests in which various levels of concentration of the precursor solution were studied, it was observed that the variation of the concentration of the solution utilised to synthesise the $LaFeO_3$ had a different effect on the first temperature cycle, in which O_2 was not present in the gas reacting mixture and on the second temperature cycle in which O_2 was fed.

When O_2 was not fed, the two $LaFeO_3$ synthesised with precursor solution with different concentrations had similar catalytic performances in the dynamic part of the tests, but different catalytic performances in the stationary part. Instead, when a lean O_2 gas reacting mixture was fed to the reactor the opposite occurred; in fact, the CO and NO profiles reached the same maximum conversions but had different trends in the dynamic part of the temperature cycle.

However, the expected result was not obtained because the $LaFeO_3$ synthesised with the less concentrated solution did not have a significantly larger catalytic activity even if the ESEM images showed that the sample had a higher percentage of smaller particles. But, the fact that the difference in the particle size was not substantial between the two samples and that smaller particles were present in the $LaFeO_3$ batch synthesised with the more concentrated solution and bigger particles were present in the one synthesised with the less concentrated solution might have influenced the results. The particle size of the batch synthesised from a solution with a halved level of concentration with respect to the initial one was not substantially different from

the particle size of the initial one because the particle diameter is proportional to the cubic root of the molar concentration of the solution.
Therefore, for the $LaFeO_3$ used to catalyse the CO oxidation and simultaneous NO reduction, it was not enough to halve the precursor solution concentration to have a substantial reduction of the particle size and a significant increment of the catalytic activity as a consequence. The solution should have been diluted more in order to try to considerably decrease the particle size so to increase the catalytic activity.

5.8 $LaFeO_3$ recovered with different procedures

Here it is examined if the recovery method of the perovskites (either obtained by scraping the filters or by cleaning them in the ultrasonic bath) could have some influence on their catalytic activity.
Therefore, two samples of $LaFeO_3$, obtained from the same synthesis executed with flames fed with 7 l/min of H_2 and 6 l/min of O_2 and with a precursor solution with the reference concentration (undiluted), were catalytically tested with a WHSV of 170,000 $cm^3/g_{cat}h$. The only difference between the two samples was the catalyst recovery at the end of the synthesis which was either obtained by scraping the filters or by cleaning them in the ultrasonic bath.
As it was explained in Chapter 2, the catalyst, that was scraped from the filters, did not undergo any further treatment; while the one that was obtained from the ultrasonic cleaning of the filters was also placed in the muffle to evaporate all the deionised water utilised for the cleaning.
To understand if a different recovery method could have brought an improvement to the results of the tests in which the perovskites had been scraped from the filters, a WHSV of 170,000 $cm^3/g_{cat}h$ was chosen because it was the condition in which the $LaFeO_3$ had the worst results and therefore any kind of improvement would have been very noticeable.

5.8.1 Mixture without O_2

As it happened in the previous paragraphs, first the conversion profiles obtained with the gas reacting mixture without O_2 are compared and then the ones acquired from the temperature cycle in which O_2 was inserted in the reacting mixture.
In Figure 5.24, the comparison between the CO conversion profiles is reported. In both cases, the CO conversion started at around 200 °C, but it is in the dynamic part of the test, when the temperature is changing, that it is possible to observe a significant difference between the two profiles. The rate of conversion of the catalytic test, in which the $LaFeO_3$ utilised was recovered through ultrasonic cleaning, is much greater. For example, at 350 °C the CO conversion value of the test in which $LaFeO_3$ recovered via ultrasonic cleaning is 40 % higher than the other one, with the two values being 20 % and 60 % respectively. Following this example, at each temperature value, the CO conversion profile, of the test in which $LaFeO_3$ recovered via

ultrasonic cleaning was used, reached higher values of conversion with respect to the other profile; in fact, in that test, the maximum conversion value was reached at around 530 °C, while in the other test, in which $LaFeO_3$ scraped directly from the filters was used, it was obtained only at 600 °C. The maximum CO conversion reached employing the scraped powder was slightly higher than the one achieved with the catalyst from ultrasonic cleaning, but while the first one did not have a constant value during the isotherm, the second one did. In fact, apart from obtaining a high conversion, it is also important that this value is maintained and that it does not decrease when the temperature is constant.

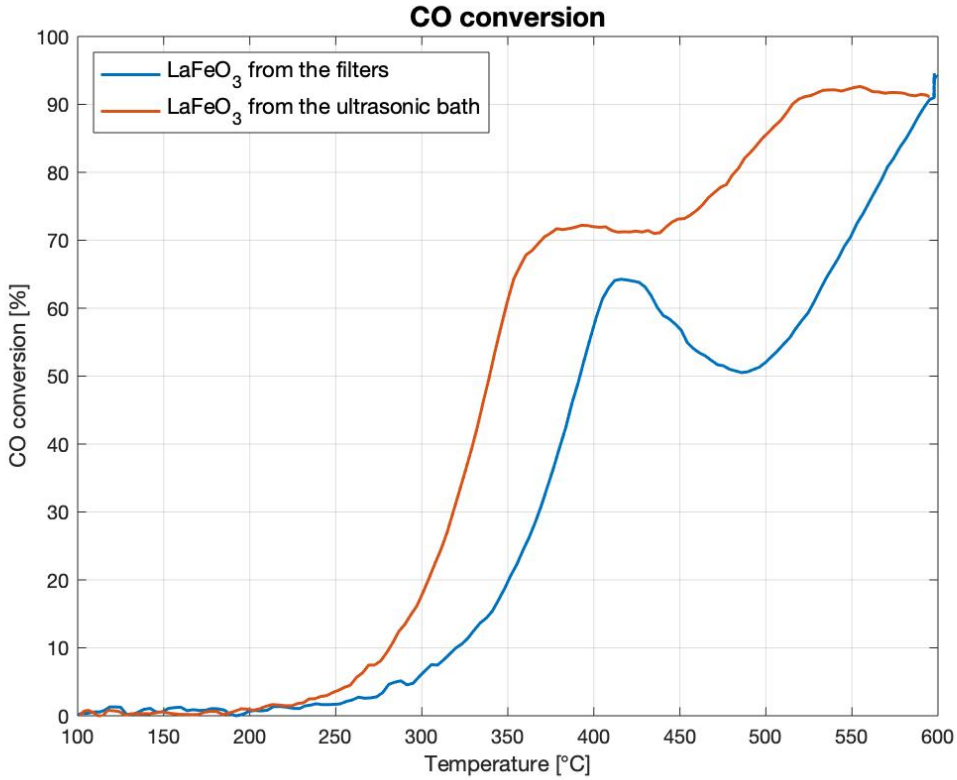

Figure 5.24: CO conversion on $LaFeO_3$ recovered with different methods

Because the reaction model assumed is the reduction of NO with the simultaneous oxidation of CO, the conversion of CO and NO have similar profiles and therefore the assertions about the CO conversion are also valid for the NO profiles reported in Figure 5.25.

The dynamic catalytic activity of the $LaFeO_3$, recovered via ultrasonic cleaning, was much greater with respect to the other test; for each temperature, a higher NO conversion value was reached.

NO reached complete conversion at around 530 °C and its consumption remained stable after that in the test catalysed by the $LaFeO_3$ from the ultrasonic cleaning. Instead, the $LaFeO_3$, scraped from the filters, brought the NO to complete conversion but it was not able to stabilise its value which started to decrease immediately.

Moreover, the NO consumption started at a slightly lower temperature with the powder recovered from the ultrasonic cleaning.

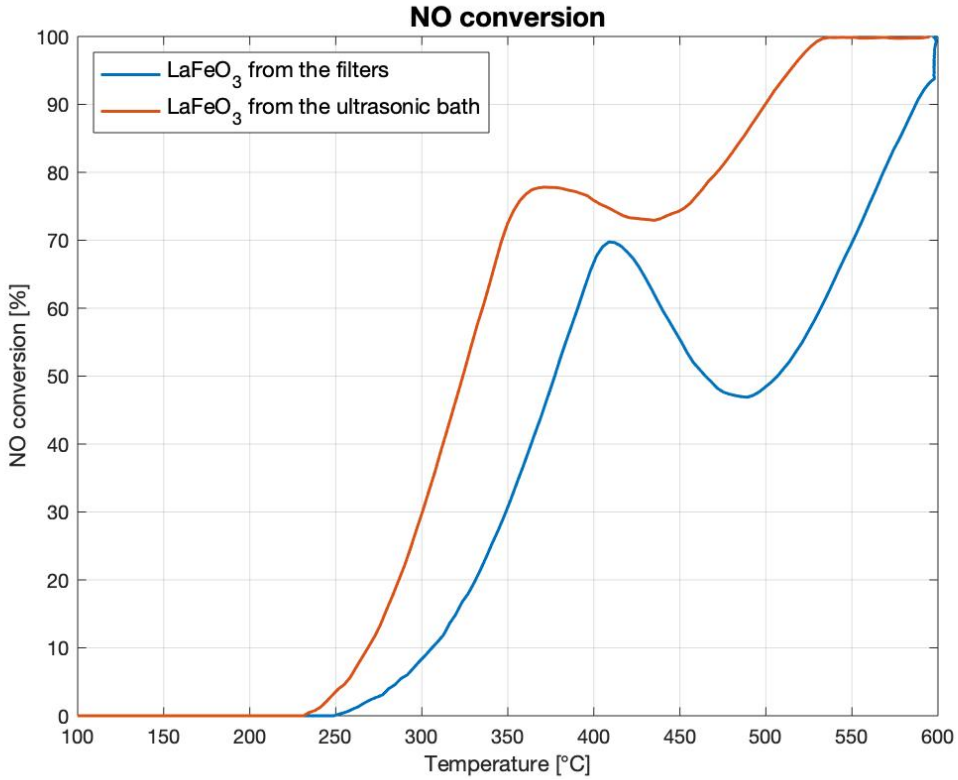

Figure 5.25: NO conversion on $LaFeO_3$ recovered with different methods

After analysing the behaviours of both reactants, it is possible to affirm that the catalytic performance of the $LaFeO_3$ recovered from the filters after the ultrasonic cleaning is much better than the one of $LaFeO_3$ scraped directly from the filters. Between the two performances, it is possible to observe a substantial improvement mostly based on the enhancement of the catalytic activity during the heating and cooling ramps of the temperature cycle. The complete conversion of NO was reached before, which means that the catalyst required lower temperatures to be catalytically active and consequently the reactor did not necessitate to be heated up to 600 °C and therefore less energy could have been wasted.

5.8.2 Mixture with O_2 in defect

The reactants' behaviour was examined also for the second temperature cycle in which O_2 was added to the gas reacting mixture.

In Figure 5.26, the comparison of the CO conversion profiles is reported. The test, that utilised the $LaFeO_3$ recovered after the ultrasonic cleaning, was the one with the best catalytic performances because the carbon monoxide reached complete conversion at the maximum temperature of 600 °C and this remained constant during all the isotherm.

Another important improvement of that catalytic test with respect to the one that used the scraped $LaFeO_3$ is that the oxidation of CO by means of the O_2 present in the gas reacting mixture was catalytically activated at a lower temperature; CO started to oxidise at 150 °C instead of 200 °C.

These are the significant enhancements achieved by utilising the perovskites recovered after the ultrasonic cleaning.

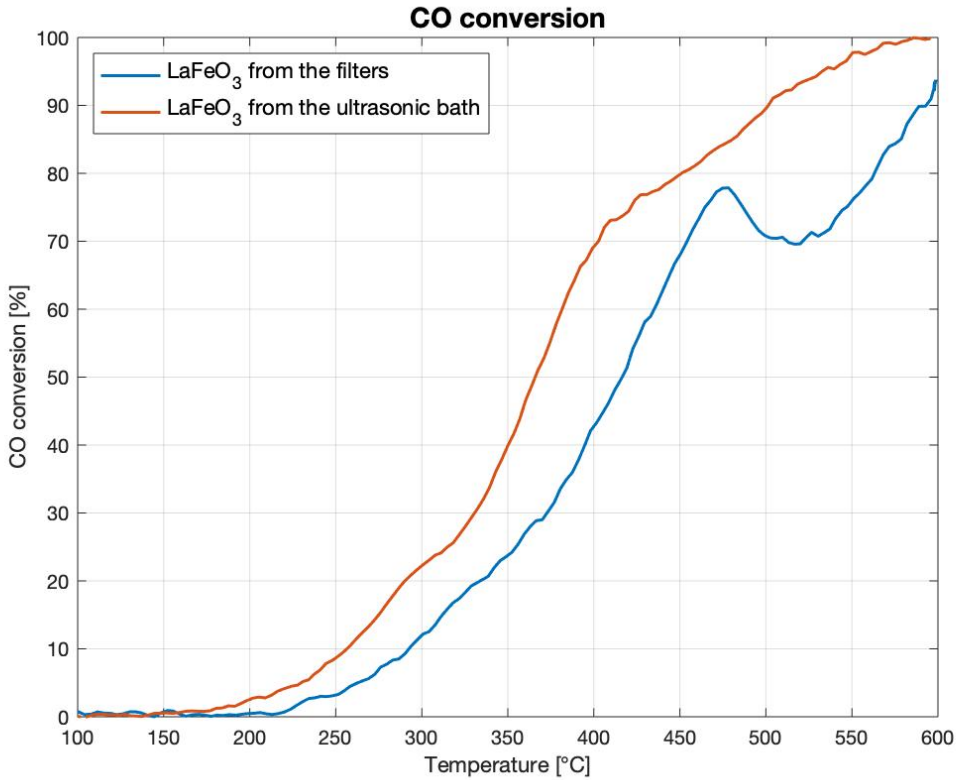

Figure 5.26: CO conversion in the presence of O_2 on $LaFeO_3$ recovered with different methods

The NO conversion profiles are reported in Figure 5.27. As it happened for the comparison of the CO conversion profiles, also while considering the NO conversion, the catalytic test which utilised the $LaFeO_3$ obtained from ultrasonic cleaning resulted the one with the best performance.

It is possible to assert this because, during that catalytic test, the maximum conversion obtained had a much higher value, almost reaching complete conversion even with the presence of O_2.

Moreover, during that test, the reaction was catalytically activated at 300 °C, 50 degrees before the other one. This is also a significant enhancement of the performance because it implicates that the temperature at which both the conversion of CO and the conversion of NO started occurring is lower, which means that the $LaFeO_3$ is more catalytically active.

At low temperatures, the NO conversion was not null because a certain percentage NO was oxidised to NO_2, which is a harmful compound. Its production should be limited to a minimum if it cannot be avoided. Also in this occasion, the test which utilised the $LaFeO_3$ recovered after

the ultrasonic cleaning of the filters had the best performance because, even if the conversion of NO into NO_2 was very limited in both cases, in that test the oxidation of NO was inferior and it stopped at lower temperatures.

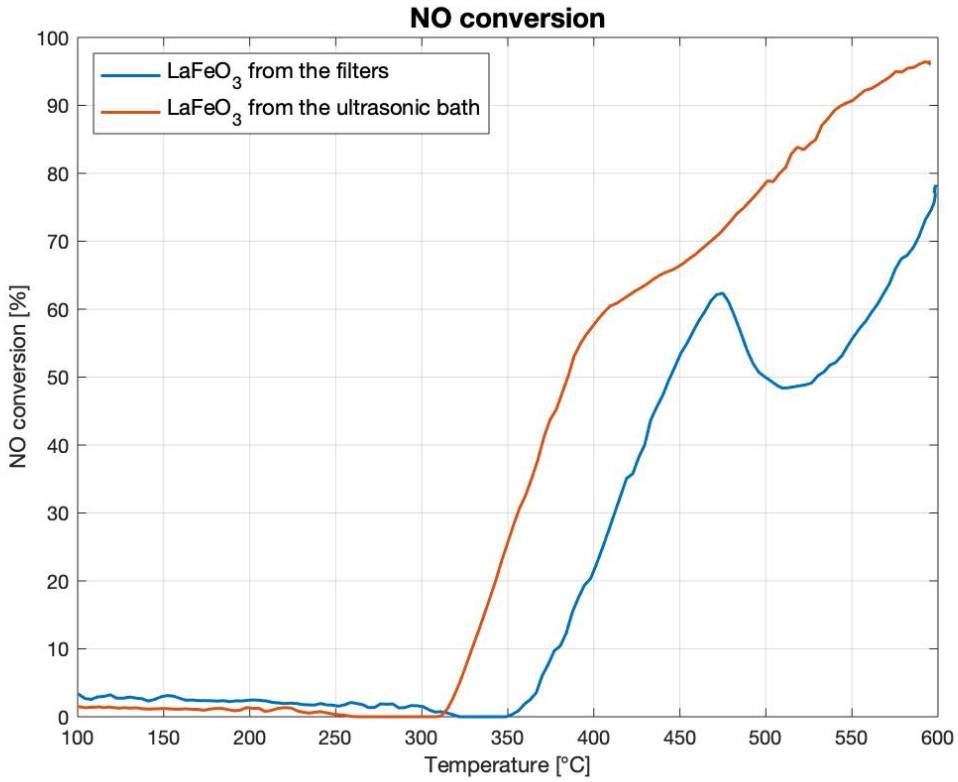

Figure 5.27: NO conversion in the presence of O_2 on $LaFeO_3$ recovered with different methods

It is possible to conclude that obtaining the perovskites with different recovery methods will lead to have powders with different catalytic activities.

The substantial improvement that was obtained in the results of the catalytic test, carried out with the $LaFeO_3$ recovered after the ultrasonic cleaning of the filters, could have been a consequence of multiple factors. Among these, there was the fact that the perovskites had been stabilised by the "thermal pre-treatment" to which they were subjected when they were put in the muffle so that the deionised water, utilised for the cleaning, could be evaporated. This stabilisation could have enhanced the catalytic activity of the $LaFeO_3$.

Moreover, as it was demonstrated in Chapter 4, where the ESEM images of $LaFeO_3$ were reported, the particle size of the perovskites recovered after the ultrasonic cleaning, was significantly inferior to the one of the scraped powders. Smaller particles translate into a higher specific surface area which leads to a higher catalytic activity as it was demonstrated by the tests' results.

This could be the explanation of why the $LaFeO_3$, recovered from the ultrasonic cleaning of the filters, provided a better catalytic performance when tested.

5.9 Activity in excess of O_2

As it was explained in the paragraph 5.2, during the cooling ramp of the second temperature cycle of each catalytic test, the concentration of O_2 in the gas reacting mixture was increased. The amount of O_2 that was fed during this ramp was in excess with respect to the stoichiometric quantity needed to completely oxidise the carbon monoxide present in the reacting mixture.
A mixture with that composition was fed to the catalytic reactor because the purpose was to test the $LaFeO_3$ and understand if it was enough catalytically active towards the reduction of NO and the simultaneous oxidation of CO to favour that reaction over the oxidation of CO with O_2. In all the catalytic tests carried out, with the presence of an excess of O_2, the reduction of NO to N_2 was null and CO completely oxidised by reacting just with O_2. Furthermore, at high temperatures the O_2, that did not react with CO, oxidised NO into NO_2, a harmful compound, whose production should be avoided or limited to a minimum. The oxidation of NO into NO_2 did not occur only at high temperatures but also at ambient temperature.
During the catalytic tests, the production of NO_2 depended on the quantity of O_2 present in the reacting mixture, but it also varied depending on the type of $LaFeO_3$ that was being used to catalyse the reaction. In each test, the maximum volumetric concentration of NO_2 in the gas mixture exiting the reactor was obtained at ambient temperature when an excess of O_2 was present in the reacting mixture.
In order to have a better idea of how much NO_2 was produced with respect to the theoretical quantity that could have been obtained, the percent yield was calculated as it follows:

$$Y\% = \frac{y_{NO_2}^{produced}}{y_{NO_2}^{theoretical}} \cdot 100 \qquad (5.4)$$

Figure 5.28 reports the maximum values of the NO_2 percent yield for the catalytic tests carried out at a WHSV value of $150{,}000\ cm^3/g_{cat}h$ and $170{,}000\ cm^3/g_{cat}h$ and with $LaFeO_3$ synthesised with a solution at a concentration of 100% in flames fed with decreasing flowrates of H_2 and O_2. All the perovskites utilised were scraped directly from the filters.
It is noticeable that the maximum NO_2 percent yields of the tests considered in this plot have similar values to each other. Therefore, it is possible to say that the WHSV at which the test is carried out and the flowrate of H_2 utilised to feed the flames in which the $LaFeO_3$ is synthesised do not influence the value of the NO_2 percent yield and as a consequence the volumetric concentration of NO_2 present in the gas mixture exiting the reactor.

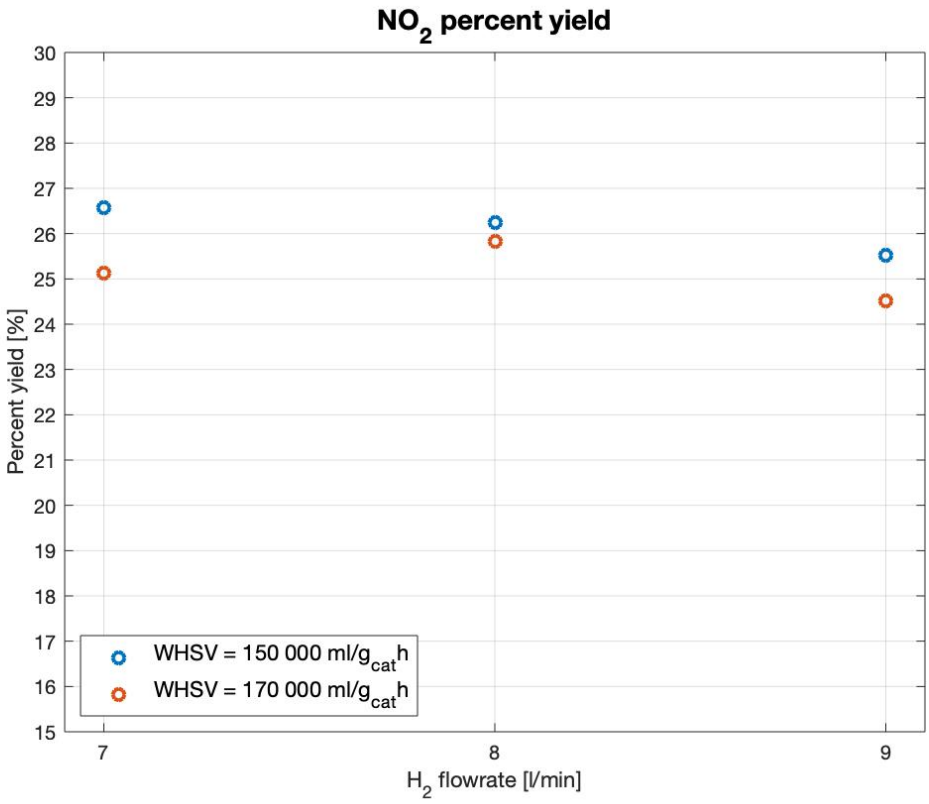

Figure 5.28: Maximum NO_2 percent yields on $LaFeO_3$ obtained using different H_2 flow rate at the flame

The two plots reported in Figure 5.29 and Figure 5.30 are referred to the catalytic tests carried out at a WHSV value of $170{,}000\ cm^3/g_{cat}h$ and employing $LaFeO_3$ synthesised in flames fed with 7 l/min of H_2 and 6 l/min of O_2.

In Figure 5.29, there is the comparison between the perovskites scraped directly from the filters but synthesised with precursor solutions with different concentration levels. It is observable that in the catalytic test, in which the $LaFeO_3$ synthesised with a less concentrated solution was utilised, the maximum NO_2 percent yield is lower.

In the test, in which the $LaFeO_3$ synthesised from a less concentrated solution was used, the catalyst was not as active towards the oxidation of NO into NO_2; but, as it was observed in the previous paragraphs, it was also not as active towards the oxidation of CO and simultaneous reduction of NO. Therefore, even if the production of NO_2 was inferior, also the conversion of CO and NO were lower and therefore it cannot be affirmed that this type of perovskite had a better catalytic performance.

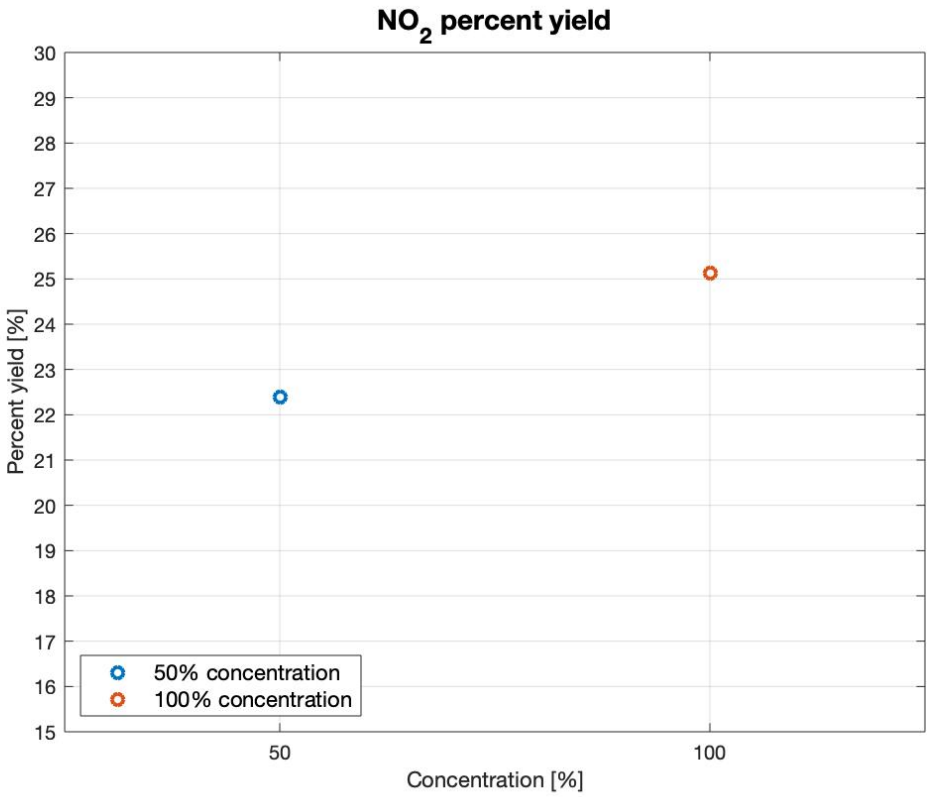

Figure 5.29: Maximum NO_2 percent yields on $LaFeO_3$ obtained from solutions with different concentrations

In Figure 5.30, there is the comparison between the perovskites produced with a precursor solution with a 100% concentration but recovered with different methods. It is noticeable how the maximum NO_2 percent yield obtained in the test in which the $LaFeO_3$ recovered after the ultrasonic cleaning of the filters was utilised is significantly inferior to the one of the other tests. Once more, this is the proof that the $LaFeO_3$ recovered from the ultrasonic cleaning of the filters had the best results because, apart from being the most catalytically active towards the reduction of NO and the simultaneous oxidation of CO, it was also the least active towards other reactions such as the oxidation of NO, which had to be limited to a minimum.

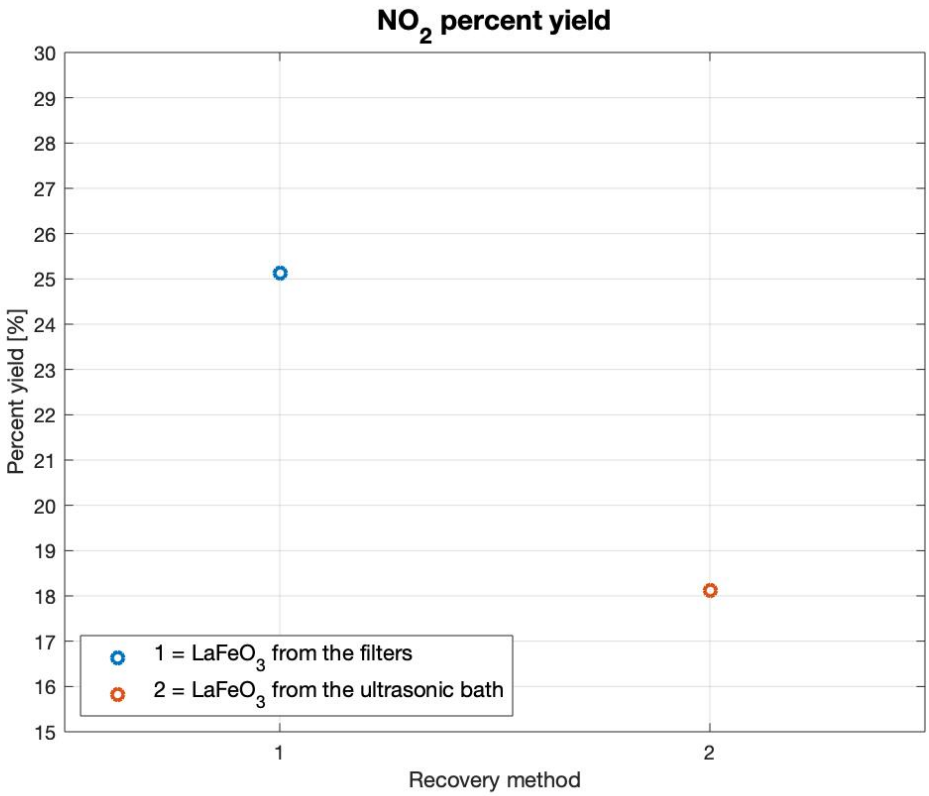

Figure 5.30: Maximum NO_2 percent yields on $LaFeO_3$ recovered with different methods

Therefore, after analysing all the performances of the various types of $LaFeO_3$, it is possible to conclude that the $LaFeO_3$ was not active in reducing NO by CO oxidation if the gas reacting mixture contained an abundance of another oxidant, such as O_2, which could oxidise the CO and NO more easily.

Moreover, it is affirmable that the $LaFeO_3$ which was less active towards the oxidation of NO and guaranteed the lowest NO_2 percent yield, and as a consequence the lowest volumetric concentration of NO_2, was the one recovered after the ultrasonic cleaning of the filters, confirming once again its better catalytic performances compared to the others.

5.10 Conclusions

The results of all the tests executed during this thesis work are summed up in Table 5.5. To compare the catalytic activity of all the $LaFeO_3$ synthesised, the temperatures at which the conversion profiles reached a value of 50 % (T50) are reported for each test. The tests, which have the lower values of T50, are the ones in which the $LaFeO_3$ with the greatest catalytic activity were utilised.

All the synthesis parameters that were varied for the production of different batches of $LaFeO_3$ are listed. It was important to decrease the flowrate of H_2 so that the flame synthesis of perovskites could become economically sustainable. Therefore, the first parameter that was

investigated was the flowrate of combustible gas fed to the burner to understand if it could be decreased without invalidating the catalytic activity of $LaFeO_3$.
Then, it was studied how a variation in the concentration of the precursor solution would affect the catalytic activity of $LaFeO_3$ and if the recovery method of the powder could have an influence on its catalytic performance.
In the Table 5.5 the maximum CO and NO conversions are reported for both the temperature cycles, the one in which O_2 was not fed and the one in which a lean O_2 gas reacting mixture was fed.
Moreover, the results are divided based on the value of weight hourly space velocity at which the tests were executed. It is important to notice that those values of WHSV are extremely high with respect to the ones set in the tests cited in literature and therefore obtaining good results with such high WHSVs is to be considered a great achievement.

Table 5.5: Tests results

WHSV [$cm^3/g_{cat}h$]	150,000			170,000				
H_2 flowrate [l/min]	7	8	9	**7**			8	9
Solution concentration	100%	100%	100%	50%	**100%**		100%	100%
Recovery method	Filters	Filters	Filters	Filters	Filters	**Ultrasonic bath**	Filters	Filters
T50 for CO conversion [°C]	380	360	366	387	391	**339**	503	383
T50 for CO conversion [°C] (O_2 in defect)	411	424	407	428	416	**367**	506	431
T50 for NO conversion [°C]	366	345	354	376	376	**324**	520	372
T50 for NO conversion [°C] (O_2 in defect)	438	507	479	532	444	**385**	589	510

By analysing the results summed up in Table 5.5, it is possible to affirm that the best results were obtained with the $LaFeO_3$ recovered from the ultrasonic cleaning of the filters because those catalyst particles, that were embedded in the filters, were the smallest ones and therefore the most active.
In the tests conducted with a WHSV of $150{,}000\ cm^3/g_{cat}h$, the differences between the T50s of the various tests are not significant. However, if the catalyst is tested with a higher WHSV ($170{,}000\ cm^3/g_{cat}h$) the differences between the T50s are substantial in some cases. It has to be remembered that during the test, in which the $LaFeO_3$ synthesised in flames fed with 8 l/min

of H_2 was used, the catalytic bed shrunk and therefore the results might not be truthful. The T50s of the other two profiles were similar when O_2 was not in the gas reacting mixture, but they were quite different when O_2 was present.

Therefore, the flowrate of H_2, fed to the flames in which the $LaFeO_3$ is synthesised, could be decreased up to a certain point without worsening the activity of the catalyst. Decreasing the flowrates of combustible and oxidising gases fed to the flames is essential to have an economically sustainable process.

The tests, in which the catalysts synthesised with precursor solutions with different concentrations were used, did not give the expected results because the $LaFeO_3$, which was synthesised with the less concentrated solution and that had the smaller average particle size, did not provide better results than the one synthesised with a more concentrated solution.

Therefore, the parameter that has the greatest influence on the catalytic activity of the $LaFeO_3$ is the diameter of the particles synthesised. In future projects, it will be crucial to be able to recover efficiently and in large quantities the finest particles of every synthesis, because those, as it was observed, are the ones with the greatest catalytic activity.

Conclusions

The first objective of this thesis work was the optimisation of the lab-scale plant for the flame synthesis of perovskites that had been constructed during previous thesis projects.
The sections, that necessitated the most improvement, were the feeding section and the filter pack. The old feeding system was substituted with a new one composed of four atomisers that nebulised the precursor solution by means of ultrasonic membranes. The particles synthesised with this new method were much smaller than the ones produced with the spray gun, which was a great result in terms of the enhancement of the catalytic activity of $LaFeO_3$.
One of the main issues of the experimental set-up, utilised in the previous thesis projects, was the particles sticking on the internal surface of the column. The employment of the new feeding system solved this problem because the direction of the flow of nebulised solution could be controlled and adjusted more easily.
In order to collect the smaller particles synthesised with the new feeding system, a new filter pack was constructed. In fact, the filters utilised to block the particles needed to have extremely fine mesh spacings which consequently created substantial pressure drop. To counteract this effect, the surface area of the filters had to be increased with respect to the one of the existing collection set-up and therefore a new filter pack was built.
Moreover, a pressure control was programmed on the inverter that regulated the blower to obtain a better control on the quantity of air that was sucked in by the blower. It was important for the blower to aspire constantly the same quantity of air during the synthesis because if the air entering the blower were too hot, it would have damaged its internal components compromising its correct functioning. This was a significant implementation of the experimental set-up because it assured the reliability of the lab-scale plant of always working in the same conditions.
Once the lab-scale plant was optimised, the $LaFeO_3$ was synthesised varying the production parameters. The objective was to identify the best economically sustainable conditions for the synthesis of the perovskites which would lead the catalyst to have the greatest catalytic activity possible.
The first parameter that was studied, to understand if it had an influence on the properties of the perovskite, were the flowrates of combustible and oxidising gas fed to the burner. The pairs of flowrates investigated were 9 l/min H_2 and 8 l/min O_2, 8 l/min H_2 and 7 l/min O_2 and 7 l/min H_2 and 6 l/min O_2. The second parameter, that could have influenced the properties of $LaFeO_3$, was the concentration of the precursor solution nebulised into the flames. Moreover, it was also observed if the recovery method of the particles was influential on their properties.

An environmental scanning electron microscope was utilised to observe the particle size of the $LaFeO_3$ produced and characterisation analyses were executed to identify possible residues still present in the powder and to assure that the $LaFeO_3$ produced had a complete crystalline perovskite structure. Then, the batches of $LaFeO_3$ synthesised were catalytically tested to examine their catalytic performances and identify the one with the greatest catalytic activity towards the simultaneous reduction of NO and oxidation of CO.

The catalytic tests, which employed $LaFeO_3$ synthesised with decreasing flowrates of H_2 and O_2, obtained very similar results. In fact, the CO and NO conversion decreased of only 4% and 2% respectively between the test which employed the $LaFeO_3$ synthesised with 9 l/min of H_2 and the one that employed the one synthesised with 7 l/min. These results were considered very satisfying because these slight decrements in conversion could be tolerated to make the process more economically sustainable.

It is affirmable that decreasing the combustible and oxidising gas flowrates fed to the burner up to a certain point does not influence the catalytic properties of the perovskites.

The catalytic tests confirmed what had been observed from the ESEM imaging. The $LaFeO_3$ recovered after the ultrasonic cleaning of the filters was the most active out of all the samples because it was the one with the smallest average particle size and consequently the greatest specific surface area.

The catalytic tests were dynamic because of the variation of temperature during the test and because gas reacting mixtures with different compositions were fed to the reactor during the same test; the initial gas reacting mixture was composed of CO and NO, while O_2 was added after a certain interval of time to study the effect that the presence of the oxidant in the mixture could have had. It was discovered that with a lean O_2 gas reacting mixture, the reduction of NO worsened; while an excess of O_2 in the gas reacting mixture did not allow the reduction of NO into N_2 because the oxidation of CO by means of O_2 was favoured over the simultaneous reduction of NO and oxidation of CO.

The catalytic tests were executed at two different values of WHSV to identify the limit after which the catalyst would not have a satisfying performance. The performances of the catalysts in the tests executed at a WHSV of $150{,}000\ cm^3/g_{cat}h$ were all satisfying, while a WHSV of $170{,}000\ cm^3/g_{cat}h$ was too high because the catalysts were not able to provide a consistent performance, apart from the one recovered after the ultrasonic cleaning of the filters. However, it is crucial to affirm that a value of $150{,}000\ cm^3/g_{cat}h$ is extremely high compared to the values usually imposed in the catalytic tests cited in literature. Therefore, synthesising a catalyst able to perform well with a WHSV of $150{,}000\ cm^3/g_{cat}h$ is a great result.

The knowledge acquired, on the best synthesis conditions for the production of perovskites with a great catalytic activity, could be utilised for the synthesis via flame assisted spray pyrolysis of doped $LaFeO_3$ to further enhance its catalytic performance.

Nomenclature

N_A	=	Avogadro number
λ	=	Beam wavelength
X_{CO}	=	Carbon monoxide conversion
m_{cat}	=	Catalyst mass
r_A	=	Cation A radius
r_B	=	Cation B radius
V_{uc}	=	Crystal unit cell number
D_d	=	Droplet diameter
ϕ	=	Equivalence ratio
$\dot{n}_F$	=	Fuel molar flowrate
t	=	Goldschmidt's tolerance factor
θ	=	Incident angle
y^{in}	=	Initial molar fraction
y	=	Molar fraction in gas phase
Z	=	Molecules per unit cell
$\dot{n}_{OX}$	=	Oxidant molar flowrate
r_O	=	Oxygen ion radius
D_p	=	Particle diameter
$Y\%$	=	Percent yield
M	=	Solution molar concentration
d	=	Spacing between diffracting planes
$\dot{V}$	=	Total volumetric gas flowrate

Acronyms

DPF	=	Diesel Particulate Filters
EDS	=	Energy X-ray Dispersive Spectroscopy
ESEM	=	Environmental Scanning Electron Microscopy
FASP	=	Flame Assisted Spray Pyrolysis
FID	=	Flame Ionisation Detector
FSP	=	Flame Spray Pyrolysis
FT-IR	=	Fourier Transform Infrared Spectroscopy

GC	=	Gas Chromatograph
NO_x	=	Nitrogen Oxides
OPC	=	Optical Particle Counter
PGMs	=	Platinum Group Metals
PSD	=	Particle Size Distribution
RI	=	Refractive Index
SEM	=	Scanning Electron Microscopy
SSA	=	Specific Surface Area
TCD	=	Thermal Conductivity Detector
WHSV	=	Weight Hourly Space Velocity
XRD	=	X-Ray Diffraction

References

[1] Strobel *et al.,* Aerosol flame synthesis of catalyst. *Advanced Powder technology.* 2006; 457-480.

[2] Frison E., Sintesi, Drogaggio e attività di perovskite mediante flame spray. - University of Padua; 2017.

[3] Franchin R., Continuous flame-assisted synthesis of perovskites nanoparticles: reactor optimization. - University of Padua; 2019.

[4] Garbujo *et al.*, On A-doping strategy for tuning the TWC catalytic performance of perovskite based catalysts. *Applied Catalysis A, General 544.* 2017; 94-107.

[5] Varandili S. B., Nano-structured Pd doped $LaFe(Co)O_3$ perovskite; synthesis, characterization and catalytic behavior. *Materials Chemistry and Physics*. 2018; 228-239.

[6] Vieten J. *et al.*, Citric acid auto-combustion synthesis of Ti-containing perovskites via aqueous precursors. *Solid State Ionics*. 2018; 92-97.

[7] Nunes *et al.*, Synthesis, design and morphology of metal oxide nanostructures. *Metal Oxide Nanostructures. Synthesis, Properties and Applications.* 2019; 21-57.

[8] *Law, C.K.*, Combustion physics. Cambridge, UK. *Cambridge University Press.* 2006.

[9] *Glassman I.*, *Yetter R.,* Combustion. USA. *Elsevier.* 2008. 4th edition.

[10] Chiarello *et al.*, Flame-spray pyrolysis preparation of perovskites for methane catalytic combustion. *Journal of Catalysis 236.* 2005; 251-261.

[11] Rudin *et al.*, Towards carbon-free flame spray synthesis of homogeneous oxide nanoparticles from aqueous solutions. *Advanced Powder Technology 24.* 2013; 632–642.

[12] Mueller *et al.*, Nanoparticle synthesis at high production rates by flame spray pyrolysis. *Chemical Engineering Science 58*. 2003; 1969 – 1976.

[13] Betancur-Granados *et al.*, Flame spray pyrolysis synthesis of ceramic nanopigments $CoCr_2O_4$: The effect of key variables. *Journal of the European Ceramic Society 37*. 2017; 5051–5056

[14] https://www.explorermaterials.wordpress.com/basic-concepts/perovskite-structure/

[15] Blonda C., Kinetic studies on perovskite-based four-way catalysts (FWC) for automotive applications. – University of Padua; 2018.

[16] Donald A., The use of environmental scanning electron microscopy for imaging wet and insulating materials. *Nature Materials, Vol 2.* 2003.

[17] https://serc.carleton.edu/research_education/geochemsheets/techniques/XRD.html

Ringraziamenti

Ringrazio i miei genitori che in tutti questi anni di studio mi hanno sempre appoggiata e mi hanno concesso la possibilità di intraprendere sempre nuove avventure in giro per il mondo.
Ringrazio Riccardo per aver creduto in me, sempre.
Ringrazio mia cugina Anna, che per me è come una sorella, la mia famiglia italiana e la mia famiglia canadese.
Ringrazio Francesca, Martina, Natalia e Roberta perché dopo tutti questi anni ancora mi sopportano. Ringrazio la mia squadra di nuoto per tutte le ore passate insieme in piscina e davanti ai giochi da tavolo. Ringrazio la compagnia di Bassano per le costanti risate.
Ringrazio il Professor Paolo Canu per avermi dato la possibilità di lavorare ed imparare molto in laboratorio. Ringrazio Nicola per avermi seguito durante questo progetto di tesi, per tutti i consigli e gli insegnamenti. Ringrazio Benedetta per tutta la pazienza che ha avuto nei miei confronti e per essere sempre stata pronta ad aiutarmi. Ringrazio Mattia per avermi fatto scoprire il mondo del GC.
Ringrazio Marco, Luca e Pierre per i pranzi e le pause merenda, Giovanni e la sua stufa per aver riscaldato le fredde giornate estive in laboratorio, Filippo mio fedele compagno di lavori di gruppo e Luca per non essersi mai tirato indietro quando si trattava di giocare con le fiamme ad idrogeno. Ringrazio Davide, Elisa, Matteo, Riccardo, Simone, Sofia e tutti gli altri compagni di corso che mi hanno accompagnata in questi cinque lunghi anni.